RRFM

EUROPEAN RESEARCH REACTOR CONFERENCE 2011

Transactions

Rome, Italy
20 -24 March 2011

EUROPEAN NUCLEAR SOCIETY

ENS CONFERENCE

organised in collaboration with:

ENEA · IAEA International Atomic Energy Agency · Università di Pavia · INFN Istituto Nazionale di Fisica Nucleare · Consiglio Nazionale delle Ricerche

European Nuclear Society
Rue Belliard 65
1040 Brussels, Belgium
Phone + 32 2 505 30 54
Fax +32 2 502 39 02
E-mail ens@euronuclear.org
Internet www.euronuclear.org

ISBN 978-92-95064-11-9

These transactions contain all contributions submitted by 18 March 2011.

Wednesday 23 March 2011

REVIEW OF MAIN SPECIFICATIONS AND ALLOWANCES FOR RESEARCH REACTOR MATERIALS AIMING DECOMMISSIONING

PAULO ERNESTO DE OLIVEIRA LAINETTI

Centro de Química e Meio Ambiente – CQMA
INSTITUTO DE PESQUISAS ENERGÉTICAS E NUCLEARES IPEN-CNEN/SP
Av. Prof. Lineu Prestes, 2242 C. Universitária São Paulo – SP, Brazil CEP- 5508-000
Telephone: 55 11 3133-9333 Facsimile: 55 11 3133-9249 E-mail: lainetti@ipen.br

ABSTRACT

The decommissioning of nuclear facilities, especially research reactors, can be facilitated, with significant reduction of the costs and amount of wastes, if suitable choice of the employed materials and their chemical composition is made during the design phase. It deserves special attention the reactor regions where activation of materials is possible, since the presence of determined elements in the composition of alloys and structural materials can affect significantly the future decommissioning. Then, the proper selection of the materials and their chemical composition and respective allowances will reduce the impact in the future decommissioning costs, amount of high level wastes generated during the process and in the safety of the involved personnel. In this paper is presented a review of the main criteria employed in the choice of materials used for fuel elements and structural components for research reactors.

1. Introduction

The shutdown of a research reactor and their related supporting facilities, such as radioisotope production and waste treatment facilities, leaves an important nuclear decommissioning legacy. Interest for reducing the residual radioactivity in construction materials employed in research reactors evolves from the impact that this reduction will have in the decommissioning and dismantling future activities. To facilitate future research reactors' dismantling and decommissioning projects some recommendations, such as the clearance levels of the most important isotopes for different materials employed in the reactors' construction, should be included in the regulatory norms and procedures on national and international levels. The decommissioning of nuclear facilities, especially research reactors, can be facilitated, with significant reduction of the costs and amount of wastes, if suitable choice of the employed materials and their chemical composition is made during the design phase. Regarding the decommissioning issues involved in the design of a new research reactor, the main concern should be to take into account the lessons learned and the worldwide accumulated experience in the decommissioning of such facilities [1] avoiding mistakes and reducing the amount of problematic wastes in the future.

2. Brazilian regulatory procedures regarding research reactors

In Brazil, CNEN is the Regulatory Body in charge of regulating, licensing and controlling nuclear energy. Since 2000, CNEN has been under the Ministry of Science and Technology - MCT (Ministério da Ciência e Tecnologia). Some of CNEN responsibilities include: the preparation and issuance of regulations on nuclear safety, radiation protection, radioactive waste management, nuclear material control and physical protection; licensing and

authorization of sitting, construction, operation and decommissioning of nuclear facilities; regulatory inspection; acting as a national authority for the purpose of implementing international agreements and treaties related to nuclear safety, security and safeguards; participating in the national preparedness and response to nuclear emergencies.

The Brazilian legislation defines the operating organization as the prime responsible for the safety of a nuclear or radioactive installation, including the management of spent fuel and radioactive waste. The licensing regulation CNEN-NE-1.04 establishes that no nuclear facility shall operate without a license. It also establishes the necessary review and assessment process, including the specification of the documentation to be presented to CNEN at each phase of the licensing process. It finally establishes a system of regulatory inspections and the corresponding enforcement mechanisms to ensure that the licensing conditions are being fulfilled. The enforcement mechanisms include the authority of CNEN to modify, suspend or revoke the license. The licensing process is divided in several steps: Site Approval; Construction License; Authorization for Nuclear Material Utilization; Authorization for Initial Operation; Authorization for Permanent Operation; Authorization for Decommissioning Federal Law 9756, approved in 1998, establishes taxes and fees for each individual licensing step, as well as for the routine work of supervision of the installation by CNEN. Other governmental bodies are involved in the licensing process, through appropriate consultations. The most important ones are the Institute for Environmental and Renewable Natural Resources (Instituto Brasileiro do Meio Ambiente e dos Recursos Naturais Renováveis - IBAMA), in charge of environmental licensing [2].

Nevertheless, Brazil does not have yet a national regulation that establishes rules for decommissioning of nuclear facilities and no decommissioning policy has been adopted until now regarding research reactors. As the Brazilian nuclear program and related facilities are relatively new in comparison with other countries, it should be taken into account the international experience for the decommissioning of shut down nuclear facilities. These activities have increased within the last ten years and are constantly increasing as older facilities retire and the need for their dismantling or safe enclosure becomes prominent.

3. Decommissioning requirements for research reactors and nuclear facilities

Decommissioning of large facilities such as research reactors and associated units is a technically complex task and has significant implications for the local social and economic situation. Regulatory requirements are an opportunity to improve the technical aspects of design, construction and operation of nuclear installations, and they will affect the safety and the decommissioning costs of such facilities. Many issues should be solved before successful decommissioning can be achieved and include clearly defined regulatory requirements for decommissioning of nuclear facilities.

Decommissioning is defined to include all activities after the final termination of operation of a nuclear facility. Decommissioning consists of: the final shut down of a nuclear facility; sometimes followed by transferring it into safe store condition; decontamination and dismantling of systems and components; demolition of some or all of the buildings; the clearance and release of the site to the green-field state if possible.

The phase of decommissioning is the last life cycle phase of a nuclear facility. All these activities are considered to be kept under regulatory control, in continuation from the operational phase. This includes licensing procedures where legally required or regulatory approval as well as regulatory inspection by the authorities. Some countries are planning to introduce further legal requirements for licensing of decommissioning activities and develop

corresponding standards and guidelines. In general, most countries see the need for more precise legal requirements and regulatory guidelines to regulate or license and to inspect decommissioning activities of nuclear facilities [3].

4. Clearance of waste material - release and clearance criteria

An important feature of decommissioning is the possibility to clear waste material for recycling, reuse or conventional disposal. The clearance might be unrestricted or subject to conditions after clearance e.g. a prescribed installation for processing or disposal. Related regulations for this, i.e. clearance criteria and procedures, are developed and applied in almost all countries. The clearance criteria are in most cases based on the internationally agreed criteria for the resulting radiation exposure.

Related to future regulatory requirements for new projects**, s**ome countries develop further requirements for licensing of decommissioning activities and develop corresponding standards and guidelines. For instance, the members of the European Union are in the process of introducing the EURATOM 96/29 directive into their legal framework. In general, most countries see the need for more precise legal requirements and regulatory guidelines to regulate or license and inspect decommissioning activities of nuclear facilities.

Is interesting that, even in Europe, most countries have no specific regulations in place and some countries plan to introduce a licensing regime for decommissioning. Decommissioning is regulated mostly on a case by case basis by approval of the regulatory body similar to plant modifications. Safety reviews for these activities are generally required. Some countries require submission of preliminary decommissioning considerations (feasibility study) as a license condition already for operation. Such data are to be revised regularly. In all countries the regulatory bodies continue to be in charge of regulating safety and radiation protection as the plants change over from operation to decommissioning activities. The relevant regulations (safety, requirements, rules, standards), normally applicable to construction and operation, continue to be valid also for decommissioning, sometimes including adaptations or amendments as appropriate [3,4].

An important aspect of the decommissioning task is to describe the specific activity and surface contamination clearance criteria and clearance procedures for the release of waste material for unrestricted use, and authorized reuse. The release of waste material (containing radioactivity below prescribed limits) for unrestricted use, conventional disposal, recycling or reuse is possible in most of countries. By this provision the amount of radioactive waste to be disposed off can be kept small. If necessary, the release of waste material is regulated on a case by case basis.

Some countries have not yet established release and clearance criteria and procedures but are in progress of developing such criteria. In most countries release criteria refer to the international criteria discussed at the IAEA or the European Union. The international criteria are based on a dose of the order of 10 µSv/y to the public for each practice of release pathways. The development of an integrated approach for clearance criteria to release waste material from licensed activities taking into consideration the fundamental international guidance on acceptable radiation exposure is commendable practice.

5. Specifications and allowances for research reactors materials

The commendable practices are not international standards or guidelines. The preparation of an efficient, safe and economic decommissioning project begins during the design phase,

since a lot of problems can be avoided by the proper choice of construction materials, mainly those employed in regions subjected to activation.

The decommissioning items listed below should be considered already during design and construction of the reactor or for any modernization or refurbishment during the operational life. These items include: - Minimizing the potential for activation of the materials and / or contamination; - Provision of equipment and systems in order to have adequate space to allow for the easy implementation of decommissioning activities; - Management of radioactive waste to be generated during the lifetime of the reactor to minimize the need for treatment and disposal during the decommissioning.

Therefore, a design principle related to decommissioning to be adopted is that the design of the reactor facility must minimize contamination and activation of components. The design of the reactor facility should take into account the need of monitoring the parameters, during the life of the reactor, that can affect the inventory of radioactivity and the radiological factors needed to estimate the potential radiation levels during the decommissioning phase. Materials near the reactor core or passing through it are activated and become sources of contamination and/or activation of other materials. Of particular importance to the decommissioning activities is the reduction of the amount and intensity of radiation sources existing in the reactor building.

The neutron flux generated in the reactor core induces radioactivity in materials nearby. At the time of decommissioning, it is advisable to plan a period of decline prior to handling these materials in order to decrease the dose to workers and decrease the volume of tailings. Still in design phase or during the reforms, the choice of materials should take into consideration the following characteristics: physical properties depending on operational requirements; Mechanical properties to ensure good performance of the material; the range of possible activation products that can be generated and half lives; for those materials in contact with water, consider the resistance to corrosion.

An important recommendation is that materials which are subject to high neutron fluxes must be specified according to nuclear standards, because they restrict the presence of impurities that raise the levels of radiation. The main characteristics of some materials used in this type of project are presented bellow. Aluminum alloys are used preferably in materials subjected to high-flow regions in the reactor, since Al has low cross-section of neutron capture and good mechanical performance under neutron radiation. These alloys are widely used in the manufacture of the plate array and other reactor components. The main advantage is that most of the isotopes resulting from irradiation of Al have a short half life, being ^{24}Na the main one. Therefore, these components can be handled as low-activity waste in a relatively short space of time after the final shutdown of reactor. The zirconium alloys have benefits under neutron irradiation, and mechanical properties (low absorption cross section and high resistance under neutron flux). These alloys must be manufactured to standards for nuclear pattern, limiting the content of hafnium as an impurity. Nevertheless, the irradiation produces radionuclides with longer half life than the aluminum alloys such as ^{60}Co, ^{125}Sb and ^{93m}Ni. The stainless steel is a material with excellent corrosion resistance and has been used in various structures of the reactors. Despite the use of special alloys with low cobalt content, the activation products such as ^{60}Co, ^{51}Cr, ^{55}Fe, ^{59}Fe, ^{56}Mg, make these alloys difficult to handle before the decay, and therefore usually require the use of shields. Therefore, the use of these alloys has been avoided, particularly in regions of high flow. The concrete that is used as shielding has small amount of impurity such as iron, cobalt and europium which tend to become radioactive under intense neutron flux. Wherever possible,

activation sources should be positioned away from concrete bioshields or other shield walls in order to reduce the quantity of activated concrete. Given the nature of the materials that make up concrete, it is difficult to source these so as to reduce activation [5].

5. Conclusion

Designing for decommissioning is the best long term facilitator of the decommissioning process [6,7]. In reactors, the trace elements that are always present in construction material will be activated in a neutron flux. The resulting radioactive isotopes contribute to operational doses (e.g. ^{60}Co) and can become significant for waste management (e.g. long lived isotopes such as ^{36}Cl from graphite and ^{14}C from most construction material). It may not be practicable or cost effective to eliminate relevant trace elements entirely, but care should be taken in construction material selection and samples should be retained for future analysis to support characterization campaigns for decommissioning; for example, the use of aluminum rather than stainless steel for research reactor containment tanks reduces the quantities of low and intermediate level waste (LILW), since all commercial stainless steels contain significant quantities of elemental cobalt (although most aluminum alloys contain some residual traces of cobalt) [8]. The international exchange of information concerning the specifications and allowances of materials employed in the construction of components of research reactors is of fundamental importance for the reduction of the waste volume and for workers safety during the decommissioning phase. The international availability of information on specifications and tolerances for the materials used in research reactors should be encouraged and emphasized.

6. References

[1] ***Decommissioning of Research Reactors: Evolution, State of the Art***, ***Open Issues***, Technical Report Series 446, IAEA, Vienna, 2006.
[2] Silva, E. F., ***National Report of Brazil – Legal and Regulatory Framework on Decommissioning of Research Reactors***, CNEN, June, 2006.
[3] ***Regulatory Practices for Decommissioning of Nuclear Facilities with Special Regard of Regulatory Inspection Practices*****,** Working Group on Inspection Practices (WGIP), NEA/CNRA/R(99)4**,** Paris, Feb. 2000.
[4] ***Review of Existing and Future Requirements for Decommissioning Nuclear facilities in CIS*****,** European Commission, Direct. Gen. XI, Jan. 1999.
[5] ***Design Concepts to Minimize the Activation of the Biological Shield of Light Water Reactors***, European Commission, Rep. EUR-8804, EC, Brussels, 1985.
[6] ***Application of the Management System for Facilities and Activities***, IAEA Safety Standards Series No. GS-G-3.1, IAEA, Vienna, 2006.
[7] ***Design and Construction of Nuclear Power Plants to Facilitate Decommissioning***, Technical Reports Series 382, IAEA, Vienna 1997.
[8] ***Decommissioning of Research Reactors and Other Small Facilities by Making Optimal Use of Available Resources***, Technical Reports Series 463, IAEA, Vienna, 2008.

7. Acknowledgments

The author would like to express his gratitude to the CNPQ – *Conselho Nacional de Desenvolvimento Científico e Tecnológico* / MCT – *Ministério da Ciência e Tecnologia do Brasil* for the financial support for his participation in the RRFM 2011 - European Research Reactor Conference 2011.

THE BORON NEUTRON CAPTURE THERAPY (BNCT) PROJECT AT THE TRIGA REACTOR IN MAINZ, GERMANY

G. HAMPEL, C. GRUNEWALD, C. SCHÜTZ, T. SCHMITZ, J.V. KRATZ
Nuclear Chemistry, University of Mainz
D-55099 Mainz, Germany

C. BROCHHAUSEN, J. KIRKPATRICK
Department of Pathology, University of Mainz
D-55099 Mainz, Germany

S. BORTULUSSI, S. ALTIERI
Department of Nuclear and Theoretical Physics University of Pavia, Pavia, Italy
National Institute of Nuclear Physics (INFN) Pavia Section, Pavia, Italy

P. KUDEJOVA
Forschungs-Neutronenquelle Heinz Maier-Leibnitz (FRM II),
Technische Universität München, D-85748 Garching, GERMANY

K. APPELMAN, R. MOSS
Joint Research Centre (JRC) of the European Commission,
NL-1755 ZG Petten, The Netherlands

N. BASSLER
University of Aarhus, Norde Ringade, DK-8000, Aarhus C, Denmark, Denmark

M. BLAICKNER, M. ZIEGNER
Molecular Medicine, Health & Environment Department, AIT Austrian Institute of Technology GmbH, Austria

P. SHARPE, H. PALMANS
National Physical Laboratory, Teddington TW11 0LW, Middlesex, UK

G. OTTO
Department of Hepatobiliary, Pancreatic and Transplantation Surgery, University of Mainz,
D-55099 Mainz, Germany

Abstract

The thermal column of the TRIGA reactor in Mainz is being used very effectively for medical and biological applications. The BNCT (boron neutron capture therapy) project at the University of Mainz is focussed on the treatment of liver tumours, similar to the work performed in Pavia (Italy) a few years ago, where patients with liver metastases were treated by combining BNCT with auto-transplantation of the organ. Here, in Mainz, a preclinical trial has been started on patients suffering from liver metastases of colorectal carcinoma. *In vitro* experiments and the first animal tests have also been initiated to investigate radiobiological effects of radiation generated during BNCT. For both experiments and the treatment, a reliable dosimetry system is necessary. From work elsewhere, the use of alanine detectors appears to be an appropriate dosimetry technique.

Introduction

Every second patient, suffering from colorectal carcinoma, gets metastasis in the liver. For half of them the liver is the only organ where metastases occur. Therapy, such as resection, conventional radiotherapy or local ablation, is only available in 25 % of these cases (for 10% of the total number of patients), caused by the location and the number of the metastases [1]. Extended involvement of the liver by primary and secondary cancer is life limiting even if the tumour is confined to this organ. So far in this situation only palliative treatment using chemotherapy is applicable. For a large group of patients, who are not suitable for a curative therapy, BNCT could be a promising alternative.
In 2001 and 2003, at the TRIGA in Pavia (Italy), two patients with liver metastases were treated successfully by combining BNCT with auto-transplantation of the organ. This led to a BNCT project focussed on liver tumours to be applied at the TRIGA Mainz [2, 3]. The successful treatments in Pavia gave rise to the assumption that BNCT could be a beneficial option for a large number of patients suffering from primary and secondary cancer. Taking also into consideration the treatment options of hepatocellular carcinoma (HCC) and intrahepatic cholangiocarcinoma (CCC), about 12,000 patients per year in the European Union could profit from this kind of treatment. Therefore, at the University of Mainz, a multinational research consortium conducts research in BNCT to explore the possibilities of a curative treatment of the liver.
BNCT is a biologically-targeted form of radiotherapy, which uses the ability of the isotope ^{10}B to emit He-4 (alpha) particles and Li-7 recoil ions following the capture of thermal neutrons with a very high probability (cross-section: 3837 barn). The fragments produced in this reaction ($^{10}B(n,\alpha)^{7}Li$) have high linear energy transfer (LET) properties and a high relative biological effectiveness (RBE) relative to photon irradiation. The range of these particles in tissue is limited to 8 and 5 µm, respectively, thus confining the destructive effects to about one cell diameter. Therefore, if the ^{10}B can be selectively delivered to cancerous tissue, the short range of the high LET charged particles offers the potential for a targeted irradiation of individual tumour cells while the healthy liver parenchyma would be spared [4].
The critical prerequisite to achieve this effect is a sufficient concentration of ^{10}B inside the target cells. Such a concentration is achieved by a ^{10}B-carrier, which is administered to the patient, which shows a high uptake rate in the specifically targeted cells. The uptake of the tumour cells has to be higher (≥3) compared to the uptake in the surrounding healthy tissue, which causes the dose to the tumour to be much higher than the dose to the healthy tissue. Only in such a case, a lethal damage is inflicted to the tumour while the healthy tissue remains intact. For this task, the boron compound, 4-borono-phenylalanine (BPA), is a suitable choice.

Clinical Study to determine the boron uptake

For successful treatment, it is necessary to identify the kind of tissue or cells, where the ionised radiation is generated. Furthermore, knowledge of the differences of the boron concentration in cancerous and healthy tissue is required to calculate the correct dose released by ionising radiation in the different tissues. Work is currently in progress on a pharmacokinetic study with 15 patients at the Department of Transplantation Surgery of the University of Mainz, to investigate the uptake of the boron carrier under conditions identical to the proposed therapeutic situation in prospective patients [5].
During surgery, blood and tissue samples of the tumour and the tumour free liver are taken to assess the pharmacokinetic behaviour of the BPA. Blood samples are measured with prompt gamma ray analysis (PGAA) and quantitative neutron capture radiography (QNCR). PGAA measurements have been performed at the HFR in Petten, The Netherlands [6] and at the FRM II in Munich, Germany [7]. Figure 1 shows the results of the blood samples for the first four patients in the preclinical trial for both facilities [8].

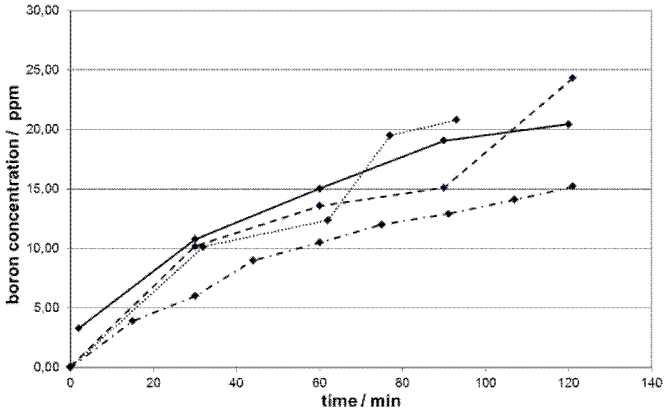

Fig. 1. Pharmacokinetic curves for Patient 1 (dashed); Patient 2 (dotted); Patient 3 (solid); Patient 4 (dashed-dotted)

While PGAA is a spectroscopic method that cannot perform a local selective analysis, radiography is a method to visualize the distribution of particular isotopes by image analysis. This can be done qualitatively and quantitatively using adequate standard reference materials. These images are obtained from the irradiation of a particular solid state detector, more specifically, a polyallyl-diglycol-carbonate polymer film (TASTRAK, CR-39), which is sensitive only to charged particle radiation. On such films, cryo-sections are mounted from cut samples. Upon irradiation, the fragments produced during the $^{10}B(n,\alpha)^{7}Li$ reaction leave so called “latent tracks” on the surface of the films, which are made visible by etching. Hence, a precise image of the concentration distribution inside the tissue slices is created. With this method it is possible to determine the boron concentration on the millimetre scale. This has a greater advantage compared to other methods in BNCT, which very often perform bulk-analysis of tissue samples, where local information is inevitably lost.
Tissue samples obtained from tumour-free tissue were also measured with PGAA, as to confirm the results of the QNCR analysis. Tumour samples were excluded, as with PGAA, it is not possible to determine the spatial distribution within the analysed sample, which was crucial for the analysis. Tumour-free liver tissue provides eligible sample material, as it is very homogeneous in its cellular structure and composition. The analysis of the same samples with all three methods showed a good correlation, especially for the measurements with PGAA (Fig.2).

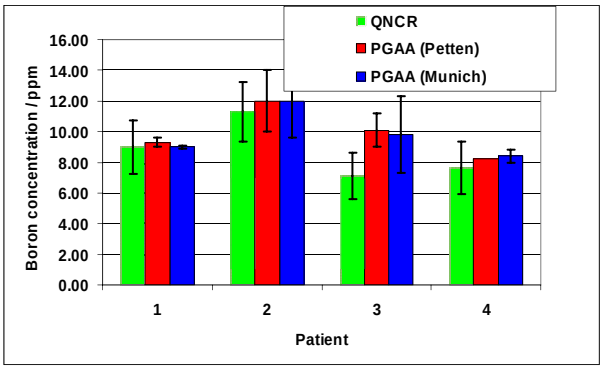

Fig 2: Results from the tumour-free tissue samples of the first four patients (ppm ^{10}B), samples measured in Petten, Munich and Mainz.

The regions of cells in tumour and tumour-free tissue were analysed by QNCR and in parallel characterised by the pathologist to be able to deduce a cell-type dependence of the boron enrichment. The data vary greatly between the different types of cells. As expected, the uptake is highest in metabolic active tumour tissue (20 to 34 ppm) and lowest in necrotic tissue (4 to 7 ppm), compared to an uptake of 7 – 11 ppm in tumour-free liver tissue.

Neutron irradiation of cell cultures

Currently, at the thermal column of TRIGA Mainz, experiments with human hepatoma cell lines are carried out to expand the research on the treatment of liver cancer in the BNCT project. To estimate an organism's or complex organ's reaction of a therapeutic radiology, either animal or alternative cell experiments are required. For both experiments, the thermal column is an excellent facility, and a standard protocol for further trials has been created.
In particular, results of experiments with human liver cells correlate more with results of human *in vivo* analyses than with animal experiments. For this purpose, the cell line Huh7 was selected, which stems from a well-differentiated hepato-cellular carcinoma. The cell culture media were treated with p-borono-phenylalanine enriched with *99% ^{10}B* before the cells were irradiated in the thermal column. The aim of the cell experiment was to calculate the survival of cells depending on different doses, incubation times and boron concentration. The survival curves allowed the determination of a relative biological effectiveness (RBE) specific to the liver, which is an important parameter to evaluate later for the radiotherapy. So far, the experimental findings prove qualitatively the ability to deprive HuH7 cells of their proliferation abilities. To derive RBE values from our data, a more precise follow-up study will be required to collect more data for the creation of a cell survival calculation model.
Additionally, the first experiments were carried out to prove the selective enhancement of the BPA uptake into the same cells by stimulation of the metabolic pathways by preloading of the cells by supposedly, metabolically-similar acting structural analogues. For that purpose, L-DOPA and L-tyrosine were chosen. As a result, a significant enhancement of the BPA-uptake in HuH7 cells by preloading with L-DOPA or L-Tyrosine was achieved. Nevertheless further experiments with longer incubation times will be carried out to improve the results and animal tests are in preparation.

Dosimetry in mixed neutron and gamma fields

During treatment of the liver, the irradiation will need to be performed outside of the body, as otherwise there would be relevant tissue damage inflicted to the surrounding organs and tissues by neutron and gamma radiation from the radiation source. The organ was therefore explanted, after infusion of BPA in the operating theatre, and then irradiated in a suitable facility, such as the thermal column of a research reactor. Monte Carlo simulations have demonstrated the potential for an effective BNCT treatment for extracorporeal livers irradiated in the modified thermal column. Simulation of the gamma dose has shown the necessity to shield the organ from all sides, due to the secondary gamma photons induced within the graphite of the thermal column, which contribute considerably to the total gamma dose [9].
To monitor the mixed neutron and gamma field in the thermal column, an alanine detector system was established and tested [10]. The alanine pellets had a diameter of 5 mm and a thickness of 2 mm, consisting of 90% finely-grained, crystalline alanine powder. Irradiation of alanine forms the stable radical CH3–C·H–COOH. Using an electron spin resonance (ESR) reader, the radical electron at the carbon atom can be detected. The value of the ESR signal correlates to the amount of absorbed dose.
The dose in each pellet correlates to an equivalent gamma dose by a factor called relative effectiveness (RE). To determine the RE values and to predict the dose for each pellet, the Hansen & Olsen alanine detector response model is used together with FLUKA, a multipurpose transport Monte Carlo code, able to treat particle interactions up to 10,000 TeV. The only information needed for the calculations is the neutron and gamma spectrum for the TRIGA Mainz and the description of the thermal column.
Figure 2 a) and b) shows the results of the dose measurements in a phantom and a resected liver in the thermal column and the connected simulations with the two codes. The RE value was determined to be 0.83 ± 0.07. The presented data are preliminary and calculations are still being improved.

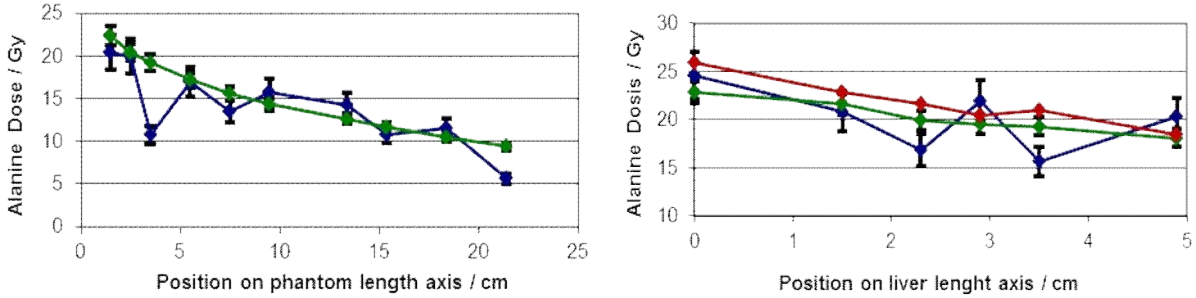

Fig. 2. First results of the dose measurements (green) and simulations (MCNP – red, FLUKA – blue) (a) position for a phantom along the phantom length axis and (b) along the liver length axis

Conclusion

The BNCT project at the University of Mainz is focussed on the treatment of liver tumours. The thermal column of the TRIGA Mainz is an excellent facility to conduct *in vitro* experiments, and a standard protocol for further trials has been created. In particular, a preliminary clinical trial is conducted to explore BPA pharmacokinetics and boron concentration behaviour in patients suffering from liver metastases. So far, the results from the first four patients have been achieved. The study will continue with changes in some study parameters and will be extended to hepatocellular carcinoma (HCC) and intrahepatic cholangiocarcinoma (CCC). From measurements taken at the PGAA facilities at Petten and Munich, it was possible to obtain the pharmacokinetic curves for the blood concentrations. The results from each facility for both blood and tissue samples show a good agreement and also a good correlation between the surgical procedure and the boron concentration in the blood. With the QNCR it could be demonstrated that the BPA uptake into cells depends on the cell type. In-vitro experiments together with preloading with either L-tyrosine or L-DOPA can enhance the BPA-uptake in HuH-7 cells. To understand this mechanism, more knowledge and research on the molecular biological processes is necessary.
Alanine pellets are able to measure the dose values in the mixed neutron and gamma field in the thermal column. The application of the FLUKA and MCNP codes allows the simulation of neutron fluences and absorbed doses for these pellets. With further investigations, it will be possible to develop a reliable dosimetry monitoring system for a liver treatment and *in vitro* experiments at the TRIGA Mainz. To increase the sensitivity of the alanine to thermal neutrons, the alanine in the detectors shall be modified with boron to give a higher thermal neutron dose in the pellet, which would lead to even more detailed dosimetry results.

References

[1] Kemeny N., Fata F., 1999. J. Hepatobiliary Pancreat. Surg. 1, 39-49.
[2] T. Pinelli T. et al., In: M.W. Sauerwein, et al. editors. International Proceedings Division 2002, 1065-1072.
[3] G. Hampel, et al., RRFM conference, Marrakesh, Morocco, March, 2010.
[4] Current status of neutron capture therapy, *IAEA-TECDOC-1223,* International Atomic Energy Agency IAEA, Wien, 2001
[5] C. Schütz, et al., NEUDOS-11, Cape Town, South Africa, October, 2010.
[6] C.P.J. Raaijmakers et al., Acta Onco 34, 1995, 517-523.
[7] P. Kudejova et al., J Radio Nuc Chem 278, 2008, 691-695.
[8] T. Schmitz et al., App Radiat Isot, accepted.
[9] G. Hampel et al., App Radiat Isot, 67, 2009, 238-241.

[10] T. Schmitz et al., Acta Onco 49, 2010, 1165-1169.

R&D on Control Rod Magnetic Suspension

Drive Mechanism of CARR

Wu Xinxin, Yan Huijie

Institute of Nuclear Energy Technology, Tsinghua University

Neng Ke Lou (INET) Tsinghua University,100084 Beijing-China

ABSTRACT

This paper deal with the research and develop(R&D) on Control Rod Magnetic Suspension Drive Mechanism(MSDM) of CARR. The MSDM is made up of tube, coil, armature, step motor, lead screw etc. . The MSDM use electromagnetics as its main principle. The open solenoid electromagnet technique is employed to implement suspension function. It has advantages of high drive precision, high safety feature, good running reliability, easy maintenance and good economical property. The R&D process of MSDM has three phases including single coil electromagnet, principle prototype and engineering prototype.

Key words: Control rod; Magnetic Suspension; Drive Mechanism; single coil electromagnet; principle prototype; engineering prototype

1 Introduction

The China Advanced Research Reactor (CARR), composed of reactors, auxiliary systems and testing facilities, is a safe, reliable and multifunctional research reactor with high performance. The CARR is a large-scale nuclear science project providing an important testing platform for nuclear science and research of China. The Control Rods Magnetic Suspension Drive Mechanism (MSDM) of CARR is researched and developed independently by the Institute of Nuclear Energy Technology (INET) of Tsinghua University in China. The MSDM is a new type of electromagnetic apparatus, as well as is a completely new scheme for reactor control rod drive, in China. This paper presents MSDM's system composition, operating principle, R&D processes and the main features.

2 System Composition[1]

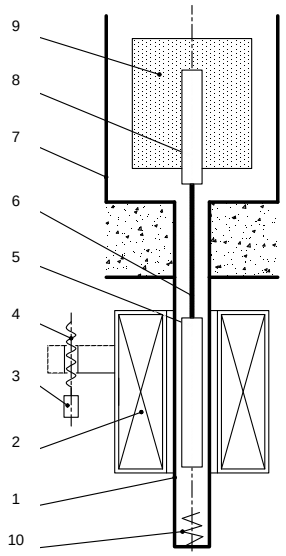

Fig 1. MSDM principle sketch

1-tube; 2-coil; 3-step motor; 4-lead screw; 5-armature; 6-linkage; 7-shell; 8-control rod; 9-in-core; 10-buffer.

The MSDM system mainly is made up of ten parts, shown in the principal sketch (Fig 1). The tube(1) guarantees the reactor's pressure border integrity. The armature(5) and linkage(6) are in the tube. The linkage is used to connect armature and control rod(8).

The coil(2), step motor(3) and lead screw(4) are outside the tube. The lead screw is connected to the coil, and they are driven by the step motor.

At the bottom of tube, a buffer(10) is set to protect the control rod when it shuts down.

3 Operating Principle[1]

The Control Rods Magnetic Suspension Drive Mechanism is designed mainly based on the electromagnetic principle. The key technique is the Open Solenoid Electromagnet technique, which is used to implement suspension function.

The MSDM's operating principle is as following:

Firstly, the coil(2) which is outside of tube(1) is turned on by power supply, and the armature(5) which is inside of tube will be pulled together with coil by electromagnetism. In the other words, the armature is suspended by the electromagnetism. When the coil is moving, the armature will move with it, which drives the movement of the reactor control rod(8).

Then the step motor(3) is powered on, and it rotates the lead screw(4). The coil is thus able to move up and down along the lead screw. The MSDM implements the function of reactor control in this way.

When the coil or step motor power is shut off, the control rod will drop to in-core(9) by gravity in case of emergency.

4 MSDM R&D Processes

R&D process on the MSDM includes three phases. In order to understand the performance of the Open Solenoid Electromagnet, the single coil electromagnet was studied firstly; the principle prototype was then designed for the purpose of dealing with some unsolved problems in the single coil electromagnet study such as overall structure practicability, space limitation, drive element selection etc.; as well as some predicted problems that must be considered in the engineering prototype design such as the static property and dynamic property. The property experiment on principle prototype was carried out. Thirdly, the engineering prototype was designed and manufactured. The test for the control rod drive line performance, full-life and anti-seismic were accomplished.

4.1 Study on Single Coil Electromagnet [2]

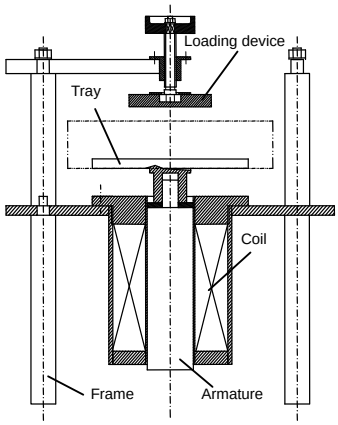

Fig 2. Single Coil Electromagnet

Finite Element Analysis (FEA) is employed to study the open solenoid electromagnet technique. In order to make sure the functional performance of the open solenoid electromagnet, we designed and fabricated the single coil electromagnet as shown in Fig 2. Series tests, such as rigidity experiment, carrying capacity experiment, turn off response experiment and temperature experiment etc. were carried out.

The results of the single coil electromagnet experiment indicate that:

- The equilibrium temperature of the coil which is air-cooled is about 65 Centigrade when the current of coil is 1.5A.
- The maximum carrying capacity is larger than 100kg.
- The single coil electromagnet has good shut off response ability. The time between coil power off to control rod begin drop is about 0.047s.
- The rigidity of electromagnet is about 100N/mm.

4.2 Principle Prototype Study[3,4]

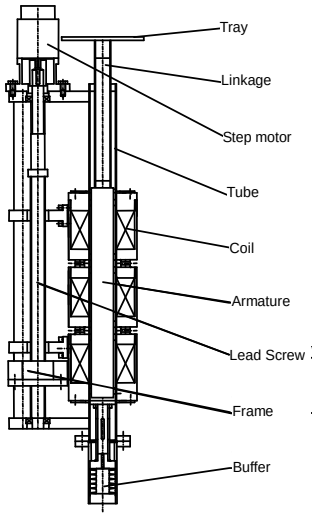

Fig 3. Sketch for the principle prototype

Fig 4. Principle prototype test-bed

After the single coil electromagnet study, with the consideration of overall structure practicability, space limitation, drive element selection etc., we designed the principle prototype which combined three single coil electromagnets together and include tray, linkage, step motor, tube, armature, lead screw, frame, buffer etc. as shown in Fig 3. The distance of run is 200mm.

A test-bed was built as shown in Fig 4 after the principle prototype machining is ready. In the test-bed the static property experiment and dynamic property experiment were carried out regarding on some predictable problems in engineering prototype design.

The results are as follow:

- The carrying capacity is linear with the coil electric current. The maximum carrying capacity meets the demand of design which shall be not less than 300kg.
- The rigidity, which varies with load and current, has an optimum value.
- The electromagnet coil has a good heat radiation property.
- The drive system runs smoothly and do not have significant vibration; steady transform can be achieved under all kind of work conditions.
- The location precision and dynamic carrying capacity meet the demand of

design.

- Armature displacement needs offset when it is measured indirectly, and the offset value is related with load and electric coil current.

4.3 Engineering Prototype Study

The structure of coil and machine are improved regarding to the problem which appeared in the principal prototype study. Moreover, several engineering factors were taken into account, such as the motor and the rod overtravel-limit switch, rod position indicator, refuelling device, inservice inspection etc.. The engineering prototype in accordance with the ratio of 1:1 was then developed, shown in Fig 5-A. Its distance of run is 920mm.

A test system was built up. Fig 5-B shows the testing frame and testing loop. The following tests were carried out: MSDM's performance, drive line performance, 2000 times normal running, 2000 times shut off. The shut off time is less than 1.0s; the rod kinematic accuracy can be controlled less than 0.1mm; and the other qualifications such as carrying capacity, shut off response ability, coil temperature, operating property etc. completely meet the expectance.

After the drive line performance and life testing experiments, anti-seismic test were employed. Fig 5-C shows the seismic test frame. The control rod was shut off before/during/after the seismic events, which included 5 Operating Basis Earthquake (OBE) and 1 Safe Shutdown Earthquake (SSE). All shut off times met the requirement, and all system parts kept the structural integrity.

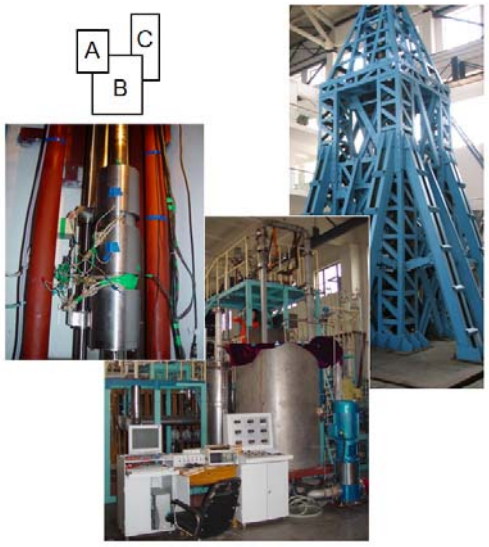

Fig 5. Test photo

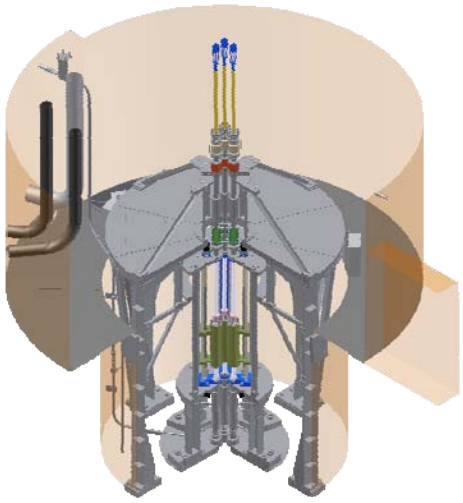

Fig 6. Engineering plan in CARR

Based on the results of the tests, we designed the engineering plan for the CARR project. Fig 6 indicates the MSDM arrangement design in CARR, and the Fig 7 is final appearance of the MSDM.

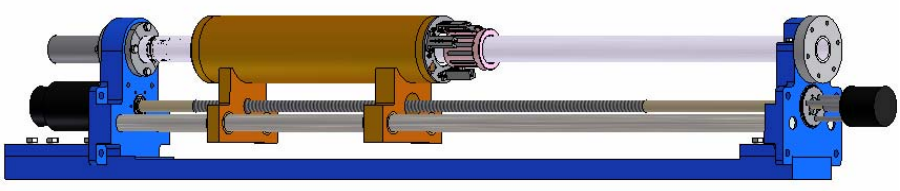

Fig 7. Engineering design photo

The installation of MSDM in CARR has been completed and CARR has reached critical in May 2010. The operation of MSDM has shown good safety and functional performance.

5 Main Features of MSDM

The MSDM's main features are as follow:

- Continuously movement rather than step movement was achieved using lead screw, pinpoint controlled by step motor. The rod kinematic accuracy is lower than 0.1mm.
- The drive system runs smoothly and do not have significant vibration, steady transform can be achieved under all work conditions.
- Good shut off response ability; the time between coil power off and control rod begin to drop is 0.047s.
- The electromagnet coil has a good heat radiation property. When coils total current is 4.5A, the coil temperature was about 65 Centigrade.
- The system has advantages of low current and large carrying capacity with the maximum capacity larger than 300kg.
- There is no mechanism inside the boundary of reactor main loop. The structure of the driving chain is simple and is able to operate safely and reliably.
- All mechanism are located outside the boundary of reactor main loop, and use normal drive equipment and material; so it is easy to maintain, and has good economy.
- The shut off time is less than 1.0s.

6 Conclusions

Because the MSDM has the superiority of high drive precision, high safety, good operating reliability, easy maintenance and economical property, the CARR choose it as its control rod drive mechanism. Moreover, the MSDM can be applied in not only pool reactor but also shell reactor. It can drive from top to bottom or vice versa. Therefore we believe MSDM can contribute to more reactors.

References:

[1] WU Yuanqiang,WANG Minzhi, Mobilizable coil electromagnet drive for reactor control rod[J].J Tsinghua University,2000,40(S3):299-302.(in Chinese)

[2] ZHANG Jige,WU Yuanqiang, Experimental study on property of a new electromagnet drive for reactor control rod[J].Nuclear Power Engineering, 2001.22(4):365-369.(in Chinese)

[3] ZHANG Jige, WANG Xiaoguang, WU Yuanqiang, ZHANG Zhengming, Experiment Monitoring System of a New Electromagnet Drive for Nuclear Reactor Control Rod[J]. Atomic Energy Science and Technology, 2003.37(5):438-441. (in Chinese)

[4] ZHANG Jige, WU Yuanqiang, SHENG Xuanyu, ZHANG Zhengming, Experiment Study on Dynamic Property of a New Electromagnet Drive for Reactor Control Rod[J]. Chinese Journal of Nuclear Science and Engineering, 2003.23(2):123-126. (in Chinese)

APPROXIMATION OF FAST REACTOR SPECTRA AT THE JHR

T. STUMMER
Institute of Atomic and Subatomic Physics, Vienna University of Technology
Stadionallee 2, 1020 Wien - Austria

M. Blanc, B. Pouchin
CEA, DEN, DER, SRJH
Cadarache, F-13108 Saint-Paul-lez-Durance - France

ABSTRACT

Due to the limited availability of fast reactors, some experiments supporting fast reactor development have to be conducted in MTRs whenever possible. At the Jules Horowitz Reactor, currently under construction in Cadarache, studies are underway to determine the range of possibilities at this reactor for basic neutron cross section, material and fuel behaviour experiments before ASTRID, the presently studied fast reactor prototype, becomes operational. One of the examined options is to aim for a similar neutron physics environment by hardening the neutron spectrum with Cd and Hf shields. Because reactor is designed to be strongly under moderated with a fast flux of 5.5 10^{14} n/cm²/s in core, the neutron flux conditions come reasonably close to low power density fast reactors as long as the thermal part of the spectrum can be excluded. This paper presents calculations for adjusting the neutron spectrum in the JHR with neutron shields and compares it to a SFR core spectrum. The examined irradiation positions are located in the reflector close to the core, in the central tube into a fuel element and as a replacement of a fuel element. An estimation of the effect on the neutron economy of the reactor is also given.

Introduction

There are currently several fast reactor/ADS projects in various stages of planning in Europe but, because of the limited availability of operational ones worldwide, some supporting fuel research has to be done in MTRs whenever possible. In order to estimate the possibilities at the Jules Horowitz Reactor [2] several proposals for neutron physics and fuel behaviour studies are currently investigated at CEA Cadarache. While for some experiments like power ramping the neutron spectrum is of secondary concern, others like a fuel pin irradiation test require an environment, which is as close as possible to the real case. In the following test cases for approaching a fast reactor spectrum with the help of neutron shields in the JHR are presented together with their expected reactivity costs.

Concept and Geometry

According to the current plans (fig 1), there will be seven fuel elements with a central irradiation channel with a diameter of 4 cm and three irradiation positions replacing a fuel element with a diameter of 9.6 cm in the JHR core. For this study a pre-existing device, CALIPSO [4], was adapted with neutron shields consisting out of 1 mm Cd and 2 mm Hf to give an estimate for the resulting neutron spectrum and the reactivity costs on reactor operation. CALIPSO has a NaK cooling loop for high temperature / high power fuel pin experiments and provides room for a sample with a diameter of 9.5 mm at outer device diameter (in core) of 33.1 mm. Due to the low melting temperature of Cd, the Cd shield has to be outside of the device and the investigated location is inside the device's water cooling tube (between the fuel element and the CALIPSO device). For the calculations four positions

were chosen: two near the centre of the core (101 and 103), one in the outer fuel element ring (313) and one in the reflector close to the core (C313) as a low reactivity cost fall back option. The position 103 was included in case the available space (about 4 mm shield thickness) in the centre of a fuel element would prove insufficient for the needed shield thickness and cooling.

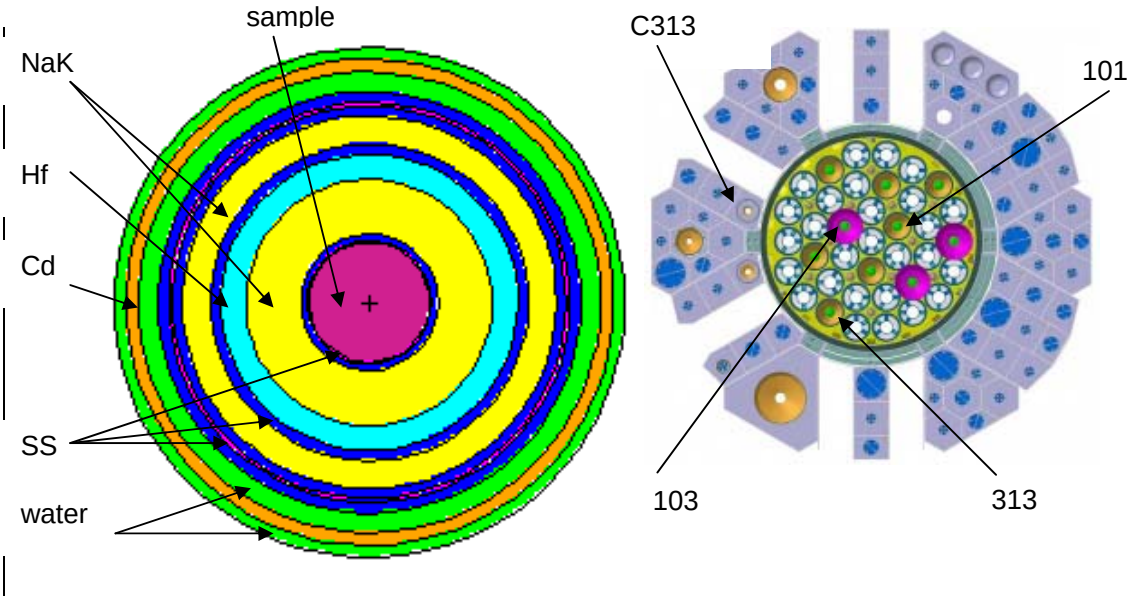

Fig 1: Assumed irradiation positions and device cross section

Methodology

All the JHR calculations were done with TRIPOLI-4 [2] using the JEF2.2 library because this is the reference model for the CEA JHR core calculations. The reactivity effects and overall flux distribution were calculated with the full core model for the cases with 1 mm Cd + 2 mm Hf as neutron shields and without shielding. For further variation of the shield thickness, the core flux distribution was assumed as constant and a smaller model of the device itself was used. As a reference sample serves a 9.43 mm thick $(UPu)O_{1.97}$ rod with a density of 11 g/cm^3 and the following isotopic composition:

	238Pu	239Pu	240Pu	241Pu	242Pu	241Am	235U	238U
at%	0.62	8.25	5.16	1.43	1.81	0.14	0.21	82.39

Tab 1: sample actinide composition

The basis for SFR reference case was calculated by V. Brun-Magaud and L Buiron [1] with ERANOS. The average total core flux is given as 2.5×10^{15} n/s/cm² and the spectrum is shown in fig 2 and 3.

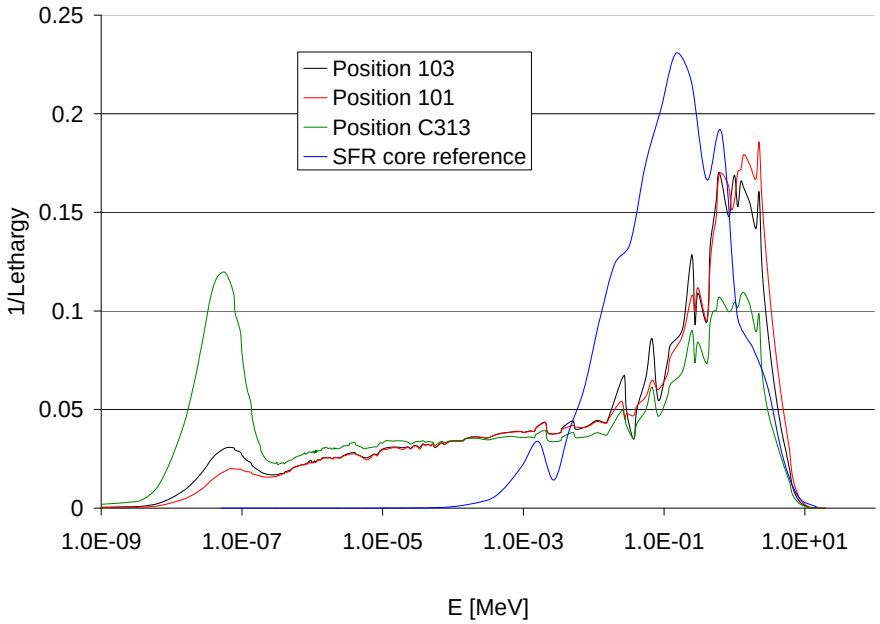

Fig 2: Neutron spectra used in the calculations

Results

As seen in figure 2 above the fuel element (27% enriched U_3Si_2) in position 101 acts as thermal neutron shield for the device, increases the fast flux and reduces the reactivity cost for the reactor (table 3). Additionally because there are 7 possible in-fuel element positions versus 3 fuel element replacements available, such a setup would be preferable if the experiment is to be placed inside the core. The resulting spectra inside a 1 mm Cd + 2 mm Hf shield in figure 3 show a strong equalizing effect between the positions in the thermal an low epithermal energy range, so the criterions for the position selection will most likely be the achievable neutron flux and the reactivity cost.

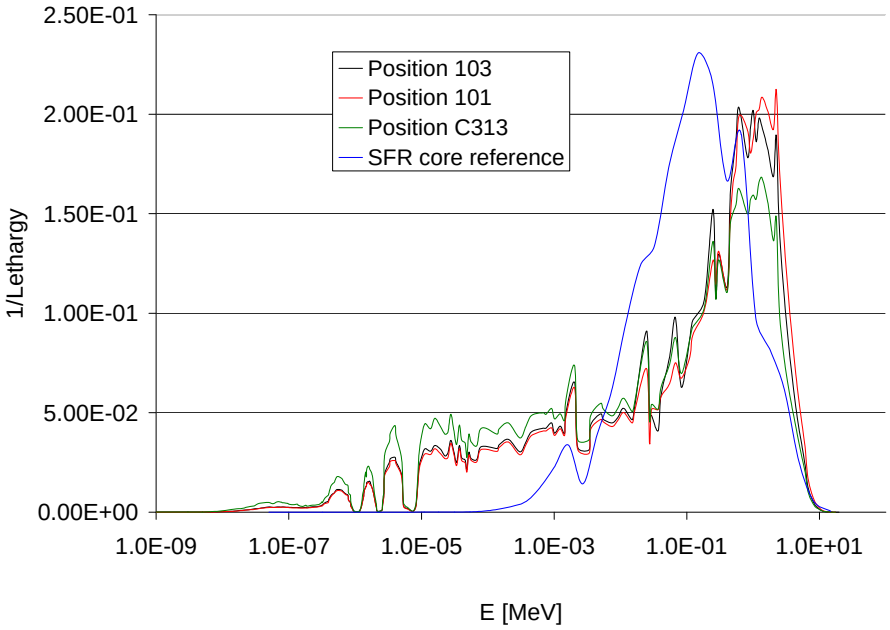

Fig 3: Resulting neutron spectra inside 1 mm Cd and 2 mm Hf shields.

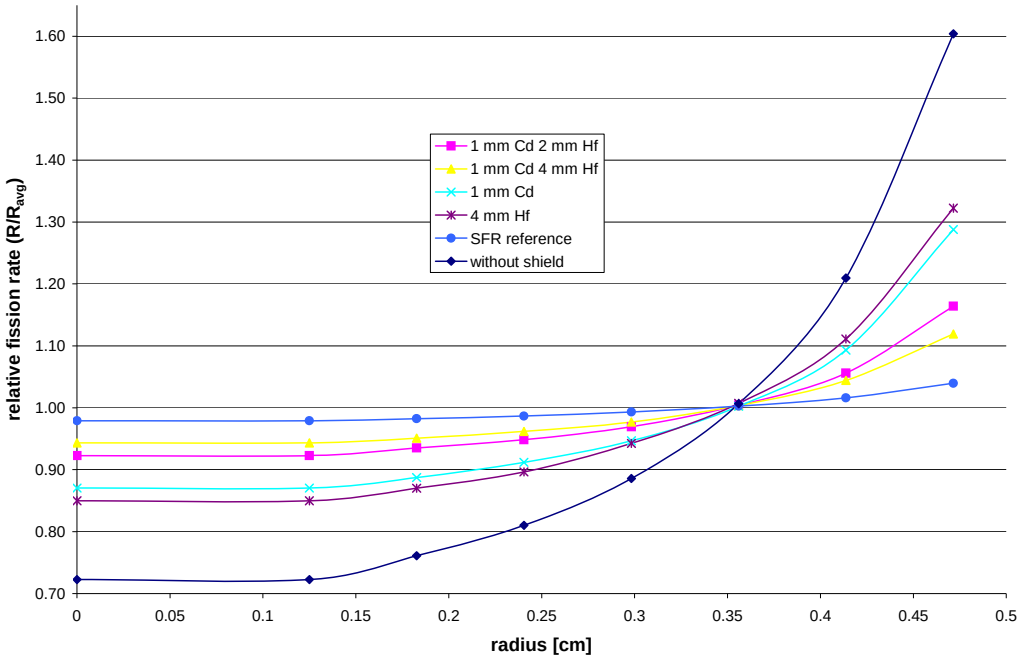

Fig 4: radial power distribution in sample.

One of the key problems of utilising MTRs for FR fuel research is generating a similar power profile in the fuel sample due to the strong self shielding effects in the thermal and low epithermal energy ranges. With shielding the problem can be mitigated but not fully resolved as figure 4 above shows. The acceptable deviation from the SFR case will determine the neutron shield needed and in turn strongly depend on the planned duration of the experiment.

	101	103	313	C313
Δk_{eff} [pcm]	-1450	-1580	-550	-150
total flux [n/s/cm²]	5.48E+14	5.44E+14	3.36E+14	8.84E+13

Table 2: reactivity cost of full core height shielding depending on position.

The negative reactivity value of an experimental device with full core length neutron shields is unsurprisingly close to a fully inserted control rod. For comparison a day of operation costs between 200 and 300 pcm of reactivity with 25-26 efpd between scheduled refuelling and the total average core flux of the SFR is given as 2.5×10^{15} n/s/cm². Depending on the experimental requirements the effect on the core can be reduced by either reducing the height of the shield or by shifting the experiment towards the rim of the core. Because of a much smaller reactivity drop, the later option is particular attractive as long as the maximum JHR neutron flux is not strongly needed.

	< 0.625E-6 MeV	0.625E-6-0.9 MeV	> 0.9 MeV	Fast/thermal ratio
No shielding	1.14E+14	4.96E+14	2.03E+14	1.78
1 mm Cd	8.10E+12	5.84E+14	8.91E+13	11.00
4 mm Hf	5.74E+12	4.40E+14	8.25E+13	14.36
1 mm Cd 2 mm Hf	1.98E+12	4.63E+14	8.36E+13	42.25
1 mm Cd 4 mm Hf	9.28E+11	4.32E+14	7.78E+13	83.83

Table 3: fast/thermal ratio for position 101 depending on shielding.

Conclusions

This preliminary study was primarily intended as a starting point for more detailed work. So far the results indicate that the remaining difference in the radial power distribution between SFR reference case and the heavily shielded JHR cases can be attributed to differences in the low epithermal neutron spectrum. Unfortunately reducing it further would require more volume, which restricts the available experimental positions inside the core. Additionally, although this study used Cd as a baseline option for its excellent thermal neutron shielding capabilities, Cd is unlikely to be used in an actual device inside the reactor core. Because Cd has very low melting point, it is problematic inside a core with a high power density like JHR and should be replaced with either a thicker Hf or an Europia shield.
The primary objectives for the follow up neutronic study are to replace the Cd shield and to estimate the effect of the different radial power profile on the radial burn up. A fuel element experiment would likely last up to two reactor years (400 efpd) and the later effect could set the minimum necessary shield thickness.

References

1. L. Buiron et al., “Minor actinides transmutation in SFR depleted uranium radial blanket, neutronic and thermal hydraulic evaluation”, *Proceedings GLOBAL 2007,* Boise, Idaho USA, September 9-13 2007.
2. G. Bignan et al., “The Jules Horowitz Reactor: A new European MTR (Material Testing Reactor) open to International collaboration: Description and Status “, *Proceedings RRFM 2009*, Rome , Italy, March 20-24 2011.
3. O. Petit et al., “TRIPOLI-4 User’s Guide”, ISSN 0429-3460, January 2008.
4. D. Moulin et al., “Thermal assessment of the CALIPSO irradiation device for the Jules Horowitz reactor”, *Proceedings IGORR 2010*, Knoxville, TN, USA, September 19-23 2010.

THE DESIGN OF A PROMPT GAMMA NEUTRON ACTIVATION ANALYSIS BEAM FOR BNCT PURPOSE AT THE TRIGA MARK II REACTOR IN PAVIA

S.STELLA[1,2], A.BAZANI[1,2], F.BALLARINI[1,2], S.BORTOLUSSI[1,2], P.BRUSCHI[1], N.PROTTI[1,2], and S.ALTIERI[1,2]

[1]*Department of Nuclear and Theoretical Physics, University of Pavia, Italy*
[2]*Istituto Nazionale di Fisica Nucleare (INFN), Section of Pavia, Italy*

ABSTRACT

In preclinical and clinical Boron Neutron Capture Therapy studies the knowledge of the amount of ^{10}B in blood and tissues is very important. The boron concentration measurements method used in Pavia (Italy) is based on the charged particles spectrometry of thin tissue cuts irradiated in the Thermal Column of the TRIGA reactor of the University. In order to perform measurements in biological liquids such as blood and urine, or in other tissue that cannot be cut in slices, a Prompt Gamma Neutron Activation Analysis (PGNAA) [1] facility is being designed, which measures ^{10}B concentration detecting the prompt gamma from boron nuclear capture reaction.
At the TRIGA reactor in Pavia, there are four horizontal channels, potentially available for PGNAA. The choice of the suitable channel, and the design of its configuration, were achieved using the Monte Carlo neutron transport code MCNP4c2. To perform the simulations, an input code already validated, describing the reactor structure and the neutron source, was used. The calculations were implemented applying non-analog techniques for the neutron transport, that are necessary to obtain a sufficient statistic in every positions along the channel and especially at its end.
The selection of the channel for PGNAA installation was carried out by comparing the simulated fluxes obtained in the different channels at the present configuration. The channel shielded by the core reflector was chosen, because the graphite lowers the fast component of the neutrons, with no need to insert additional material in the facility. The thermal flux at its end is 1.7 $x10^8$ n/cm^2 s with thermal-to-total neutron flux ratio around 0.8.
Subsequently a bismuth block for gamma radiation shielding and blocks of single crystal sapphire as filter for fast neutron component were inserted in the channel. Other components of the facility that are under study are a collimator and the beam catcher.

1. Introduction

The knowledge of boron concentration in tumor and in healthy tissues is one of the most important issues to achieve an effective BNCT treatment [2]. Currently, in Pavia, a well established quantitative method is used, based on α spectroscopy. With this method it is possible to determine the boron concentration in different kinds of tissue. However, due to the fact that the samples are under vacuum during the measurement process, this method cannot be exploited for liquid samples. In order to perform measurements in biological liquids such as blood and urine, a Prompt Gamma Neutron Activation Analysis (PGNAA) facility is being designed at the TRIGA Mark II reactor of the University of Pavia. This technique allows to analyze every element (except 4He) detecting the γ radiation emitted after a neutron capture reaction. There are two types of γ radiations following a neutron capture reaction: the prompt and the delayed γ characteristic of a particular element. The γ prompt is related to the binding energy released by the nucleus as soon as the reaction occurs (typically 6-9 MeV), while the second takes place only if the product nuclide is radioactive (with energies up to 2-3 MeV). PGNAA exploits mainly the prompt γ radiation for elemental analysis. The neutron capture reaction in ^{10}B produces an α particle and a ^{7}Li ion. With a probability of 94%, the Li ion is produced in an excited state, and it decays by emission of a 478 keV γ ray.

A Germanium detector is used to collect these γ rays and from the obtained spectrum it is possible to calculate the boron concentration present in the sample.
The main requirement of a PGNAA facility is the availability of a thermal neutron flux of about 10^7 n/cm^2 s at the irradiation position, with a low gamma background. In this conditions, boron measurements with a resolution suitable for BNCT can be performed.
In this work the results of the filtering of the neutron beam performed by Monte Carlo simulation are presented.

2. Material an Methods

The Applied Nuclear Energy Laboratory (LENA) in Pavia is equipped with a TRIGA MARK II research reactor. This reactor operates at a maximum power of 250 kW. It is provided of 4 lateral channels; two of them, named A and B, are radial beam ports that stop at the outer edge of the graphite reflector. Another channel named C is tangent to the outer edge of the core and a fourth, D, is a radial piercing beam port that crosses the graphite reflector and stops in front of the core. Among these channels, the most suitable to install the prompt gamma facility is B. The graphite reflector thermalizes neutrons, in a way that the epithermal and fast components are lower if compared to the others channels. Even if the total flux at the B beam port is lower than at the port of the other channels, a brighter and cleaner thermal neutron source is more suitable for a PGNAA facility.
In order to reduce the γ background coming from the core a bismuth shield was inserted in the channel, and calculations were performed to study the suitable thickness and position. Furthermore, to decrease the epithermal and fast neutron components of the neutron beam a sapphire filter was tested. All the simulations were performed using the Monte Carlo transport code MCNP4c2 [3].

2.1. Neutron flux simulations

To perform the simulations, an input code describing the complete reactor geometry and the neutron source, already validated with experimental measurements in the thermal column [4], was used. Non-analog techniques for the neutron transport were applied, in order to obtain reliable statistic in every position of the channel and especially at its end. First of all, a geometry splitting/Russian roulette was applied, by dividing the channel into cells and assigning the cells an importance increasing towards the end of the channel. In the other parts of the reactor the importance was set to zero; causing the neutrons that enter that cells to be automatically killed, thus reducing the computer time. Furthermore, a set of space-energy weight windows was assessed by a weight windows generator, in order to increase the efficiency of the calculation. The calculation of thermal neutron flux after a single-crystal sapphire filter, requires the thermal treatment for the specific materials, to take into account the effect of the crystal lattice on the thermal neutron transport. In fact, normally MCNP uses the approximation of free gas for all the materials of the geometry [5].

2.2. Gamma flux simulations

About the gamma simulation, some considerations about the source of γ radiation are necessary. The contribution of γ background come from: 1. prompt gamma coming from fission reactions, 2. gamma-rays coming from the fission products and 3. gamma-rays coming from the secondary interaction of neutrons with the materials (including the gamma ray coming form the inelastic scattering of the fast neutron).
The problem was approached by considering only prompt gamma radiation, i.e. ignoring the interaction of the neutrons. For this purpose a source of prompt gamma was implemented in the MCNP input file, shutting down the neutron source and the neutron transport.
The gamma source was obtained sampling the gamma rays from each fuel element, and using a decreasing exponential probability distribution function [6], ranging from 0.2 to 7.6 MeV[1].

[1] When the reactor operates at the maximum power of 250 kW, the intensity of the prompt gamma source is 5.4 x10^6 s^{-1}, since 7 gamma rays are emitted during a single fission and 0.76x10^6 fission per seconds occur.

This source was used to test the effect of a bismuth shield in a proper position inside the channel, whose function is to clean as much as possible the neutron beam irradiating the sample thus lowering the background that could spoil the measurement.
In the next section the results for the neutron and gamma flux simulations are presented.

3. Results and discussion

Different simulations were first performed to get the neutron energy spectrum at the end of the channel for several energy binning (Fig.1).

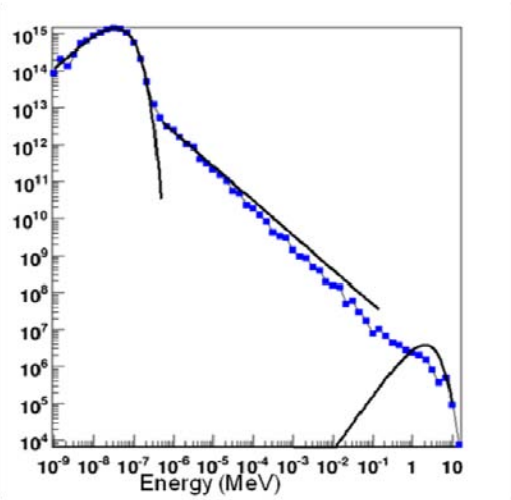

Fig 1. Neutron energy spectrum at the end of the channel without any filter

The typical features of a neutron beam from reactor can be recognized; a Maxwellian part in the thermal region (meV), an epithermal slowing-down region (eV) and fission fast component in the high energy region (MeV) $\Psi(E) = \Psi e^{-E} \sinh \sqrt{2E}$.
Energy lower than 0.2 eV was considered for the thermal neutrons, from 0.2 eV to 0.5 MeV for the epithermal component and from 0.5 MeV to 20 MeV for the fast one . Without any filter in the channel, the thermal flux is 1.07×10^8, the total flux is 1.35×10^8 , with a thermal-to-total neutron flux ratio around 0.8.
A poly-crystal bismuth filter, 7.7 cm radius, was than placed in the channel, 45 cm far from the external edge of the graphite in order to absorb the gamma radiation (Fig.2).

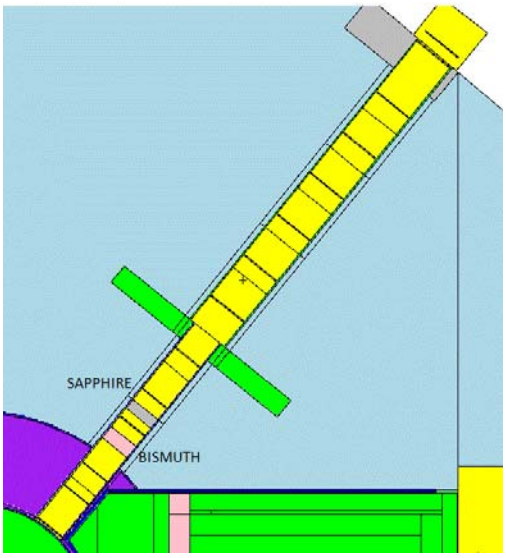

Fig 2. MCNP geometry for the channel B with the bismuth and sapphire filter inside.

Simulations were performed to study the γ attenuation due to the bismuth and the thermal neutron absorption as a function of the filter thickness. A flux tally was put in the middle of the channel.
Figure 3 shows the comparison of the gamma flux after a 5, 7 and 10 cm thickness of bismuth and with no filter. For γ energy < 1 MeV, the average attenuation coefficient is 0.015 for 5 cm, while 7 cm and 10 cm it is $\cong$ 0.008. For γ energy > 1 MeV the average attenuation coefficient decreases with increasing of thickness, taking the value 0.14, 0.07, 0.05 respectively for 5, 7, 10 cm.

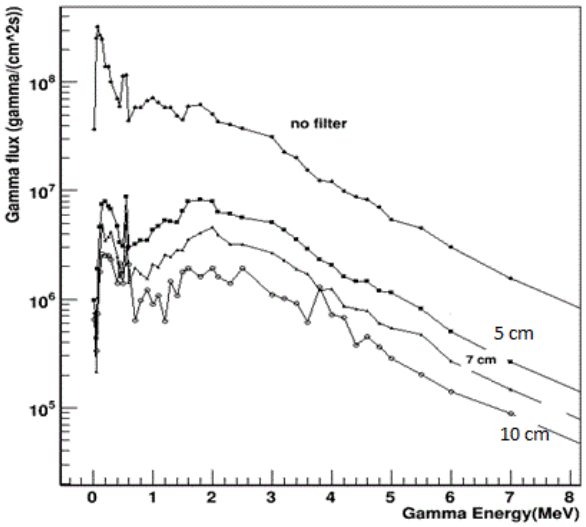

Fig 3. Comparison of the gamma spectra for different thickness of bismuth

The bismuth shield also affects the neutron beam. The attenuation factor (F) for the different beam component as a funcion of the bismuth thickness are showed in Table1.

	Thermal		**Epithermal**		**Fast**		**Total**
no filter	1.07E+8		2,26E+7		5.80E+6		1.35E+8
		F		F		F	
5 cm Bi	3.53E+7	0.33	6,72E+6	0.29	3.07E+6	0.53	4.51E+7
7 cm Bi	2.34E+7	0.22	4,27E+6	0.19	1.98E+6	0.34	2.82E+7
10 cm Bi	1.23E+7	0.11	2,20E+6	0.09	1.29E+6	0.22	1.58E+7

Tab 1: Attenuation factor (F) and neutron flux for the different thickness of bismuth block.

A 7 cm thick bismuth was chosen in order to obtain a good gamma radiation shielding without attenuating much the thermal neutron beam.

A single-crystal sapphire, 7.7 cm radius, was inserted 10 cm after the bismuth as a filter of fast neutron beam [7] (Fig.2). Two thickness were tested: 5cm and 10 cm. Table 2 shows the combined effect on neutron beam of the bismuth shield (7 cm thick) and the sapphire filter (5 cm thick).

	Thermal		**Epithermal**		**Fast**		**Total**
7cm Bi	2.34E+7		4.27E+6		1.98E+6		2.96E+7
		F		F		F	
7 cm Bi + 5 cm sapph	1.93E+7	0.83	9.65E+5	0.22	4.91E+5	0.25	2.07E+7

7cm Bi + 10 cm sapph	1.62E+7	0.71	3.53E+5	0.12	2.11E+5	0.11	1.67E+7

Tab 2:Attenuation factor (F) and neutron flux for sapphire and bismuth filter

The introduction of the sapphire filter 10 cm thick, determines the decrease of the unwanted neutron beam components of about one order of magnitude, without affecting the thermal neutrons. The choose of a even bigger thickness is an economic limitation. The effect of the sapphire filter on gamma radiation is also positive, allowing a further reduction of the background.

4. Conclusion and future work

The PGNAA facility will be installed in the B channel of the Triga Mark II reactor in Pavia.
The insertion in the beam tube of a 7 cm thick bismuth shield and a 10 cm thick single crystal sapphire, rapresent a good compromise between the reduction of the gamma background and the shaping of the neutron beam.
New simulations are under way for the design of a collimator that will allow a uniform neutron flux in the sample position, reducing, however, the thermal neutron flux depending on its shape and length.
This new set of simulations will also explore the possibility to replace the 7.7 cm radius sapphire with a tighter one, for practices and economic purposes.
The design of the beam catcher and the shielding of the Germanium detector are also in progress.

References

[1] G.L.Molnar “Handbook of Prompt Gamma Activation Analysis” Kluwer Academic Publisher (2004)
[2] R.F.Barth, J.A.Coderre, M.Graca H.Vicente and T.E. Blue, “Boron Neutron Capture Therapy of Cancer: Current Status and Future Prospects”, Clin.Cancer Res. 11(11), 3987-4002 (2005)
[3] “MCNP^{TM}- A General Monte Carlo N-Particle Transport Code”, Version 4C, Judith F. Briesmeister, Editor, LA-13709-M (2000)
[4] S.Bortolussi and S.Altieri “Thermal neutron irradiation field design for boron neutron capture therapy of human explanted liver”, Med. Phys. 34 (2007)
[5] F.Cantargi, F.Sanchez, J.R.Granada, R.E.Mayer, “Seccione eficaces de neutrones thermicos para un filtro de zafiro” , AATN congress "XXXVI Reunión Anual" (2009).
[6] Reactor Shielding Design Manual, 1965
[7] D.F.R. Mildner, G.P. Lamaze “Neutron Transmission of Single-Crystal Sapphire”, J . Appl. Crystallography 31, (1998) 835.

VIBRATION CHARACTERISTICS OF A PLATE TYPE FUEL ASSEMBLY

J.S.YIM, H.J.KIM, Y.W.TAHK, J.Y.OH, B.H.LEE
Nuclear Fuel Design for Research Reactor, KAERI
305-353 Daeduck Daero 1045, Yuseong-Ku, Taejon, KOREA

ABSTRACT

A flat fuel plate and a box type fuel assembly for a research reactor were modeled to be finite element meshes of the ANSYS to predict dynamic characteristics, such as natural frequencies and mode shapes. These characteristics provide the basic information about their vibrations. If the model is properly prepared, it can be used for further calculations of the dynamic behaviors under the SSE or even in the static stress calculation. With the FE Model, the natural frequencies and the mode shapes of a fuel plate and a FA were obtained in air and in water environments. The effects of fluid surrounding the fuel plate and the FA as well as the combs on the natural vibration of the FA are discussed.

1. Introduction

The dynamic analyses of a Fuel Plate (FP) and a Fuel Assembly (FA) are essential procedures in the design of nuclear fuel in order to avoid the resonance failure from coolant flow fluctuation caused by the pump blades passing frequencies. For the purpose of obtaining the dynamic behavior of a FP and a FA, they are modeled to be the Finite Element meshes of the ANSYS[1] and the natural frequencies and mode shapes were calculated. The calculation model will also be used in the analysis of FA integrity during the Safe Shutdown Earthquake (SSE). IF the dynamic model is pertinent, the subsequent calculation will result in reliable results. Thus it is necessary for the model of the FE dynamic calculation to be validated by tests using a dummy fuel plate and/or fuel assembly.
As the first step of the analysis, the designed fuel parameters can be used to model for the modal analysis to yield the natural frequencies and mode shapes. After determining such data, the dynamic characteristics as well as the model can be checked by comparing the test results for the validation of the model. After confirming the model, the model further can be used to calculate the dynamics behavior during the SSE. Since the mesh size and the nodal numbers of the model affect significantly on the calculation cost, the fine meshes of the fuel plate needs to be constructed in simplified equivalent meshes while preserving the same dynamic properties. By way of simplification, the calculation time can be reduced drastically. The natural frequencies and mode shapes of the FP were obtained with two boundary conditions, all edges were free and two lateral edges fixed. To investigate the fluid effect on the natural vibration of a fuel plate, the frequencies were obtained with varying fluid sizes. With the FE model of the FA, where all fuel plates were assembled, the natural frequencies and mode shapes of the FA were calculated. Since the FA was inserted in the fuel hole on the grid plate, fixed boundary condition with bottom end fitting was imposed. With the results of the FA natural vibration, the characteristics of dynamic behavior of the FA were discussed.
All the frequencies and mode shapes will be validated by experimental tests, scheduled to be performed in the future.

2. Calculation Model and Input

2.1 Description of the FA

The design of a fuel assembly (FA) for a research reactor is based on well-proven box-type

concepts. A plate type fuel which has been almost standardized one is adopted due to its high heat removal capability and successful uses in many research reactors. The U3Si2 dispersion fuel developed in connection with non-proliferation policy is chosen in the standpoint of well-proven performance.
The FA is composed of a fuel box assembly (FBA) and an end fitting. The height of the FA is 1015 mm. The upper part of the end fitting is inserted into the lower part of the fuel box assembly, then they are joined together by welding or screwing.
The material of the FA components, except fuel plates, is aluminum alloy 6061-T6 for its high strength and good performances in the reactor core. The rectangular duct at the upper part of the end fitting is reduced to a circular duct for a smooth transition of the flow area. When the FA is loaded in the core, the lower cylindrical part of the end fitting is inserted in the fuel hole on the grid plate, and then the FA can stand alone in its position without any lateral support.
The FBA has 21 flat fuel plates and the envelope dimension is 76.2 mm x 76.2 mm x 830 mm excluding wear pads on 4 edges of the FBA out surface at top. Each fuel plate one after another is inserted in the groove inside of the side plates and then fixed by applying plastic deformation on the crests in between the grooves, by means of moving wedge or roller, i.e. roll-swaging or crimping.
The LEU fuel plate, 1.27mm thick, is composed of a fuel meat with the surrounding cladding of 0.38mm thickness. The fuel meat is made of a fine and homogeneous dispersion of U3Si2 particles in a continuous aluminum matrix. The fuel is LEU with a 235U enrichment of 19.75 wt% and the uranium density in the fuel meat is 4.8 g-U/cm^3. The fuel meat is hermetically sealed with aluminum alloy cladding. In addition, the fuel meat is bonded rigidly to its surrounding cladding for structural integrity. This type of fuel plate has been routinely fabricated for decades [2].

2.2 FE Model of the Fuel Plate and the Fuel Assembly

The Model of the fuel plate and the FA calculation are shown in Fig. 1 and Fig. 2, respectively. In the detailed model, cladding and meat was modeled with 4 element layers in the normal to the thickness direction, with Solid45 element of the ANSYS. Since the detailed model required too long time for the calculation, it was needed to make simplified finite element model to have less elements and nodes in the meat, to be only one element layer in the thickness direction of the FP.

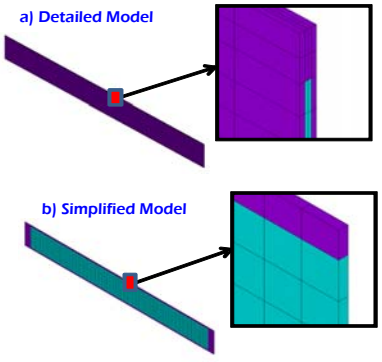

Fig. 1 Fuel Plate FE Model

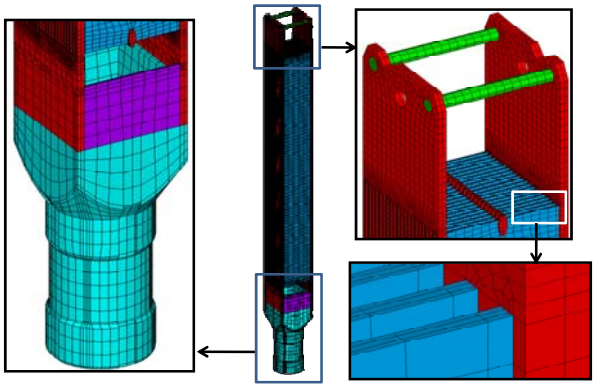

Fig. 2 Fuel Assembly FE mode

Material properties of the simplified model were controlled to preserve the same dynamic characteristics by adjusting the material properties, density and Young's Modulus.
In order to get the natural frequencies of the fuel plate, both ends of the fuel plate in the longitudinal direction were fixed to simulate the swaging condition. As for the boundary

condition (BC) of the FA, the end fitting in the hole of the grid plate was fixed. After getting the natural frequencies in an ascending order, the mode shapes corresponding to the natural frequencies were found which took rather tedious and time consuming work.

3. Calculation Results and Discussions

3.1 Natural Vibration of the Fuel Plate

The natural frequencies of the fuel plate with all 4 edges free and two lateral edges fixed are listed in Table 1. The mode shapes and the natural frequencies of the FP in air with detailed model under both sides fixed are shown in Fig. 3.

Table 1 Frequencies of a Fuel Plate under various Conditions (Hz)

B.C	Detailed Model				Equivalent Simplified Model			
	Free-Free B.C		Fixed-Fixed B.C		Free-Free B.C		Fixed-Fixed B.C	
Mode	Air	Water	Air	Water	Air	Water	Air	Water
1	13	26	1266	929	13	26	1264	925
2	35	50	1275	934	35	50	1273	931
3	70	53	1289	944	70	53	1287	941
4	73	83	1310	958	73	83	1308	954
5	115	107	1338	976	115	107	1336	973

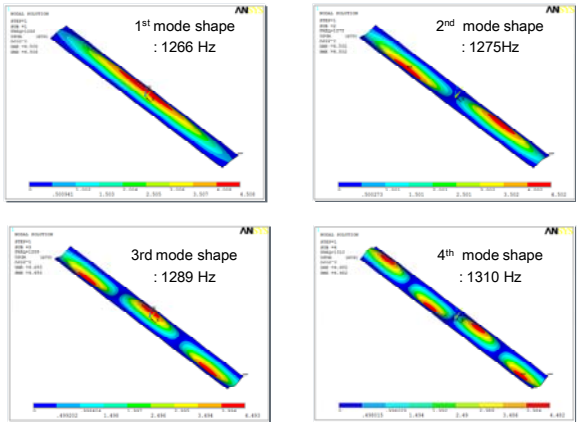

Fig. 3 Fuel Plate Mode Shapes

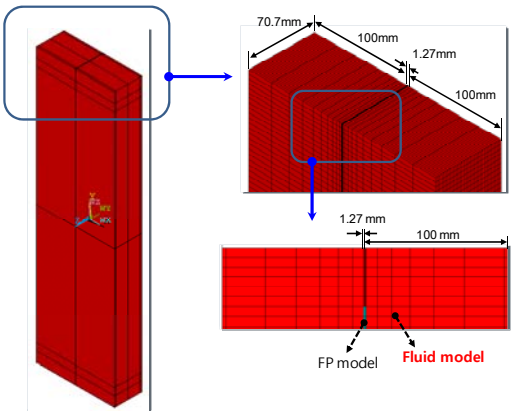

Fig. 4 FP FE Model in Water

A fuel plate with all 4 edges free boundary conditions, which eliminate the boundary effects on the vibration, reveals very low frequencies starting from about 12 Hz in air and shows relatively slightly lower frequencies than those in air. For the simulation of the FP in water condition, the fuel plate was surrounded by 100mm of water as shown in Fig. 4. Comparing the frequencies of all the edges free BC, the natural frequencies of the both sides fixed condition show fairly higher frequencies, starting from 1266Hz in air and they show slightly lowered in water condition. To investigate the effects of the size of the surrounding fluid on the natural frequencies of the plate, the frequencies with variation of the fluid thickness were obtained as in Table 2 for the fixed BC. It is significant that as the size of the surrounding fluid becomes smaller, the frequencies increase significantly. Since the fluid size of 2.35mm is the actual size of the flow gap in the FA, the frequencies of the FP under this condition seems to

be the real frequencies in water. The reason why the frequencies of FP decreased with the fluid amounts is due to the added mass effect of the water which is a portion of the surrounding fluid that is accelerated as though it were rigidly attached to the FP. On the contrary if the fluid gap becomes smaller, the fluid needs more energy to escape from its place which results in a resistance to the motion of the FP so that it may increase the frequencies of the FA[3]. This phenomenon can be validated by the vibration test in water with dummy fuel plates in the future.

Table 2 Natural Frequencies of the Fuel Plate as variation of Fluid Size (Hz)

Mode number	Fluid thickness(mm)			Air condition
	200	100	2.35	
1	425	424	929	1266
2	430	430	934	1275
3	440	439	944	1289
4	453	452	958	1310
5	470	469	976	1338

3.2 Natural Vibration of the Fuel Assembly

The comparison of the natural frequencies of the FA in air and in water is in Table 3. It shows that the frequencies of the detailed model and the simplified model do not show much difference, while for those in water environment, the FA frequencies decreased by 30% lower than those of in air. It is noted that the dynamic analysis of the detailed model in water was not performed due to its high computational costs. These frequencies of the FA also will be compared with those of test results, which are scheduled to be performed in the future. The modes of the FA in water are shown in Fig.5.

Table 3 Natural Frequencies of the FA in Air and in Water (Hz)

Condition	Fuel assembly with detailed FP model		Fuel assembly with simplified FP model	
Mode	Air	Water	Air	Water
1	65	-	65	47
2	79	-	80	53
3	378	-	378	246
4	420		419	304
5	466		466	370

Investigating the frequencies and mode shapes as shown in Table 4, the combs do not affect much on the FA lateral vibration but affect only on the twisting mode of the FA vibration which implies the combs do not influence the lateral stiffness of the fuel plates.

Table 4 Natural Frequencies of the FA with Combs and without Combs in Air (Hz)

Mode No.	FA with combs	FA without combs	Relative Ratio (%)	Remarks
1	65	65	1.00	
2	80	80	1.00	
3	378	378	1.00	
4	419	419	1.00	
5	466	451	0.97	Twist mode

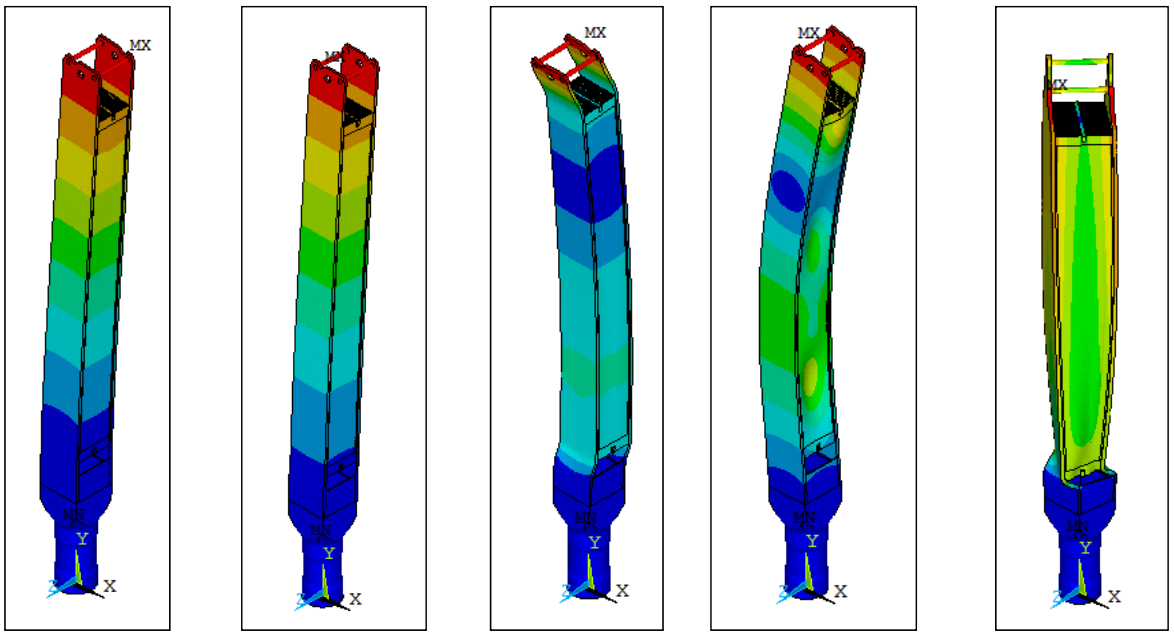

1st mode shape : 47 Hz | 2nd mode shape : 53 Hz | 3rd mode shape : 246 Hz | 4th mode shape : 304 Hz | 5th mode shape : 369 Hz

Fig. 5 FA Mode Shapes in Water

4. Conclusion

A fuel plate and a fuel assembly are modeled to be the finite element meshes of the ANSYS and the natural frequencies and mode shapes of them were obtained. The effects of boundary conditions of the fuel plate and the FA on the frequencies and mode shapes were investigated. The natural frequencies of the fuel plate were significantly reduced in water. The frequencies of the fuel plate as assembled in the FA in air were calculated which show slightly lower frequencies than FP alone. These lowered frequencies seemed to be the fact that the assembled BC of the FP is softer than that of the FP only.
The frequencies of a FA were compared in air and in water. The first frequency was about 72 % of that in air. It is shown that the assembled FPs by combs showed only affects the torsional vibration modes of the FA. Thus the combs do not affect on the frequency of the transverse mode of vibration of the FPs in the FA.
The model of the calculation will be used as the basic model for the dynamic analysis during the SSE after validation by vibration tests in air and in water using dummy FPs and/or FAs.

References

[1] ANSYS version 12, Swanson ANSYS Co.
[2] JP. Duranad, B. Duban, Y.Lavastre, S.de Perthuis, CERCA's 25 Years Experience in S3Si2 Fuel Manufacturing, 25th RERTR Meeting, Chicago
[3] Kyung-Hoon Chung, Private communication for the plate vibration with water gaps

Development of a High Flux Research Reactor with Assembly-Integral Flux Traps

S.A. KEMPF, L.-W. HU, B. FORGET
Massachusetts Institute of Technology
77 Massachusetts Ave. Cambridge, MA 02139 – USA

ABSTRACT

In recent years, the demand for irradiation services has increased as research reactors face a number of challenges. These challenges include reduction in enrichment, the need for economical use of fuel, and the medical isotope crisis brought about by the temporary shutdowns of the NRU and HFR. These challenges have inspired the design of a revolutionary research reactor assembly concept making use of the new U-Mo monolithic fuel form. Each assembly consists of a trapezoidal plate-fueled region and integral triangular flux trap. When placed in a hexagonal core, this structure permits multiple orientations of the flux trap with respect to those surrounding it. As a result, multiple orientations, sizes and shapes of the flux trap are possible. These flux trap parameters can be adjusted to provide the spectra needed to meet ever-changing experimental needs.

This assembly concept was applied to the development of a 5 MWth research reactor core, and optimized for peak thermal flux. During the design process, attention was given to making the design economical, manufacturable, and maintainable. The design was able to produce a maximum unperturbed thermal flux of 1.2×10^{14} neutrons/cm^2 s, 70% higher than existing research reactors of the same power rating. Despite this optimization for thermal flux, the reactor is still capable of producing fast fluxes in excess of 1×10^{14} neutrons/cm^2 s in other regions of the core.

The response of the resulting core to thermal hydraulic transients was also analyzed.

1. Introduction

As research and test reactors worldwide face challenges ranging from the need for increased proliferation resistance to maintenance issues, to high fuel costs, the demand for irradiation facilities continues to climb. Meanwhile, considerable opportunities in the field of new design work exist as a result of the ongoing qualification of high density U-Mo monolithic fuels at Idaho National Laboratory.

These have combined to inspire the development of a new 5 MWth research reactor concept which is both safe and economical to operate. In order to obtain the maximum benefit from this reactor, the geometric parameters of the core are optimized to maximize thermal flux while meeting safety limits. Additionally, the core contains multiple flux traps in order to allow the flux to be as fully utilized as possible.

2. Physics Analysis

In order to make the concept economical to construct, fuel and operate, the core was designed to make use of a single assembly geometry with flat fuel plates. In order to do this and still achieve the goal of making available multiple regions for high-thermal flux irradiation, it would be necessary to devise an assembly with an integral flux trap. The result was the concept shown in Figure 1.

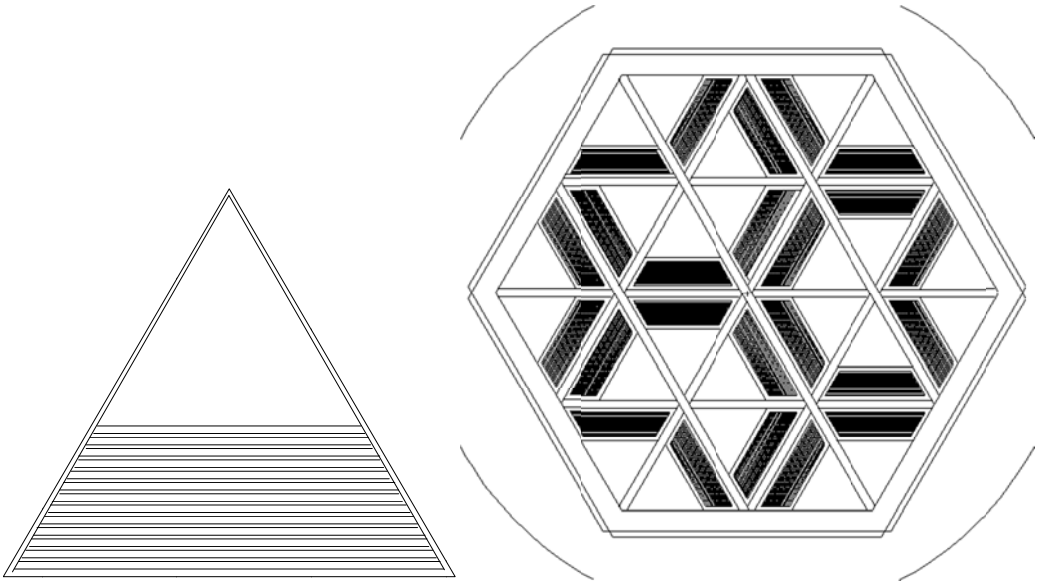

Figure 1: Assembly and Full Core Diagrams

The assembly consists of parallel fuel plates in a trapezoidal arrangement, and a flux trap region. The entire structure makes up a triangular footprint. These triangles are positioned within a hexagonal core for minimum leakage, with the assemblies rotated to form varying sizes, shapes, and spectra of flux traps.

The design concept's dimensions were subjected to constrained optimization of thermal flux, by using a mathematical technique known as kriging [2] to probe the design space for regions of potential flux increase. The resulting optimum assembly parameters and the characteristics of their loading into the fresh core shown in Figure 1 are detailed in Table 1.

Table 1: Neutronic Parameters and Performance

Assembly long edge length	5.375 cm
Flux trap edge length	3.925 cm
Fuel volume fraction	0.235
Peak thermal flux	1.20×10^{14} n/cm^{2}s
Peak epithermal flux	1.00×10^{14} n/cm^{2}s
Peak fast flux	1.69×10^{14} n/cm^{2}s
Fuel temperature coefficient	-0.0945 pcm/K
Moderator temperature coefficient	-3.221 pcm/K at 45C
Delayed neutron fraction	0.00664

While analysis of this core's application to its scientific mission is still underway, some general conclusions can be drawn from the information already available. For example, the reactor can be directly compared to the MITR-II, which has the same power rating and operates under the same thermal hydraulic conditions [1]. The MITR-II produces a peak in-core thermal flux of 7×10^{13} n/cm^{2}s, and a peak in-core fast flux of 1.69×10^{14} n/cm^{2}s. Therefore the core performs as well as the MITR-II in supply of fast flux to irradiation sites, and additionally provides more than 70% additional thermal flux. Additionally, the proposed design possesses four times the in-core irradiation volume of the MITR-II. Depletion calculations also indicate that the core can sustain operating cycles roughly twice as long as those of the MITR-II.

3. Thermal Hydraulic Performance

3.1. Steady State

One of the constraints used during neutronic optimization was the maintenance of 300% margin of safety to ONB heat flux. This large margin was chosen to delay ONB in the event of loss of forced flow. However, this margin was not sufficiently large to prevent flow instabilities from makng the core uncoolable upon loss of forced flow. As a result, the steady state flow rate was increased so that a large quantity of heat would be removed during pump coastdown, delaying ONB for long enough to allow actuation of safety injection for cooling of the core.

The resulting steady state flow velocity is high, but still lower than that of reactors like the HFIR [1]. In addition, the selected velocity provides a 200% margin of safety to the critical flow velocity predicted by Miller's method to produce channel collapse [5]. The resulting pressure drop is also high, but the economics of the high thermal flux and its utilization are expected to mitigate the costs associated with installing sufficient pumping power.

Table 2: Steady State Thermal Hydraulic Parameters

Power density	0.1755 MW/l
Average heat flux	0.212 MW/m^2
Peak heat flux	0.4785 MW/m^2
Flow velocity	10.0 m/s
Flow area	0.0088 m^2
Frictional pressure loss	2.03 x 10^5 Pa
$T_{clad,\ max}$	54.6 C
T_{in}	40 C
T_{out}	47.4 C

3.2. Loss of Flow Transient

The loss of flow transient is modeled in RELAP5-MOD3.3, and assumes a linear coastdown of the pumo over 10 seconds. The reactor scrams 1.2 seconds after loss of normal pumping power, as a result of signal transmission delay after a low-flow signal. Natural circulation and anti-siphon valves open passively 9 seconds after pump failure, and provide a flow path for natural circulation. A safety injection system is actuated 30 seconds after pump failure, providing 10 kg/s of cooling water. This actuation is necessary due to the difficulty of natural circulation cooling in the narrow channels. The results of the transient calculation are shown in figure 2.

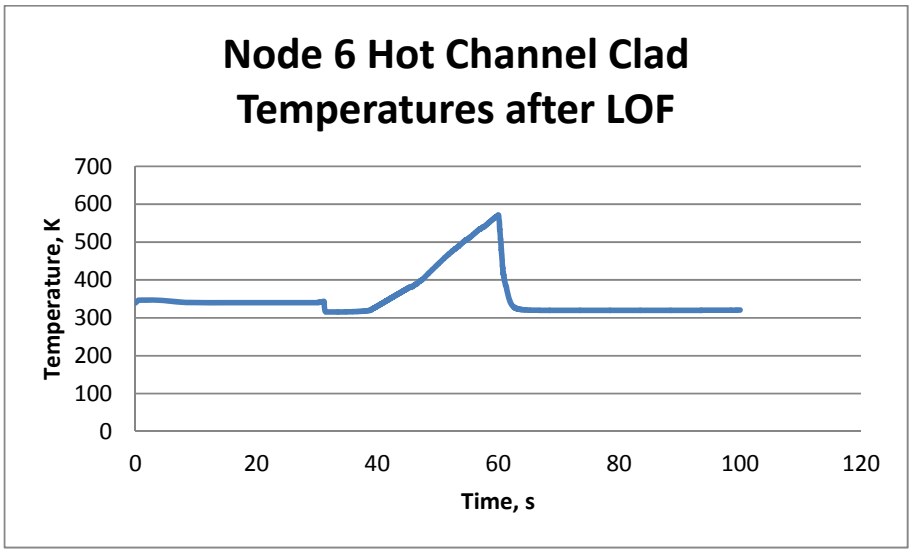

Figure 2: Peak Cladding Temperatures after LOF

As can be seen, while flow instability causes a large spike in the peak cladding temperatures in the hot channel, the introduction of safety injection causes the peak cladding temperature to maintain a nearly 150 degree C margin of safety to the clad's softening temperature for the duration of the transient.

3.3. Reactivity Insertion Transient

Fast ramp insertions of reactivity, such as may occur with sudden ejection of an experimental device, were also investigated using RELAP5-MOD3.3. The reactor was assumed to scram on 20% overpower, with a 0.1 second delay for signal transmission. The ramp rate was $1.5/0.5 s., a typical value recommended by the IAEA.

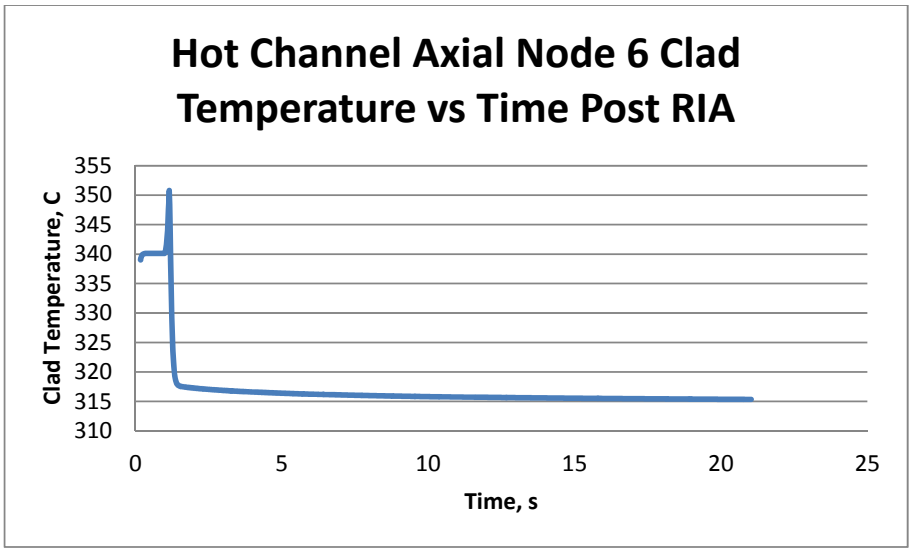

Figure 3: Peak Cladding Temperatures After RIA

As can be seen, the peak clad temperatures remain low for the duration of the transient.

The limiting case of a step reactivity insertion was also investigated, with the maximum survivable insertion being $2.1.The fact that this limit is smaller than that of other reactors is

not considered to be of concern in limiting the reactor's scientific goals. The worth of individual targets is so small that a large number of them would have to be ejected simultaneously in order to produce such a massive reactivity insertion. A recent study on prediction of reactivity worth of MURR targets indicates that the highest worth specimen in use in that reactor has a worth of -11.8 pcm [4]. Assuming that targets of comparable worth were irradiated in the present design, it would take the simultaneous ejection of 118 of these high-worth targets to produce a step insertion of $2.1. The reactor can therefore survive any foreseeable reactivity insertion transient.

4. Conclusions

A new research reactor core concept has been developed and optimized for supply of thermal flux to multiple irradiation facilities at 5 MW_{th}. This unique concept provides the experimenter the opportunity to tailor the flux spectrum, size, and position of each flux trap to meet ever-changing experimental needs. The resulting concept is capable of delivering thermal fluxes 70% greater than reactors of the same power rating, and comparable fast fluxes to those same reactors. Analysis of the potential of the design for scientific use and supply of medical isotopes is in ongoing, and appears promising. While the compactness of the core renders it difficult to cool, the expense of its large pumping power is expected to be balanced by benefits of the concept's ability to supply high thermal flux to a large volume of in-core irradiation facilities.

Simulation using RELAP5-MOD3.3 has been employed to demonstrate that the concept can survive a loss of flow transient when a modest supply of emergency cooling water is made available up to a minute after loss of forced flow. Analysis has also demonstrated that the reactor can sustain both ramp and step reactivity insertions with a large margin of safety to the clad softening temperature.

5. References

[1] R. Burn, ed. *Directory of Operating Research, Training, and Test Reactors in the United States of America*, *4th edition.* United States Department of Energy, 1997.

[2] N. Cressie, *Statistics for Spatial Data*, John Wiley and Sons, New York, 1991.

[3] S.J. Kim, Y. Ko, L.-W. Hu, "Loss of Flow Accident Analysis of the MIT Research Reactor HEU-LEU Transitional Cores Using RELAP5-3D", Proceedings of ICAPP 2010, San Diego, CA, June 13-17 2010.

[4] Z. Ma, "Development of MURR Flux Trap Model For Simulation and Prediction of Sample Loading Reactivity Worth and Isotope Production", University of Missouri-Columbia Dissertation, May 2007.

[5] D. Miller, "Critical Flow Velocities for the Collapse of Reactor Parallel-Plate Fuel Assemblies," KAPL-1954, Knolls Atomic Power Laboratory, 1958.

Safety of experiments prior to a test campaign and associated reactivity injection characterization

G. Ritter*, Th. Cadiou*, A. Rondeaux++

*CEA/Nuclear Energy Division/ Cadarache Nuclear Research Center/Reactor Studies Department
++Under contract with CEA

***Abstract*— The CABRI experimental reactor is located at the Cadarache nuclear research center, southern France. It is operated by the Atomic Energy Commission (CEA) and devoted to IRSN (Institut de Radioprotection et de Sûreté Nucléaire) safety programmes. It has been successfully operated during the last 30 years, enlightening the knowledge of FBR and LWR fuel behaviour during Reactivity Insertion Accident (RIA) and Loss Of Coolant Accident (LOCA) transients in the frame of IPSN (Institut de Protection et de Sûreté Nucléaire) and now IRSN programmes devoted to reactor safety. This operation was interrupted in 2003 to allow for a whole facility renewal programme for the need of the CABRI International Programme (CIP) carried out by IRSN under the OECD umbrella.**

The principle of operation of the facility is based on the control of ^{3}He, a major gaseous neutron absorber, in the core geometry. The purpose of this paper is to illustrate the safety computation associated to the preparation of a test campaign. It presents the schemes and tools dedicated to core characterization. Eventually, it shows an original physics offspring result of a such campaign.

***Index Terms*— RIA, Core, ^{3}He, Neutron, Kinetics, CFD.**

I. Introduction

The experiments to be performed in the CABRI facility will now be confined to a new pressurized water loop. This device is located at the heart of a pool type reactor (cf. fig. 1). The experimental fuel rod will then stand a powerful neutron flash during the core driven power transient. A vertical channel symmetrical across the core allows the hodoscope, a unique neutron camera, to monitor the course of fissions in the experimental rod along the experiment.

The core is made of 1488 stainless steel clad fuel rods with a 6% ^{235}U enrichment. The reactivity is controlled via 6 bundles of 23 Hf rods. The reactivity worth for these control rods is ~19$.

The active part of the core is the size of a small refrigerator.

G. Ritter, A. Rondeaux. DENCAD/DER/SRES CEA Cadarache, B^{t} 223. 13108 St Paul Lez Durance. France. (Corresponding author. Phone +33 (0)442 25 41 80. Guillaume.Ritter@CEA.Fr)

Th. Cadiou. DENCAD/DER/SESI CEA Cadarache, B^{t} 212. 13108 St Paul Lez Durance. France.

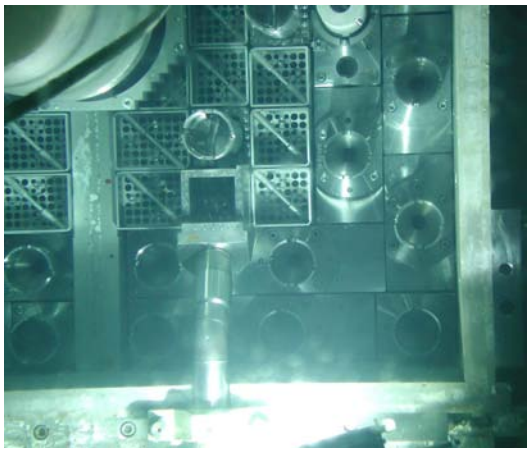

Fig. 1. ¼ CABRI core at unloading. Center up-left.

The key feature of the CABRI core is its reactivity injection system. This device allows 96 tubes filled with ^{3}He (major gaseous neutron absorber with a capture cross section $\sigma_{He\text{-}3(n,p)T}$ at least 50 times larger than Hf) up to a maximum pressure of 15 bars and located among fuel rods to depressurize very fast into a discharge tank. The absorber ejection translates into an equivalent reactivity injection possibly reaching 4$ within a few 10ms. The power consequently bursts from 100 kW up to ~20GW (cf. fig. 2) in a few ms and decreases just as fast due to the Doppler effect and other delayed reactivity feed-backs.

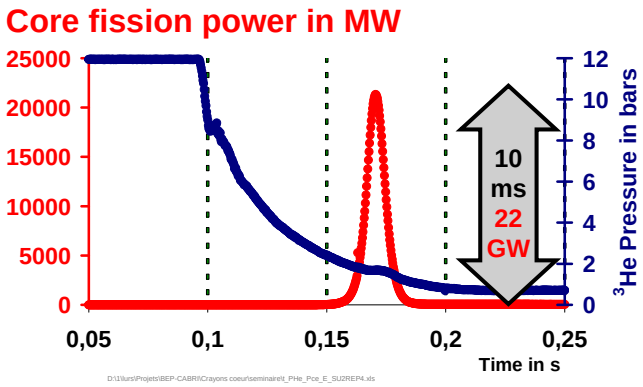

Fig. 2. Typical CABRI ^{3}He pressure and core power during a transient.

In 2008, the core safety case was upgraded. It confirmed the need for a pre computation before each new test campaign. This analysis also allowed a sharper physics characterization of the core behavior during transients. The safety issues were addressed by robust and dedicated tools in a project approach whereas these physics questions like e.g. in-core ^{3}He pressure could be answered through research oriented applications.

II. UPGRADING CABRI WITH A WATER LOOP

The CABRI International Programme was decided in order to realize tests representative of PWR accidental conditions. The facility is now being modified in order to have a water cooling in the test section.

The CABRI + project is a facility side of the CABRI INTERNATIONAL PROGRAM initiated by IRSN in the late 90's and including about 20 partners. IRSN is the Technical Safety Organization for the French Nuclear Safety Authority. The main goal of the CABRI + project was to replace the experimental sodium cooling loop by a pressurized water loop. Installing water cooling for the test rod will allow to be representative of PWR's, essentially during the post rod failure phase when there can be fuel-coolant interactions. It will be used to test future high burn up or alternate fuels like MOX and to re-assess current safety margins.

Fig. 3. The basket : support structures for the new CABRI water loop.

Figure n° 3 before shows what volume it takes to put a pressurizer, a pump, a couple of heat exchangers and a few valves.

The experiments performed in the past with sodium cooling were mostly Fast Breeder Reactor oriented but some tests were done with Light Water Reactor severe accident scenarios.

The CABRI facility is made of an experimental loop containing the test rod at the core center. A special neutron camera, called a hodoscope, allows to track the power burst in the test rod through a collimator and from outside the core.

The core fuel rods are steel clad to allow them to withstand the numerous power bursts performed in the facility. There have been about 700 pulses since the beginning.

Upgrading this facility is a major challenge that has to be carefully accounted for. Six years after the beginning of operations, several safety and technical improvements have already been achieved to fulfil the project and only a few still remain to be done, like criticality associated testing [1].

The technological upgrade issues essentially concerned replacing a major heat exchanger, inspecting and fixing all primary circuits, installing new vessels and capacities where necessary, putting a safety brake on the crane for heavy lifting, designing and realising a handling cask for experimental fuel, controlling the ^{3}He circuit and all the others, installing a new water treatment station and developing the current facility liquid waste circuit.

The safety issues were largely dedicated to strengthening the buildings, major mechanical equipments and core structures against seismic quakes, to the overall building fire protection, to the development of a new ventilation (5 times more powerful), to the design and construction of a new storage building and eventually although not the least, to a comprehensive revision of the core safety case. The safety topics were of course conducted in agreement with the prescriptions of the safety authority.

All works were realized while the nuclear facility normal operations were maintained.

III. PRINCIPLE OF OPERATION

The CABRI reactor is a world unique facility for its Reactivity injection system (cf. figure n°4 next page). The main feature of this device is to allow an accurate control of reactivity injections. Opening the valves delivers a fast ^{3}He ejection causing a reactivity injection resulting in the burst of power (e.g. 3,5 $ within 0,12 s as in figure n°2 prev. page).

There are two options for ^{3}He depressurization, a long breath or a quick blow, depending on the size of exhaust pipes. The adjustable valve aperture for each way can also be tuned to the desired flow and injection time.

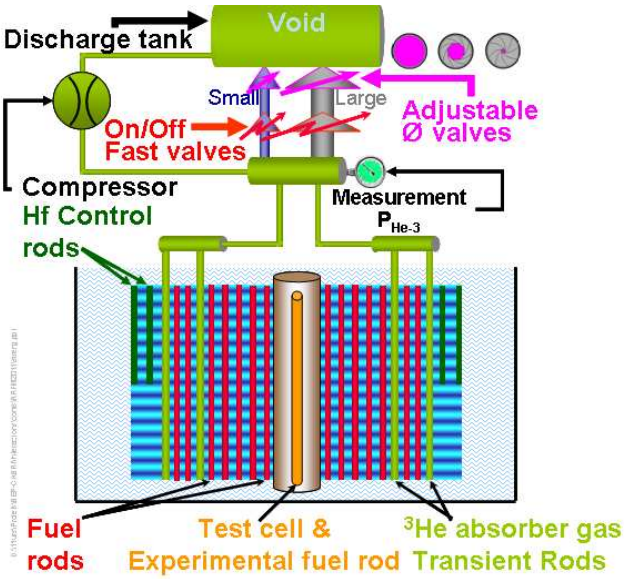

Fig. 4. Principle of operation of the CABRI facility.

A high reliability automat is dedicated to the control of valves aperture and enforces the Hf control rods insertion at the end of the experimental sequence. The device has been designed so that the risk of failure is lower than 2. 10^{-9} per test.

The design of a test basically depends on two criteria : The maximum power at pulse peak and the transient duration at half peak power. These figures are used to determine which conditions must be met with the ^{3}He reactivity injection system. Afterwards, an investigation is performed to make sure these parameters comply with the facility safety.

IV. Validation of Test Safety

The core safety now relies on three parameters and each must be evaluated with the maximum margins. The fuel temperature must not exceed 2810°C, the clad strain must remain within 3.6% and the maximum clad temperature must be lower than 1300°C.

Before any new test campaign, the envelope safety parameters are computed according to the maximum expected conditions during the campaign. The computation is made with SCANAIR, the thermal hydraulics and thermal mechanics code from IRSN [2] dedicated to fuel rod characterization during power transients. It includes a comprehensive validation on thermal hydraulics experiments as described in [3]. This code was adapted to a routine production use by experimentalists under MS Windows environment and this upgrade provides a large flexibility for test preparation.

The main input to this computational validation of test safety is the pulse power. Actually, it is the main changing variable from a test to an other for the core hot rod. There are two evaluation options for this item. The first is an existing records library based on previous measurements. Such measurements would have been performed in analogous conditions of initial power and reactivity injection either during the past sodium loop program or within the pressurized water loop commissioning campaign. It would in any case be envelope of the perspective campaign to be tested. The second option is dedicated to fast pulses only and relies on the knowledge of the ^{3}He absorber concentration in the core.

V. Core Safety Parameters Assessment

This paper concerns the realization of a fast pulse using only the large depressurization line (in gray on fig. 4) for which no data or approaching conditions would have been recorded in the past. As a consequence, it requires a specific computation. This operation will consist in assessing the core power from the injected reactivity using point kinetics. The time wise reactivity worth corresponding to ^{3}He ejection off the core is evaluated with a combination of functions :

$$\rho(t) = \rho(P_{He}) \otimes P_{He}(t) \text{ where}$$

- $\rho(P_{He})$ is given by a Monte-Carlo core computation with TRIPOLI 4 [4] and
- $P_{He}(t)$ is a preliminary measurement of ^{3}He pressure in actual test conditions but without core operation

The term $P_{He}(t)$ can be extrapolated from previous measurements. It can also be computed with the following analytical law.

$$\frac{p(t)}{p(0)} = \frac{1}{(Bt+1)^{\alpha}}$$

with :

$\alpha = 2\gamma / (\gamma - 1)$ and $\gamma = Cp / Cv$, $\gamma \approx 1.66$ for Helium

B= a term characterizing the valve flow and fitted to the experiments.

The analytical law exposed above shows $P_{He}(t)$ and thus $\rho(t)$ only depend on the initial pressure and the valve aperture.

The control of core reactivity during a transient starts with ^{3}He depressurisation and ends with the control rods automatic insertion. This last term is thus also included at the end of the $\rho(t)$ transient model.

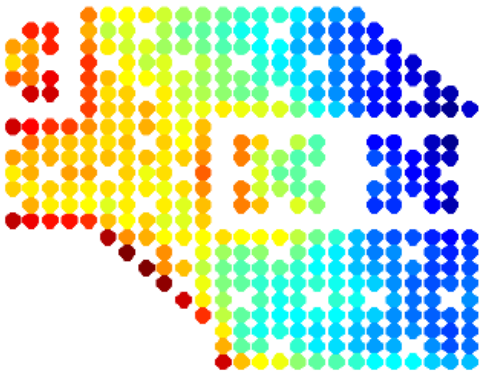

Fig. 5. CABRI Quarter core rodwise power distribution thermogram

The DULCINEE neutron kinetics code [5] converts the reactivity ρ(t) into a pulse of core power. At this point, the hot spot correction can be added to the overall core power. This correction comes again from a TRIPOLI 4 Monte Carlo transport calculation as illustrated in figure 5 above. This quarter core rod wise power distribution shows in particular how the fission rate is depleted in the ^{3}He rods region on the right of the figure. This corresponds to the situation before the power burst when the gas absorber pressure is high in the tubes. The hot spot correction accounts for the sharp evolution of power distribution during the pulse due to the disappearance of the ^{3}He absorber. This phenomenon reminds the heat rate is peaked on the hot rods region at high ^{3}He pressure and goes to the outside of the core when this absorber is gone.

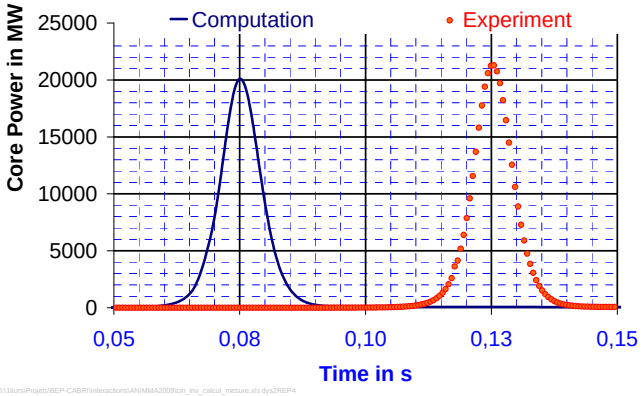

Fig. 6. Agreement between computation and experiment for DULCINEE

DULCINEE was developed at the beginning of CABRI. It was initially dedicated to fuel plate geometries and then was adapted to rod bundle cooling configurations. The geometric model is 1 D ½, corresponding to a full radial heat transfer from the fuel center to the coolant and an axial heat flux profile without transfer. It has been especially validated against low pressure coolants like sodium and LP water. In the late 80's, a fractured fuel model was inserted allowing a better validation against experimental temperatures. It was successfully validated against the CAPRI experimental Thermal-Hydraulics programme realized at CEA-Grenoble in the late 1970's.

DULCINEE uses feedback parameters that were computed with TRIPOLI 4. It includes the instant Doppler effect and all delayed phenomena like clad expansion or coolant density. The delayed neutron fraction β and generation lifetime ℓ were computed with MCNP [6]. The resulting values are now consistent and have successfully been tested with DULCINEE against experimental data acquired during the sodium loop past programs (several hundred power bursts in the past 40 years). It will be tested against the experiment with a neutron noise measurement technique [7] during core commissioning.

Figure 6 above shows the very good agreement between computation and experiment for the DULCINEE kinetics tool during a fast 10 ms duration typical fast pulse. The "experiment" plot corresponds to the measurement of an ion chamber whereas the "computation" plot corresponds to a reactivity driven DULCINEE computation. In this latter case, the reactivity comes from the above mentioned combination of functions : $\rho(t)=[P_{He\text{-}3}(t)]_{measurement.} \otimes [\rho(P_{He\text{-}3})]_{calc.}$.

Eventually, the hot rod power features are computed in SCANAIR to evaluate the three safety parameters presented in the previous paragraph (i.e. T_{fuel}, T_{clad} and ε_{clad}).

The steps exposed before to assess the safety of any upcoming experiment include several added margins. Most of this legitimate conservatism is concentrated in a large overestimation of the core power. This approach maximizes the energy deposited in the rod, which is the driving parameter for clad temperature.

VI. ^{3}HE REACTIVITY WORTH ASSESSMENT

The time behavior of ^{3}He induced reactivity is the result of two combined functions: $[P_{He\text{-}3}(t)] \otimes [\rho(P_{He\text{-}3})]_{calc}$. The reactivity as a function of ^{3}He pressure has been computed with TRIPOLI 4 Monte Carlo whole core computations and with DULCINEE in the reverse kinetics option. It has been successfully validated against past measurements. This validation first compared the computed hafnium rods criticality level to the measurement for several ^{3}He pressures in a statics approach and it also provided an assessment of the ^{3}He reactivity worth in a dynamics approach. Both methods showed a good and coherent agreement as presented in figure 7 below [8].

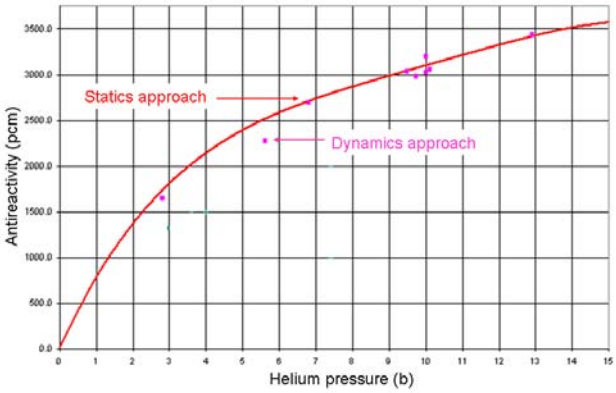

Fig. 7. Agreement between computation and experiment for TRIPOLI 4

As a consequence, the uncertainty on ρ(t) basically depends on the gas concentration in the core that is to say P_{He}(t). This pressure comes from a measurement either made during previous experimental campaigns (actual test with a power burst) or in preparation of an upcoming test (system depressurization without core operation). These records fit the analytical formula presented in chapter V as can be seen on figure 8 below. However, a couple of small bumps still remain on the experimental plot and it could hardly be modeled into

the simple analytical law.

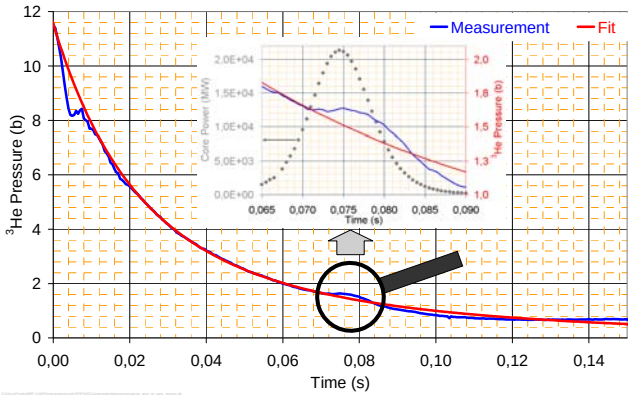

Fig. 8. ^{3}He pressure as a function of time in a typical fast pulse

The analytical approach illustrated in the fit plot of figure 8 above accounts for a perpetual critical flow. It was validated on the measurements of past experiments. However, the neutron pulse causes a delayed flash heating in the gas (see magnifier in fig. 8 above) that remains unaddressed. An attempt to better describe the physics of this ^{3}He depressurization has thus been initiated.

VII. BETTER UNDERSTANDING ^{3}HE PRESSURE PHYSICS

The validation of tests safety uses either measurements or an analytical fit to characterize $P_{He}(t)$. This approach gives satisfactory results to provide an assay of the fuel rods safety criteria, essentially because the driving parameter is the energy deposited in the rod rather than a particular power plot. However, a few specific phenomena have been observed in this $P_{He}(t)$ plot that could be better characterized using a more accurate modeling.

The characterization of $P_{He}(t)$ has been revisited and now includes two connected features :

- An explicit description of the circuit with Computational Fluid Dynamics and
- The flash nuclear heating due to the burst of power

The CFD computation is based on the actual 3D CAD model of the reactivity injection system inserted in the STAR-CD code [9] as it is well adapted to complex geometries. STAR-CD is a CFD code based on a finite volume discretization, which is largely used by the industry. It is adapted for the following calculations in laminar and turbulent flows, compressible or non-compressible and possibly with radiation modelling. The code solves the 3 basic conservation equations (mass, energy and momentum) with a refined meshing in order to provide the thermal hydraulics field for the fluid using the k, e model for turbulence. The velocity on the boundary layer is described by the wall law. A zoom on the collector head, a key element of the reactivity injection system, is showed in figure 9 hereafter.

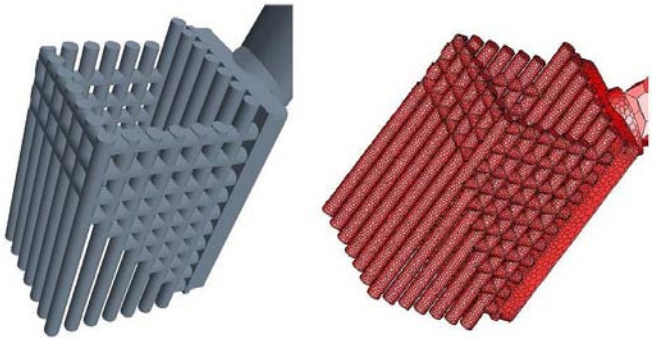

Fig. 9. Mesh of the collector head (reactivity injection system)

Figure 9 above shows the collector head, right above ^{3}He tubes located in the core. This device gathers ^{3}He flows from all 24 tubes of 1 among 4 ^{3}He absorber systems in the core. The mesh is most refined upstream, where phenomena are dense, whereas it is coarser downstream.

The CFD computation is fed by an estimate of the power rate due to nuclear heating.

The spatial distribution of *n,p* capture has been computed with TRIPOLI-4. The computation has been performed for each individual of all 96 ^{3}He rods in the azimutal, radial and axial directions and for several gas pressures. The nuclear heating of ^{3}He in the tubes is essentially due to the ^{3}He(n,p)^{3}H capture reaction whilst the γ heating is negligible. The relative heat rate thermogram shown on figure 10 below corresponds to a tube located at the inner corner of 1 among 4 ^{3}He absorber systems. It shows a significant spatial self shielding at the periphery. This effect naturally depends on the gas pressure. The peaking factor increases by 20% between 1b and the maximum ^{3}He pressure of 15b.

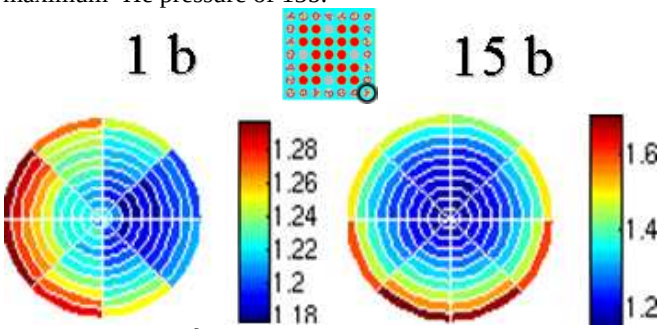

Fig. 10. In-core ^{3}He corner tube internal *n,p* reaction thermogram

On figure 10 above, the reaction rate peaking seems to move downwards when the gas pressure increases. This is due to the general shift in the core flux map as exposed below figure 5 in chapter V. The ^{3}He absorber naturally reacts as a sort of flux repellent. It allows a higher reaction rate on the inner face of the tube at low ^{3}He pressure and it keeps most reactions on the outer face of the tube at high ^{3}He pressure.

The power yield in the gas would be more important if all the energy of the $^3He(n,p)^3H$ reaction (0.764 MeV) was released at the interaction site. However, this approach does not account for the transport of *p* and ^3H resulting charged particles.

This transport has 2 consequences :

- It spreads the heat into the gas and
- It shares a part of the initial reaction energy with the *^{3}He* tube clad.

This phenomenon was modeled with a Monte Carlo routine computing and integrating the stopping power at several ^{3}He pressures for each particle from the interaction site to the final point. The model is based on simple hypotheses but gives a fair order of magnitude of the fraction of energy effectively released in the gas. It shows the energy is essentially released in the clad at low pressure (83% at 1 b ^{3}He) whereas it mostly goes to the gas at high pressure (81% at 15 b ^{3}He).

The gas nuclear heating was eventually integrated to the CFD computation. This last computation is now able to reproduce the specific characteristic observed on the pressure measurement. It also allows an assessment of the in-core ^{3}He pressure $P_{He}(t)$ as shown in figure 11 below. This new feature will be most useful to help determine the reactivity injected in the system in order to better predict the power generated during the corresponding transient.

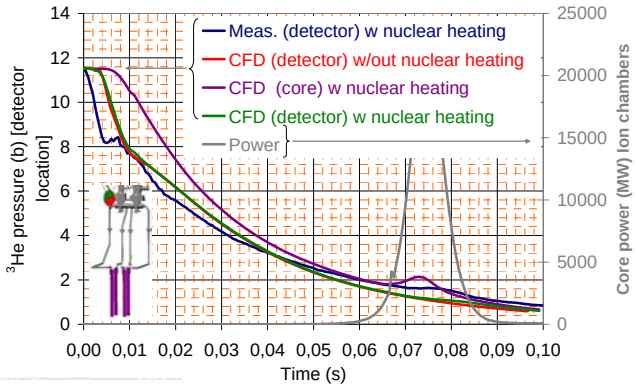

Fig. 11. $P_{He}(t)$: Measurement and CFD computation with nuclear heating

Figure 11 above shows the 2 following things.

- It is possible to characterize the so-called TOP nuclear heating effect in ^{3}He with a dedicated CFD computation.
- The phenomenon is very tight.

An option would be to improve the experimental characterization of the TOP effect. This could be possible with a dedicated test device. Such a device should be equipped with a sufficient instrumentation set up allowing the measurement of neutron flux (ion chambers and dosimeters) as well as $P_{He}(t)$ and gas temperature into a dummy ^{3}He tube undergoing the same depressurization as those of the core reactivity injection system.

VIII. CONCLUSION

This paper presented the organization set up to assure the safety of experiments in the CABRI RIA test facility.

It shows several computation steps are necessary to evaluate the margins. It presents the methodology developed to improve the characterization of power prediction in a limited amount of transients called fast pulses. This characterization allows the evaluation of an original phenomenon called the TOP effect.

The delayed repressurisation of in-core ^{3}He tubes is due to the nuclear heating caused by the $^3He(n,p)^3H$ reaction during the burst of power.

This observation can very hardly be illustrated with current computation schemes but its understanding would probably be greatly improved with the measurements provided by a dedicated test device.

REFERENCES

[1] Neutron Commissioning in the New CABRI Water Loop Facility. G. Ritter, O. Guéton, F. Mellier, and D. Beretz. IEEE TRANSACTIONS ON NUCLEAR SCIENCE, VOL. 57, NO. 5, OCTOBER 2010.

[2] SCANAIR reference documentation. version V_6_1. A.Moal F.Lamare J.C.Latché E.Fédérici V.Bessiron. February 18th, 2008

[3] Modelling of Clad-to-Coolant Heat Transfer for RIA Applications. V. Bessiron. Journal of NUCLEAR SCIENCE and TECHNOLOGY, Vol. 44, No. 2, p. 211–221 (2007).

[4] TRIPOLI-4 VERSION 4 USER GUIDE. Odile PETIT, François-Xavier HUGOT, Yi-Kang LEE, Cédric JOUANNE, Alain MAZZOLO. Rapport CEA-R-6169.

[5] DULCINEE CODE. Dutraive, P. ; Fabrega, S. ; Millot, F. CEA Internal report CEA-N—1378. 1970 Jan. 01.

[6] Forrest B. Brown, et al., "MCNP Version 5," Trans. Am. Nucl. Soc., 87, 273 (November 2002).

[7] Multimode Acquisition System Dedicated to Experimental Neutronic Physics. B. GESLOT, C. JAMMES, G. NOLIBE, P. FOUGERAS. IMTC 2005 - Instrumentation and Measurement. Technology Conference. Ottawa, Canada, 17-19 May 2005

[8] CABRI Études de coeur. Cinétique rapide. French Nuclear Society. Reactor physics section technical meeting. 10/21/2009 Paris. O. Guéton, G. Ritter.

[9] STAR-CD. Version 4.10.

COUPLED HYDRO-MECHANICAL ANALYSIS OF U-10MO FUEL PLATES FOR MANUFACTURING TOLERANCE RISK ASSESSMENT

JOHN KENNEDY AND GARY L. SOLBREKKEN
Mechanical and Aerospace Engineering
University of Missouri, E2411 Lafferre Hall, Columbia, MO 65211 – USA

ABSTRACT

The proposed new U-10Mo LEU fuel plates that are currently being considered for use in the University of Missouri Research Reactor (MURR) are being evaluated for structural integrity. Specifically, coolant flow-induced deformation of the fuel plates needs to be clearly understood. Historic work has shown that plates indeed will buckle when large enough flow velocities are applied. The analysis tools that were available to study such behavior were either experimental in nature, or else simplified fluid-mechanical analytic models. The present work is intended to move towards a more fully integrated fluid-mechanical model, without needing to make dimensional simplifications.

A study of manufacturing tolerances is used as a platform to develop the new coupled modeling tools. In any fuel plate assembly, manufacturing limitations dictate that flow channels will be of unequal size, leading to flow imbalance. The goal of the study is to determine the amount of deflection that can be expected due to the flow imbalance. The numeric modeling is carried out using Star-CCM+, a commercial finite volume thermal/fluid code, and Abaqus, a commercial finite element structural code. Since the codes use fundamentally different solution strategies, an explicit coupling approach is used. A stable solution process has been obtained through a combination of conventional pressure relaxation, flow velocity ramping, and time step relaxation. The numeric solution is benchmarked against a simple analytic model.

1. Introduction

The University of Missouri Research Reactor (MURR) is one of five high-performance research reactors in the U.S. for which fuel conversion will require the use of new LEU “monolithic” fuels. The monolithic fuels utilize U-10Mo based foils to achieve very high uranium densities and are under active development by the Reduced Enrichment for Research and Test Reactors program. The feasibility studies are currently being conducted to establish the performance and safety behavior of the monolithic structures necessary to gain regulatory approval.

From a mechanical structure standpoint, there are two key ways in which the new monolithic fuel will be different from dispersion structures. The first is that assembled monolithic fuel plates have a laminated composite structure, with clearly defined interfaces between the U-10Mo foil and the aluminum cladding. This is in contrast with the powder metallurgy approach characteristic of conventional dispersion fuel. The second way in which the monolithic fuel is proposed to be different for MURR is that individual fuel plates will be thinner than their current fuel design.

The mechanical integrity of monolithic fuel plates for MURR needs to be evaluated in light of the proposed thinner, composite structure. A major mechanical load during reactor operation is that caused by the high velocity water coolant flow. In particular, a pressure imbalance can develop across a fuel plate due to flow velocity differences between neighboring flow channels due to a difference in their cross-sectional area. A difference in the cross-sectional area between neighboring channels can be caused by natural manufacturing variations. This paper describes integrated fluid-mechanical modeling needed to support a study that evaluates manufacturing tolerances of fuel plates during operation.

2. Analytic Model Development

A simple analytic model was developed to estimate flow-induced plate deflection of a single plate with flow channels on either side. The model is intended to provide results that can be compared with the numeric model, as well as to provide parametric trend guidance. A sketch of the reference system considered is shown in Figure 1.

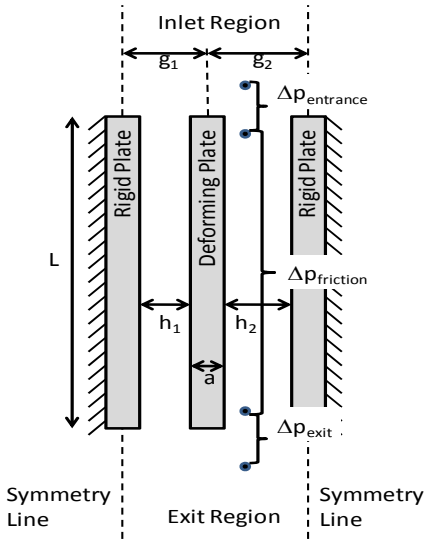

Figure 1. Sketch of Geometry Considered for Analytic Modeling

The modeling strategy is to solve for the pressure distribution on either side of the plate caused by the coolant flow, and then to use the difference in pressure distribution on either side of the plate to estimate the plate deflection using a wide beam model. A design flow velocity is set at the inlet region. The flow is allowed to distribute between the two channels. When the flow rate in each channel is known, the local pressure distribution on either side of the deflecting plate can be found using standard pressure drop relations.

As suggested by Figure 1, it is assumed that there is an inlet region before the deforming plate and an exit region after the deforming plate. Rigid plates are assumed to exist on either side of the plate. The rigid neighbor plates are assumed to have the same geometry as the deforming plate. The purpose of the neighbor plates is to provide fixed flow boundaries for the coolant flow. The distance between the rigid neighbor plates is fixed while the deformable plate is offset to simulate the manufacturing assembly variation. This means that the values of h_1 and h_2, the channel gap values, will be different. However the sum of h_1 and h_2 will remain constant.

The first step in the solution process is to calculate the mass flow rate of water in each of the two flow channels created between the rigid neighbor plates and the deformable plate. This is accomplished by defining the uniform flow velocity in the entrance region and assuming that the lateral pressure is uniform in the inlet region. The lateral pressure is also assumed to be uniform sufficiently far downstream from the plates in the exit region.

The pressure drop from the inlet region to the exit region is assumed to be fixed for a given inlet flow velocity. This is consistent with assuming that the pressure drop across the entire fuel assembly is held constant by the reactor coolant loop pump, and insensitive to small perturbations of individual fuel plates. For a given approach flow velocity, the overall pressure drop is calculated when the deforming plate is placed precisely between the two rigid plates. The pressure drop calculation approach is similar to that outlined in Kays and London [1]. The overall pressure difference can be written as:

$$\left(p_{inlet} - p_{exit}\right) = \Delta p_{entrance} + \Delta p_{friction} + \Delta p_{exit} \quad (1)$$

For the sake of brevity, it is noted that the entrance and exit pressure drops account for flow acceleration/deceleration due to flow area changes, as well as irreversible contraction/expansion losses. The frictional pressure drop through the length of the channel uses an expression for the Darcy friction factor that is based on the Colebrook equation for fully developed turbulent flow.

After the overall pressure drop is found, the deforming plate is offset between the rigid plates by some tolerance (δh in Figure 2). New expansion and contraction coefficients and friction factors are calculated for the new geometry and a guessed flow velocity. This process is repeated for both channels. The flow velocity is then solved for in each channel for the given pressure drop coefficients and the given pressure drop. If the flow velocity that was originally assumed is different than the calculated flow velocity, then new coefficients are calculated until the flow velocity converges.

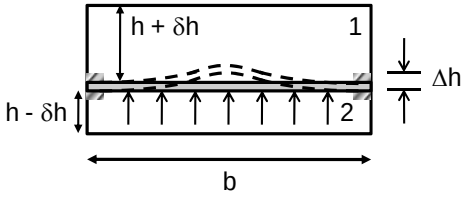

Figure 2. End View Sketch of Plate that has Deformed

The converged flow velocity in each channel is used to calculate the pressure distribution along each side of the deforming plate. The lateral pressure difference across the plate is then calculated and assumed to be the mechanical load that causes the deforming plate to bend as suggested in Figure 2. The amount of plate deformation is calculated assuming the fuel plate behaves like a wide beam with built in boundary conditions [2]. By integrating the deformed profile, an average deflection, Δh, can be calculated from:

$$\Delta h = \frac{\left(p_2 - p_1\right) b^4 \left(1 - \upsilon^2\right)}{60 E a^3} \quad (2)$$

where E is Young's modulus and ν is Poisson's ratio. It should be noted that the amount of deformation for a given pressure difference is proportional to $1/a^3$, clearly showing the risk of using thinner plates.

With the amount of plate deflection calculated, it is possible to re-evaluate the mass flow rates through the cooling channels, the resulting pressure distribution, and finally the plate deflection. This process is repeated until the plate deflection calculation converges. The converged solution is then assumed to be the actual plate deflection for a given inlet flow velocity and plate offset.

3. Numeric Model Development

A structure similar to that shown in Figure 1 was simulated using Star-CCM+ [3], a commercial CFD code, and Abaqus [4], a commercial FEM code. Aside from the fact that these two commercial codes take fundamentally different solution approaches, the primary difficulty in coupling these codes for this analysis arises from the high aspect ratio of the geometry being considered. A high aspect ratio increases the difficulty of building a mesh dense enough to provide accurate results, without being so dense that the simulation takes an extravagant amount of time to complete. Also, without careful consideration of meshing, time-stepping, and velocity ramping parameters, the solution diverges, failing to produce results.

Geometry parameters for the models evaluated are shown in Table 1. To improve the stability of the explicit coupling between the CFD and FEM

Table 1. Numeric Model Parameter Values

Parameter	Value
Plate Thickness (a)	0.9652 mm = 0.038 in
Plate Length (L)	647.7 mm = 25.5 in
Plate Width (b)	110.3 mm = 4.342 in
Front Channel Gap (h_1)	2.4 mm = 0.0955 in
Back Channel Gap (h_2)	2.2 mm = 0.0875 in
CFD Model 1 Mesh Size	6,174,614 Cells
CFD Model 2 Mesh Size	22,385,474 Cells

codes, the applied flow velocity was ramped at a prescribed rate. The two ramping profiles evaluated are shown in Figure 3. The upper flow velocity of 8 m/s is about the expected coolant flow velocity for the proposed new fuel stack.

Finally, a refined time stepping procedure was used. The CFD models utilized a time step of 0.05 seconds, while the FEM model utilized a 0.005 second time step. This allowed the FEM model to iterate 10 times for every one CFD iteration, thereby providing a more stable solution to the solid displacement model at each CFD time step.

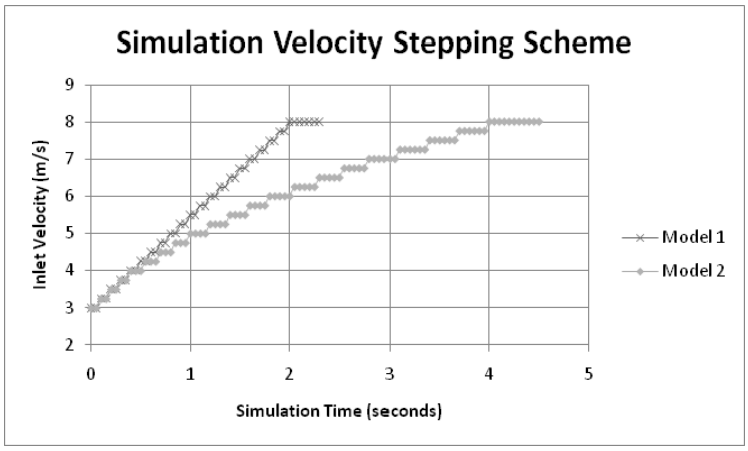

Figure 3. Flow Velocity Ramping Profiles.

4. Results

A plate deflection plot can be seen in Figure 4 based on the coupled simulation results from Model 1. Due to the coarser mesh and rapid change in fluid velocity, the Model 1 simulation diverged, and clearly showed exaggerated oscillating plate behavior. The cause was traced back to the CFD code being unable to stabilize at each step. Thus, as the solution preceded by incrementing the flow velocity, the structure continued to deform, while the flow field was not able to equilibrate. By analyzing when the solution went unstable, the flow velocity ramping rate and the number of CFD iterations-per-time step were modified to the conditions defined by Model 2 in Table 1 and Figure 3.

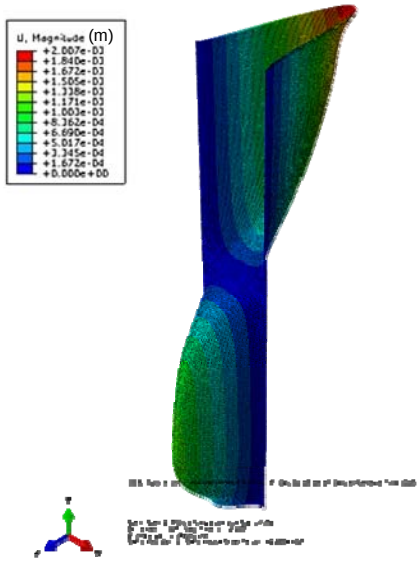

Figure 4. Unrealistic Plate Deflection Results using Model 1 Due to Diverged Solution.

The plate deflection and flow distribution for a flow velocity of 8 m/s are shown in Figure 5. It is of note that the solution process exhibited stable behavior for each velocity step shown in Figure 3 and took about 25 days on a mini-cluster to complete. The plate deflection plot shows a classic pattern where the plate deforms the most at the leading edge where the lateral pressure difference is the greatest. It should be noted that the plate deforms in the direction of the larger gap as suggested by Figure 2. This means that there appears to be a tendency for the flow channels to equalize. Along the length of the plate, the amount of deflection decreases along the length of the plate as shown in previous work [5-6]. The peak deflection at the center of the plate for the 8 m/s simulation is about 328.6 μm (0.0129 in).

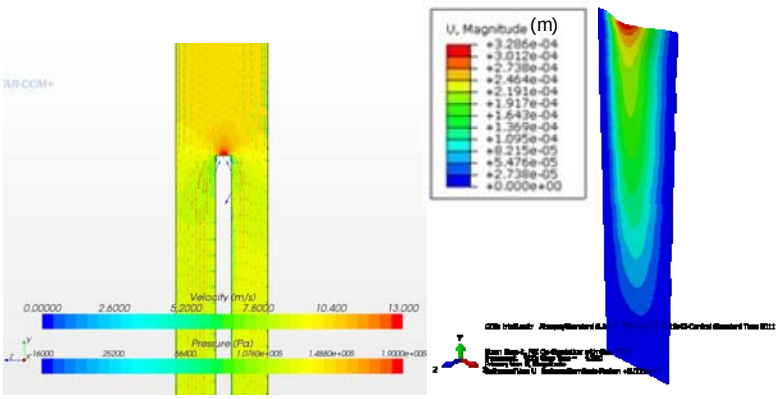

Figure 5. Pressure and Velocity Field from CFD Analysis and Plate Deflection Field from FEM Analysis. Flow Velocity is 8 m/s.

The flow velocity and pressure fields at the plate leading edge illustrated in Figure 5 from the CFD solution also support the notion that the pressure is higher in the smaller channel than the larger channel.

5. Conclusions

It has been demonstrated that coupled fluid-mechanical analysis is possible using commercial CFD and FEM codes. The means to achieve computational stability was by controlled ramping of the applied fluid velocity and by effectively employing time-relaxation. The results of the simulation agree with calculations made using the analytic model in terms of the direction of the deflection and the magnitude of the deformation within 30%. Continuing studies are being conducted to optimize the mesh for improved accuracy and shorter solution times. Experimental validation studies are also warranted and in progress.

It should be noted that while flat plates have been analyzed in this study to develop the analysis tools, the fuel plates employed by MURR have two additional stabilizing features to limit plate deflection. The first is that the plates are curved in an arc spanning about 45°. The second feature is that there is a stabilizing comb at the leading edge of the MURR fuel bundles. The combination of the curved plates and the stabilizing comb is expected to decrease the amount of deflection significantly. Both features are being analyzed with models and experiments to quantify the extent of stabilization.

6. Acknowledgements

We would like to acknowledge the support of Charlie McKibben from MURR and John Stevens from Argonne National Laboratory.

7. References

[1] Kays, W. M., and A. L. London, Compact Heat Exchangers, 3rd ed., Mc-Graw-Hill Book Company, NY, NY, 1984.
[2] Ugural, A. C., S. K. Fenster, Advanced Strength and Applied Elasticity, 2nd ed., Elsevier Science Publishing Co., Inc., NY, NY, 1987.
[3] Star-CCM+ (Version 5.06.007) {Software}, 2010, CD-adapco.
[4] Abaqus (Version 6.10-2) {Software}, 2010, Providence, RI: SIMULIA.
[5] Groninger, R. D., and J. J. Kane, 1963, “Flow Induced Deflections of Parallel Flat Plates,” Nuclear Science and Engineering, Vol. 16, pp. 218-226.
[6] Smissaert, G.E., 1968, “Static and Dynamic Hydroelastic Instabilities in MTR-Type Fuel Elements Part I: Introduction and Experimental Investigation,” Nuclear Engineering and Design, Vol. 7, pp. 535-546.

A Microstructural Model of the Thermal Conductivity of Dispersion Type Fuels with a Fuel Matrix Interaction Layer

A.F. Williams, B.W. Leitch, and N. Wang
Atomic Energy of Canada Limited (AECL)
Chalk River Laboratories
Chalk River, K0J 1J0
Canada

ABSTRACT

This paper describes a three dimensional (3D) finite element model of the micro-structure of dispersion type fuels, which can be used to determine the thermal conductivity of the fuel during irradiation. The model simulates a representative region of the fuel as a cube shaped unit cell. The elements within the unit cell are assigned material properties of either the fuel or the matrix depending on position, in such a way as to represent randomly distributed fuel particles with a size distribution similar to that of the as-manufactured fuel. By applying an appropriate heat generation rate to the fuel particles and a heat flux across the unit cell, it is possible to determine the effective thermal conductivity of the unit cell as a function of: the volume fraction of the fuel particles, the bulk temperature, and the local heat generation rate. The presence of a fuel/matrix interaction layer is simulated by the addition of a third set of material properties that are assigned to elements that surround each fuel particle. In this way the thermal conductivity of the material may also be determined as a function of the volume fraction of the interaction layer.

1. Introduction

Thermal conductivity is one of the most important material properties in determining the performance of any nuclear fuel, as the majority of the physical phenomena governing the fuel behaviour are thermally driven. UMo-Al dispersion fuels have shown great potential for replacement of the Highly Enriched Uranium (HEU) fuels in many research reactors, but have the drawback that the UMo fuel particles interact with Al matrix forming a low density and low thermal conductivity interaction layer, which results in fuel swelling and degradation of the fuel performance. The formation of the interaction layer is thermally driven [1], and the accompanying degradation in thermal conductivity of the fuel results in a positive feedback between the growth of the interaction layer and the increase in fuel temperature.

Traditional techniques for determining the thermal conductivity of two phase composites such as the Maxwell-Euken equation [2] can be successfully used to estimate the thermal conductivity of fresh fuel, but cannot accommodate the presence of the third phase interaction layer. An additional complication is the formation of fission gas bubbles, which form within the fuel particles, and precipitate on the outer boundary of the interaction layer [3]. Previous finite element modelling of the fuel performance by Ding et al [4] has met with some success by treating the dispersed particles as regularly spaced equally sized spheres, but this technique is limited by regular structure assumed for the material micro-structure. This paper describes a finite element model for micro-structure that accounts for the random distribution of the fuel particles positions and sizes, the presence of the irregular interaction layer around the particles, and also the presence of fission gas bubbles. The micro scale model is executed for a range of compositions of fuel loading, interaction layer thickness, and fission gas volume fraction, to yield values of the thermal conductivity that may later be used in macro-scale modeling of the fuel performance.

2. Model Description

Finite element techniques are used to represent of a small volume of fuel within a fuel element. This representative volume is termed the unit cell. The unit cell is constructed of

finite elements and the material properties of the elements are assigned in such a way as to be representative of the micro-structure of the dispersion fuel, including U-Mo fuel particles, the Al matrix, the fuel-matrix interaction layer, and even fission gas bubbles. The effective thermal conductivity of the unit cell is determined by applying a heat flux to one end of the unit cell and solving for the temperature field within the cell. By specifying additional boundary conditions to the unit-cell model, the influence on the thermal conductivity of the heat generation within the fuel particles and interaction layer can also be determined, The ANSYS finite element suite was used to obtain the thermal solution; however almost any of the commercially available finite element solvers could have been used.

2.1 Model Geometry

The unit cell is a simple rectangular prism representing a section of fuel of 0.45 × 0.45 × 0.9 mm, with the long axis in the x direction and short axis in the y and z directions. The elements used are cubic eight node bricks of 5.625 μm on each side. Hence the model consists of 80 × 80 × 160 or approximately one million elements. The basic unit cell is illustrated in Figure 1. An aspect ratio of 2:1 was chosen to allow for the accommodation of the edge effects associated with the packing of the fuel particles and the application of uniform boundary conditions to the ends of the unit cell. When calculating the effective thermal conductivity, only the central region of the unit cell corresponding to a cube of side 0.45 mm is considered as the representative volume.

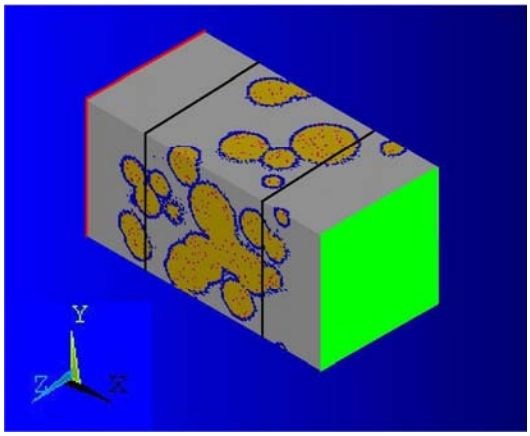

Figure 1 Unit cell showing representative volume (between the black lines), constant temperature face (green surface), and constant heat flux face (red boundary)

A Fortran computer code was written to generate a number of virtual spherical fuel particles, with random coordinates within the unit cell. The diameters of the particles were also randomly generated with a normal distribution about a mean of 112.5 μm with a standard deviation of 33.75μm. A lower and upper limit of 45μm and 360μm respectively, was also applied to ensure that extreme particle sizes were excluded from the model[1]. Fuel particles were added to the model until the required fuel loading had been obtained. No restrictions were placed the particle locations to prevent interpenetration of particles (i.e. the particles were allowed to overlap), although the fuel volume in the unit cell was calculated in such a way as to prevent the double accounting of fuel volumes in the interpenetrating regions. Restrictions were placed on the random x-coordinates of the particles to ensure that a particle free "buffer" region of 0.1125mm existed at the two ends of the unit cell. This was required to enable the correct application of uniform boundary conditions of heat flux and temperature to the ends of the unit cell. This resulted in two "edge effect" regions that were excluded from the representative volume used in the calculation of the effective thermal conductivity. The geometry of the unit cell was assumed to be cyclic in the y and z

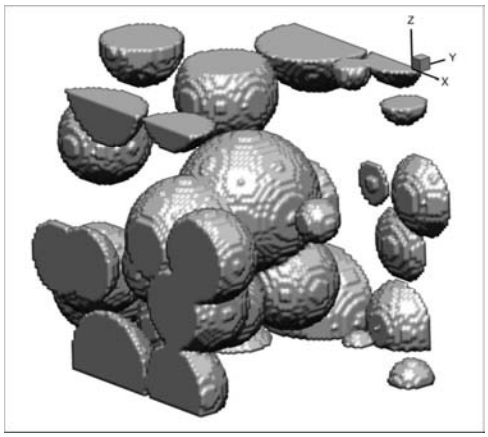

Figure 2 Typical particle distribution for 30% fuel by volume

[1] This size distribution was chosen to produce a micro-scale morphology similar to that of the UMo elements irradiated in the NRU reactor at Chalk River [7]. The model may easily be modified to represent alterative particle sizes and shapes more typical of other fuel types.

directions, and the portions of particles which penetrated the faces of the unit cell in these directions were represented at the opposite face of the unit cell. An example distribution of fuel particles within the unit cell is shown in Figure 2, and a cross section though the unit cell is shown in Figure 3. The cyclic nature of the geometry in the y and z directions is clearly visible in Figure 3.

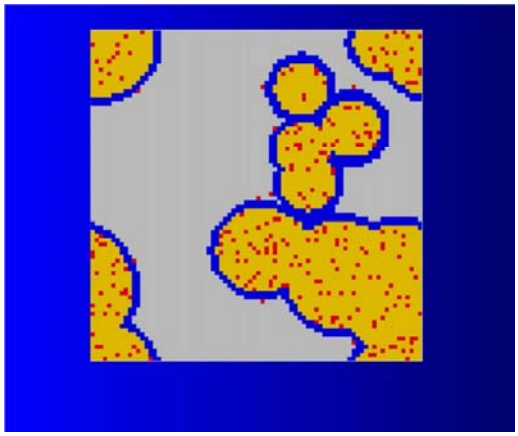

Figure 3 A cross section through a unit cell showing fuel (yellow), interaction layer (blue), fission gas (red), and Al matrix (grey)

The interaction layer between the matrix was simulated as a uniform layer around the periphery of the fuel particles. Fission gas bubbles were also simulated located on the periphery of the interaction layer. Figure 3 shows a typical cross section through the unit cell with fuel particles, interaction layer and fission gas bubbles.

The temperature dependant material properties of each finite element were assigned depending on whether the center of the element lay within the fuel particle, the interaction layer or a fission gas bubble.

2.2 Material Properties

For the simulations shown in this paper the fuel was assumed to be of 10 wt% Mo (U-10Mo) and was assigned a temperature dependant thermal conductivity determined by the correlations provided in Section 2.6 of the U-Mo Fuels hand book [5]. The thermal conductivity as a function of temperature is shown in Figure 4. The thermal conductivity of the aluminum matrix was assumed to be temperature independent and set as 220 $W.m^{-1}.K^{-1}$. The thermal conductivity of the fission gas in the bubbles was approximated as a temperature independent value of 10^{-3} $W.m^{-1}.K^{-1}$.

The composition of the fuel-matrix interaction layer is still the subject of study and the thermal conductivity of this layer remains the largest uncertainty in the model. Lee et al [6] report laser flash measurements conducted on unirradiated samples of U-Mo dispersions following various heat treatments. These heat treated samples exhibit interaction layers

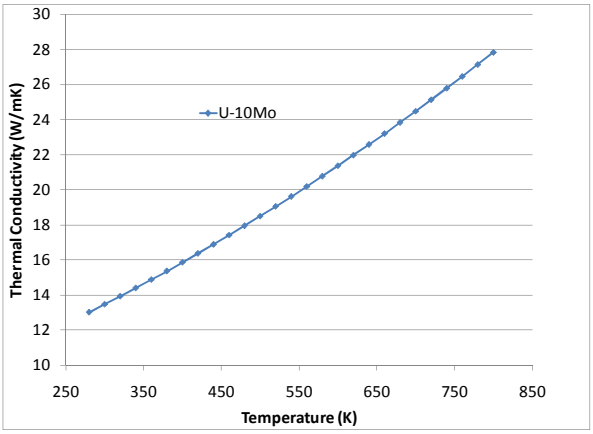

Figure 4 Thermal conductivity of U-10 fuel particles

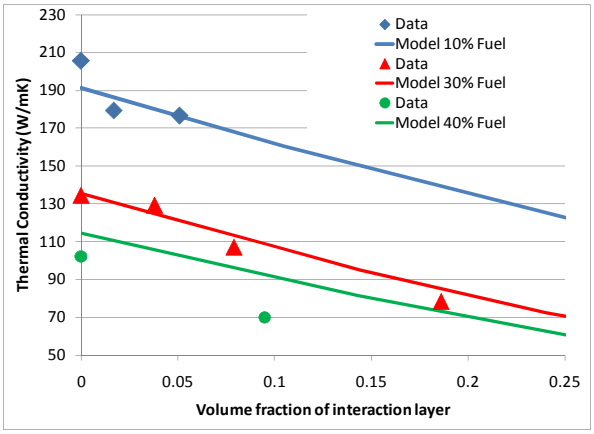

Figure 5 Thermal conductivity compared against data by Lee et al [6]

around the fuel particles, and thermal conductivity of fuel sample as a function of the volume fraction of the interaction layer is reported for several fuel compositions. It was possible to estimate the thermal conductivity of the interaction layer by choosing a value for the model

which best matched the observed degradation in thermal conductivity of the fuel sample as a function of the volume fraction of the interaction layer. The thermal conductivity as a function of volume fraction of the interaction layer for both the experiments and the model simulations is shown in Figure 5. The best match with the experimental data was obtained with an interaction layer thermal conductivity of 5.5 $W.m^{-1}.K^{-1}$.

2.3 Boundary Conditions and Constraints

Constraint equations were applied to the finite element solution to ensure that the temperature matched on opposite faces of the unit cell in the y and z directions. This is consistent with the cyclic nature of the geometry, and has the effect of making the unit cell part of an infinitely repeating pattern in the y and z directions, thus eliminating edge effects at the unit cell faces normal to these directions.

The unit cell face normal to the x direction is held at constant temperature of 400 K, while a constant heat flux of 5×10^6 $W.m^{-2}$ is applied to the opposite face (see Figure 1). These values are intended to be approximately representative of a sample of fuel in the outer portion of one of the U-Mo fuel elements irradiated in the NRU reactor at CRL [7], with a linear power of 100 $kW.m^{-1}$.

For several of the simulations shown in Section 3, a heat generation rate was also applied to the finite elements representing the fuel and the interaction layer. In all cases the applied heat generation was equivalent to a volume averaged heat generation rate of 3.2×10^9 $W.m^{-3}$ applied to the entire unit cell. It was also assume that the ratio of the volumetric heat generation rates in the fuel particles and the interaction layer was 10:1.

3. Simulation Results

The model was executed for a matrix of conditions intended to determine the impact of fuel loading, interaction layer volume fraction, fission gas volume fraction, and heat generation with the fuel particles. The results of these simulations are presented and discussed below.

3.1 Comparison to the Maxwell-Euken Equation

Traditionally, the thermal conductivity of dispersion type fuels has been estimated using the Maxwell-Euken equation [2]:

$$\lambda_m = \frac{\lambda_c\left(1 + 2\chi - 2\phi(\chi - 1)\right)}{\left(1 + 2\chi + \phi(\chi - 1)\right)}$$

where:

λ_m = thermal conductivity of the mixture (in this case the fuel meat),

λ_c = thermal conductivity of the continuous phase (in this case the Al matrix),

λ_d = thermal conductivity of the dispersed phase (in this case the UMo fuel),

χ = λ_c / λ_d i.e. the ratio of the thermal conductivity of the continuous phase to that of the dispersed phase.

ϕ = the volume fraction of the dispersed phase (in this case the volume fraction of the UMo fuel particles within the fuel).

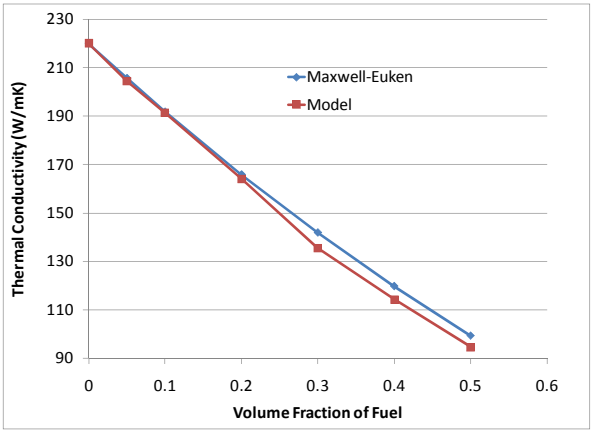

Figure 6 Comparison of model against the Maxwell-Euken equation

This equation was derived for an idealised dispersion of spherical particles in a continuous medium and is not generally applicable to dispersion fuels with significant interaction layers and fission gas bubbles. Figure 6 shows the current model compared against the Maxwell-Euken equation for several fuel volume fractions. There is no interaction layer, fission gas or

heat generation for these simulations. For fresh fuel there is good agreement with the Maxwell-Euken formula.

3.2 Effect of Interaction Layer

The impact of the growth of the interaction layer was studied by executing the model over a range of fuel volume fractions and interaction layer volume fractions. The results of these simulations are shown in Figure 7. This figure allows the thermal conductivity of the fuel to be determined from a known combination of fuel volume fraction and interaction layer volume fraction. It should be noted that for a fuel undergoing irradiation, the volume fraction of the fuel particles will fall with burnup as the interaction layer grows. In principle if the relationship between the reduction in the fuel volume fraction and the increase in interaction layer volume fraction is known as a function of burnup, it should be possible to determine the thermal conductivity as a function of burnup. Note that these simulations do not include the impact of fission gas bubble formation.

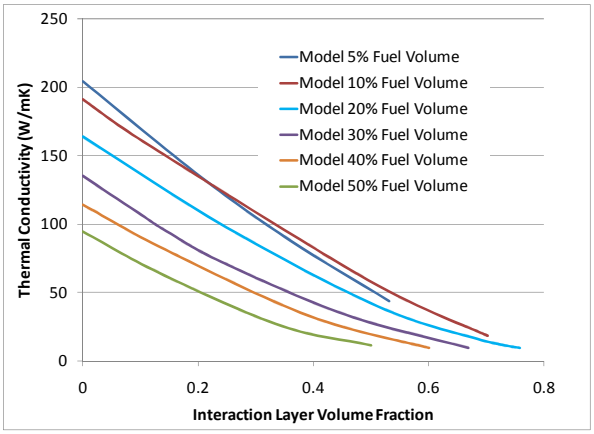

Figure 7 Thermal conductivity as a functon of fuel and interaction layer volume fraction

3.4 Effect of Fission Gas Bubbles

Fission gas bubbles were added as a fourth phase to the model. It was assumed that the fission gas bubbles are restricted to the inside of the fuel particles, and surface of the interaction layer. Figure 8, shows the thermal conductivity of a fuel sample with a 30% volume fraction of fuel and a 14.4% volume fraction of interaction layer, as a function of the volume fraction of fission gas bubbles. A cross section through the unit cell with fission gas bubbles is shown in Figure 3.

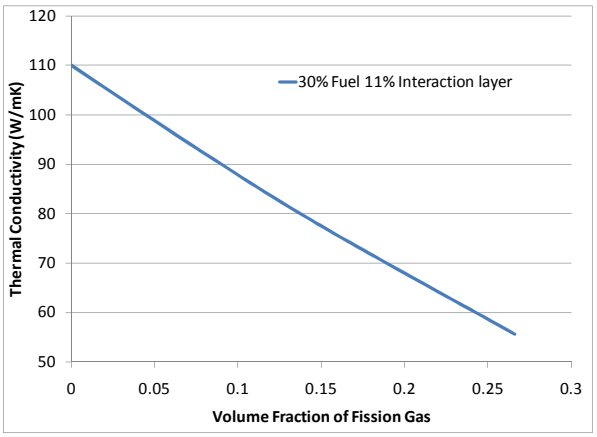

Figure 8 Thermal conductivity as a function of fission gas volume fraction

3.5 Effect of Heat Generation within the Fuel

In-reactor heat is generated within the fuel particles and the interaction layer. The volumetric heat generation rate in the interaction layer is difficult to determine as it depends on the density and loading of uranium and the various activation and fission products; however for the purposes of this model it was assumed that composition of the interaction layer is $UAl_{3.5}$. Using density measurements by Lee et al [6] it was possible to estimate the ratio of volumetric heat generation between the UMo fuel particles and the interaction layer as 10:1. Figure 9, shows the effective thermal conductivity of a fuel sample with 30% volume fraction as a function of the

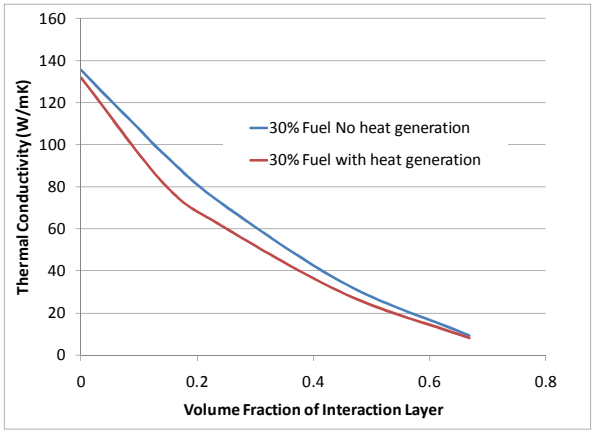

Figure 9 The affect of including heat generation

volume fraction of the interaction layer for a case with no heat generation and a case with a volume average heat generation rate of 3.2×10^9 W.m^{-3}.

Figure 10 shows a cross section through the unit cell with heat generation within the fuel particles. The temperature difference between the center of the fuel particles and the matrix is small (~ 3K).

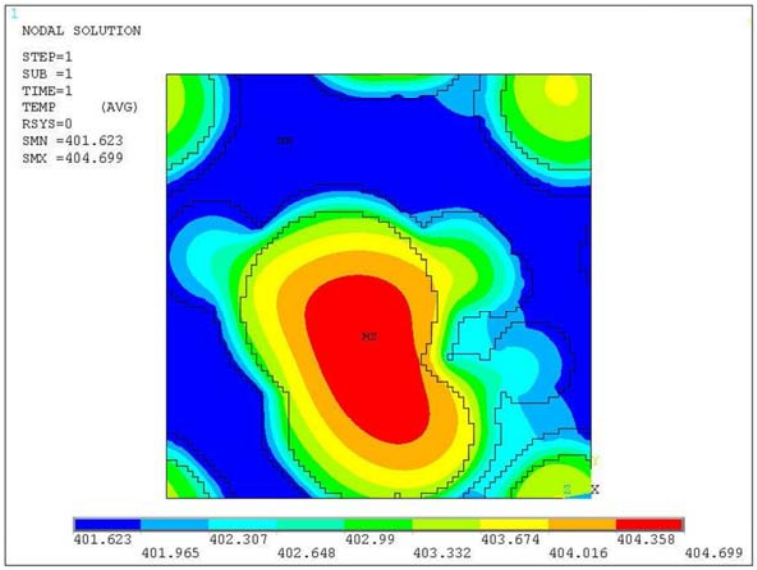

Figure 10 The effect of heat generation on the local temperatures within the fuel

4. Discussion

This micro scale model has been used to determine the thermal conductivity of dispersion type fuels over a range of fuel compositions, including various combinations of interaction layer, fission gas bubble volume fractions. The advantage of this model over many of the previous micro scale models is that morphology of the fuel in the simulation is very similar to that of real fuel, and may be readily adjusted to match many differing fuel types and compositions.

The model also has great potential for extension by directly coupling the model to a suitable thermally driven model of the interaction layer growth, such as that proposed by Soba and Denis [1]. This would allow for the simulation of the evolution of the interaction layer as a direction function of burnup under a range of physical conditions, fully representative of the conditions expected of the fuel within the reactor.

5. References

[1] A.Soba, and A. Denis, “An interdiffusional model for prediction of the interaction layer growth in the system uranium-molybdenum/aluminum”, Journal of Nuclear Materials 360, 2007 pp. 231-241.

[2] J.C. Maxwell. “A Treatise on Electricity and Magnetism” (3rd Edition), Clarendon Press, Oxford (1904), p. 440.

[3] Y.S. Kim, G.L. Hofman, and J. Rest, “Characterization of Intergranular Fission Gas Bubbles in U-Mo Fuel”, Argonne National Laboratory Report ANL-08/11, 2008.

[4] S. Ding, Y. Huo, and X. Yan, “Modeling of the heat transfer performance of plate-type dispersion nuclear fuel elements”, Journal of Nuclear Materials 392, 2009 pp. 498-504.

[5] J.Rest, Y.S. Kim, G.L. Hofman, M.K. Meyer, and S.L. Hayes, “U-Mo Fuels Handbook” Argonne National Laboratory Report ANL-09/31, 2009.

[6] S.H. Lee, J.C. Kim, J.M. Park, C.K. Kim, and S.W. Kim, “Effect of Heat Treatment on Thermal Conductivity of U-Mo/Al Alloy Dispersion Fuel”, International Journal of Thermophysics, 24 (5), 2003.

[7] D.Sears, B. Leitch, G. Edwards, I. Swainson and R. Rogge, “Effect of Burnup and Irradiation Temperature on Crystalline Phase Evolution in Al-UMo Dispersion Fuel”, RERTR 2009 - 31st International Meeting on Reduced Enrichment for Research Test Reactors, Beijing, China, 2009.

NUMERICAL STUDY OF HEAT TRANFER IN A RADIOMETRIC CALORIMETER DEDICATED TO NUCLEAR HEATING MEASUREMENTS

C. REYNARD-CARETTE, O. MERROUN, J. BRUN, M. CARETTE, A. JANULYTE, Y. ZEREGA, J. ANDRÉ, P. DI ROSA

Laboratoire Chimie Provence LCP UMR 6264 UMR 6264 CNRS-Universités Aix-Marseille I, II et III, Centre de Saint Jérôme, bâtiment Madirel Avenue Escadrille Normandie-Niemen 13397 Marseille Cedex 20, France

A. LYOUSSI, G. BIGNAN, J-P. CHAUVIN, D. FOURMENTEL, C. GONNIER, P. GUIMBAL, J-Y.MALO, J-F. VILLARD

Commissariat à l'Energie Atomique et aux Energies Alternatives CEA[2] Direction de l'Energie Nucléaire

Centre de Cadarache, 13108 Saint-Paul-Lez-Durance, France

E-mail: christelle.carette@univ-provence.fr

Keywords: IN-CORE, Heat Transfer, Calibration, MTR, JHR

ABSTRACT

Numerical analytical works on a non adiabatic radiometric differential calorimeter dedicated to nuclear heating measurements in material testing reactor are developed to focus on the heat transfers taking place into this sensor in two cases. The first case corresponds to the calibration operating mode which is performed under non irradiation conditions before an irradiation campaign. In that case the nuclear heating is replaced by an electric power imposed in the sample. Moreover the experimental results used to validate the thermal model correspond to a natural convection exchange between the calorimeter and its external surroundings. The second case concerns the in pile experiments. This paper focuses on only the first case. The differential calorimeter and its operating mode are presented. The validated 2-D axi-symmetrical numerical model, based on finite element method and solved iteratively by CAST3M code, is described. A focus on stationary results is presented. The temperature profiles and the heat flux are shown. The heat flux repartition through the external jacket of the calorimeter is studied for several electric powers. Then the response curve of the calorimeter is given. Finally the study of its sensitivity according to specific geometrical dimensions of the twin cells is presented and discussed.

1. Introduction

The present work is carried out in the frame of a collaborative research program called IN-CORE "Instrumentation for Nuclear radiations and Calorimetry Online in REactor" between the University of Provence (Marseille, France) and the CEA (French Atomic Energy Commission) - Jules Horowitz Reactor (JHR) program. IN-CORE collaborative program is inside the new CEA-Provence University join laboratory called LIMMEX[1]. The building of this new European MTR with higher performances [1] represents a real opportunity for researchers and end-users to build and then to carry out new experiments on structural material ageing and fuel behaviour under irradiation which will contribute for instance to the safety studies or to the optimization of existing or coming nuclear power reactors as well as the developments of the future ones. The JHR will allow typically ~ 20 simultaneous experiences in the core and in the reflector. In order to design experiments satisfying both safety requirements and scientific needs (to obtain consequently precise experimental results), new in pile instrumentation and measurement methods are required. At present a real challenge concerns advanced online measurements of several parameters such as specific power deposit ($W.g^{-1}$) called nuclear heating which controls temperature and temperature gradients of the experimental devices and the irradiated samples.

The IN-CORE research program deals with this important challenge. This program, started in 2009, is aimed to design a new mobile system adapted to the JRH core conditions. This

[1] Laboratoire d'Instrumentation et de Mesures en Milieux Extrêmes which roughly means « Instrumentation and Measurements in extreme medias »

device will be dedicated to the combined measurements of the irradiation condition relevant parameters in JHR experimental channels as the starting of the reactor (in core and in reflector). For simultaneous (or combined) online measurements, this device will use mixed sensors divided into three categories. The first category of sensors will concern the neutron flux quantification by using fission chambers and Self Powered Neutron Detector, the second one will correspond to the photon flux measurement with ionisation chamber and Self Powered Photon Detector and the last one category will lead to measurement of the nuclear heating with a gamma thermometer and a radiometric calorimeter.
In this program a complementary approach is developed. It is based on experimental campaigns in MTRs (for the first prototype in OSIRIS/CEA Saclay – France at the end of 2011 and then in JHR) coupled with analytical works dedicated to one sensor: a radiometric differential calorimeter. This calorimeter has been developed previously by the CEA[2] and tested inside the OSIRIS reflector [2]. The aim of these analytical studies is to develop numerical and experimental tools to improve and/or to adapt the signal delivered by the calorimeter by focusing on heat transfer inside the calorimeter and with its surroundings and to interpret in pile measurement results. This paper presents the numerical works performed under non irradiation conditions and corresponding to the sensor calibration.

2. Model of the heat transfer in the differential calorimeter

The numerical works concerns a calorimeter belonging to the fourth category called “in-reactor calorimeter” of the radiometric calorimetry in nuclear sciences and technologies [3]. This kind of calorimeter is devoted to the study of the energy deposition in specific samples for engineering purposes of structural materials or to the local measurements of nuclear heating in reactor.

2.1 Synthetic presentation of the differential calorimeter

The studied calorimeter corresponds to a simple robust design of a differential calorimeter composed by two superposed twin cells contained in a cylindrical stainless steel tube filled with nitrogen gas, instrumented by four thermocouples (K type) and two heating elements embedded in alumina.

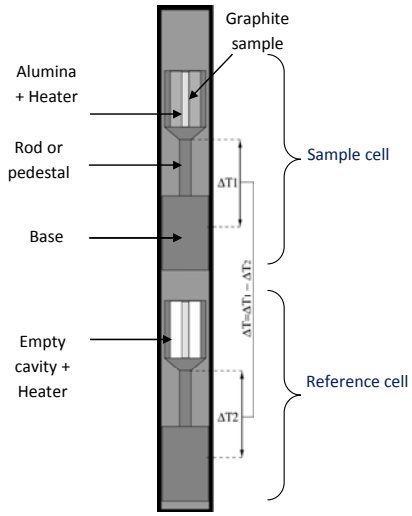

Fig 1. Differential calorimeter diagram

The upper cell contains the sample which acts like a “radiation absorber”. The sample is made of graphite. The lower one contains an empty cavity filled with nitrogen gas and is used as reference cell. The operating mode used is a permanent mode with a heat flow (or heat exchange) between the calorimeter and its surroundings (water bath during calibration in the ISIS pool at CEA[2] or water flow during irradiation in OSIRIS). The heat is transferred from the sample to the lower part of the cell thanks to two consecutive cylindrical rods. The first conduction rod has a small diameter in order to turn the heat towards the base rod which is in contact with the stainless steel tube in order to evacuate preferentially the heat in this

area. During the calibration of the calorimeter under non irradiation conditions, the nuclear heating is simulated by heating the graphite sample by Joule effect with the heater. The calorimeter is inserted in liquid bath maintained at a constant temperature. The heat exchange mode corresponds to buoyancy convection.

2.2 Thermal model

The thermal model applied is the following:

- computational domain is considered bi-dimensional due to the axi-symmetrical geometry of the twin cells
- conduction heat transfer mode is considered in the structural elements of the calorimeter as well as in the nitrogen gas surrounding the twin cells treated as a static gas cavity.
- thermal expansion effects and the radiative exchanges are neglected. The thermal conductivity of materials is calculated based on the variable temperature.
- heat dissipated in the calorimeter is evacuated through a natural convection laminar single phase fluid flow mechanism
- heat source term corresponds to the heat produced by Joule effect in the alumina by the resistance

The heat flow across the graphite sample, the pedestal/rod, the base is determined by the following equation considering the isotropic and homogenous properties of materials:

$$\rho_i Cp_i \frac{\partial T}{\partial t} = \frac{1}{r}\frac{\partial}{\partial r}\left(\lambda_i \frac{\partial T}{\partial r}\right) + \left(\lambda_i \frac{\partial T}{\partial z}\right) + Q_i$$

Where ρ_i is the mass density of a given material *i* [kg/m3], Cp_i is the heat capacity of a given material *i* [J/Kg. K]. λ_i is the thermal conductivity of material *i* [W/m. K], Q_i is the heat generation per unit of volume of a given material *i* [W/m^3].

The boundary and initial conditions are:

- bulk liquid temperature surrounding the calorimeter tube is equal to 23 °C, thermal properties of water are estimated at this temperature
- heat flux is neglected through the lower and upper sections of the stainless steel tube
- at the boundary of the stainless steel cylinder the heat flux exchanged at the interface solid-liquid is: $\varphi = \int h(T)(T - T_b)dS$

where *T* is the unknown surface temperature, *h* is the convective heat transfer coefficient and *dS* is the elementary heat exchange surface of the stainless steel tube.

In the case of the calibration, the convective heat transfer corresponds to natural convective flows around a heated vertical cylinder at a constant heat flux. The average Nüsselt number on the surface of vertical cylinder is given by the following correlation [4]:

$$Nu_{av} = 0.55\left(Ra_D^* \, D/L\right)^{0.20}$$ (for Ra_D D/L>10^4)

where Ra_D^* corresponds to the modified Rayleigh number calculated from the heat flux, L the tube length and D the tube diameter.

The calorimeter computational domain is discretized using the finite element method. It is implemented by using the 2009 CAST3M code, developed by CEA[2]. The computational domain is meshed by two kinds of element: (i) three node triangular elements are used to mesh nitrogen gas cavities and the cone of the graphite sample holder and (ii) four nodes quadrilateral meshes for the remaining calorimeter structural elements. The non-linear heat conduction equation is solved iteratively by using PASASAPS procedure of CAST3M code, from an initial temperature field To(R, z), and the Crank-Nicolson second-order scheme (implicit in time). The iterative procedure is repeated until satisfying the following convergence criterion:

$$\mathrm{Re}\,s(T) = \rho_i C_{p_i} \frac{\partial T}{\partial t} - div\left(\lambda_i \overrightarrow{grad} T\right) - Q_i < \varepsilon$$

where ε is a predefined tolerance (ε=10^{-6}) and *Res(T)* is the residual vector.

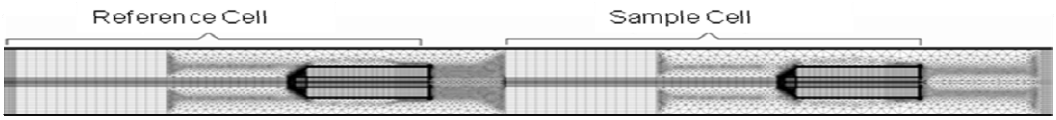

Fig 2. Computational domain meshed.

3. Numerical results on heat transfer

During the calibration under non irradiation conditions, various electric powers are imposed to the heater inserted into the sample and into the reference cell. For each power level the of rod and base temperatures are measured for the two cells. These temperatures have been used to validate the thermal model. Experimental and numerical results have a good agreement: discrepancies (simulation-experiment) are less than 6%. Afterwards the numerical results are analysed in order to obtain the temperature profiles for various simulated electric powers. Two profiles of temperature are given in Fig. 3a for two values of electric powers. Even if during calibration under non irradiation conditions the absolute value of the temperatures does not correspond to those of in pile experiments (without the nuclear energy deposition on the whole test cell), the temperature profiles are interesting in order to determine the calorimeter thermal behaviour, and in order to choose the thermocouple locations to improve the sensor sensitivity and in order to deduce the heat flux distribution. Two curves giving the local heat flux through the external tube versus the vertical ordinate are presented on Fig. 3b for the same electric powers. The location of the maximum heat flux corresponds to the base areas.

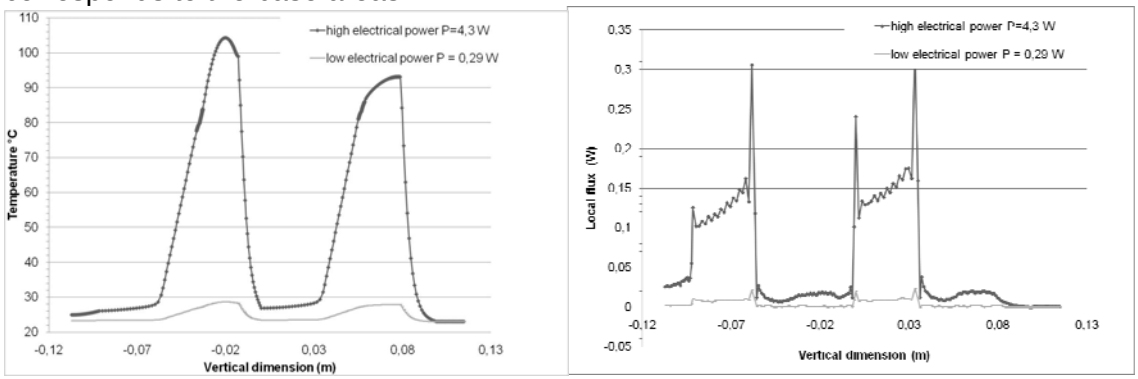

(a) **(b)**

Fig. 3: (a)Temperature along the median vertical axis for two electric powers (on the left), (b) Local flux along the external surface of the tube for two electric powers (on the right).

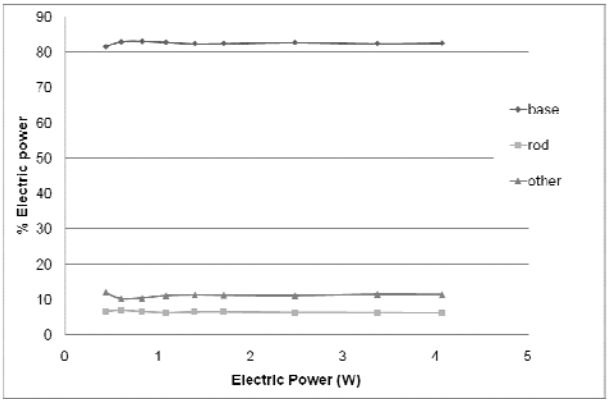

Fig. 4 : Distribution of the electric power dissipated by the sample cell along the external tube

The Fig. 4, which gives the distribution of the electric power dissipated by the sample cell for different electric powers imposed, shows that 82 % of the heat generated by the electric power is evacuated through the calorimeter base. This curve confirms that the calorimeter design ensures a good heat flow in the vertical direction. Nevertheless, an optimisation will be studied in order to increase the heat flux through this heat exchange area.

Moreover, the parametric study is completed by varying other characteristics. The aim is to define the sensor sensitivity. The main parameter presented in this paper concerns the

length of the calorimeter for several electric powers. In order to increase the available space for the other sensors, the length of the rod or the length of the base is decreased. For each simulated length value, the sensor response is determined. The Fig. 5a shows the influence of the rod length. For each value, the sample cell response or the calibration curve versus the electric power is linear for the tested range (< 5W). The slope is calculated to determine the sensor sensitivity. An increasing of the rod length (corresponding to a thermal resistance increasing) leads to the increasing of the measured temperature difference. The Fig. 5b presents the sensitivity versus the rod and base lengths. It is independent of the base length. Nevertheless, the base length has an impact on the absolute temperature value which has to be inferior to an imposed safety value. The non linearity of the sensitivity regression curve versus the rod length is induced by the thermocouple locations positioned in the rod and in the base.

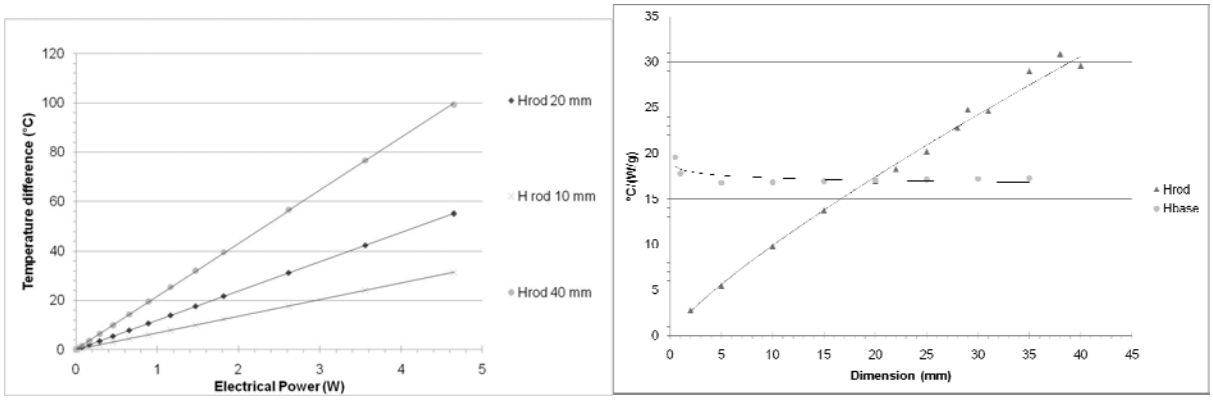

(a) **(b)**

Fig. 5: (a) Temperature difference of the sample cell versus the electrical power for three length values of the rod (on the left), (b) Sensor response versus the rod and base lengths (on the right)

4. Conclusions and outlooks

These preliminary analytical works under non irradiation conditions confirm the thermal directional behaviour of the calorimeter (82 % of the electric power pass through the base). The influence of the rod length on the sensor sensitivity is shown. These works will be completed by other parametric studies. The influence of the material thermal properties, the radius size of rod in particular, the nitrogen static cavity, the thermocouple location on the sensitivity, higher electric powers will be determined. Then these works will be performed under irradiation conditions. In that case on one hand the heat source term will be replaced by the nuclear energy deposition which depends in particular on the location of the calorimeter in the experimental reflector/core channels, on the other hand the heat exchange mode will be changed. Forced convection correlations will be used for evaluating the boundary conditions.

5. Acknowledgements

The IN-CORE program and these analytical works are supported by FEDER and Conseil Régional PACA.

6. References

[1] Materials subjected to fast neutron irradiation, Jules Horowitz Reactor: a high performance material testing reactor, D. Iracane, P. Chaix, A. Alamo, C. R. Physique 9 (2008) 445–456

[2] Patent N° FR 1060068, December 3, 2010, H.Carcreff

[3] In core Instrumentation for Online nuclear heating Measurements of Material Testing Reactor, C. Reynard et al., RRFM Transactions 2010, Marrakech, Morocco

[4] Free-Convective Heat Transfer, Oleg G. Martynenko Pavel P. Khramtsov, Springer

EXPERIENCE IN COMMISSIONING STAGE OF CARR'S DIGITAL CONTROL AND PROTECTION SYSTEM

ZHANG MINGKUI DUAN XIAO YUAN LUZHENG

CHINA INSTIRTUTE OF ATOMIC ENERGY

102413, BEIJING, CHINA

ABSTRACT

The China Advanced Research Reactor (CARR) has been erected in China Institute of Atomic Energy (CIAE). It is a multipurpose research reactor and the complete digital technology adopted, which covers supervision and control system, protection system, ATWS mitigation system, radiation protection system and others. The technique performance is briefly described. Special measures and design, such as the fast data collecting and modification coefficient adjusting for detectors due to their position changing in reactor core, are taken into account during the commissioning stage. Some problems come into being troublesome or unaccustomed due to the digital technology are discussed.

1. Introduction

The China Advanced Research Reactor (CARR) is a multi-purpose and high performance research reactor, its main technical features and properties have got the up-to-date performance of the world research reactors built. In fields of nuclear engineering, for the sake of nuclear safety, couples of years ago it was a hot subject in debate about the use of digital technology based on computer. Following the rapid development in microelectronics, computer and network communication techniques and progress of instrumentation and control (I&C) ability, to adopt the advanced computerized I&C technology and installations in nuclear energy fields has become a significant and non-reversible trend nowadays. Based on this technical background and matched with the position of synthetic disciplinary CIAE, the newly constructed research reactor CARR which is sited in CIAE has adopted the complete digital technology in I&C system especially the protection system. This paper will briefly address some experience in use of CARR's complete digital control and protection (C&P) system during its commissioning stage.

2. Composition of CARR C&P System

The C&P system of CARR covers all functions of monitoring, control, protection and data recording needed while the reactor is in normal operation, accident or post-accident conditions. It mainly includes several subsystems: the monitoring and control system, reactor protection system, mitigation system for ATWS (Anticipated Transient Without Scramming) and radiation protection system, etc.

Among these subsystems, the monitoring and control system is the basis of the C&P system of CARR, it undertakes the monitoring and control functions for main processing system, reactor power regulating system, electrical system, ventilation and air-conditioning system and others. Its hard-ware is based on the PLC structure and interlinked with 10/100Mbps self-adaptive redundant optic fiber Ethernet ring network. (Fig.1)

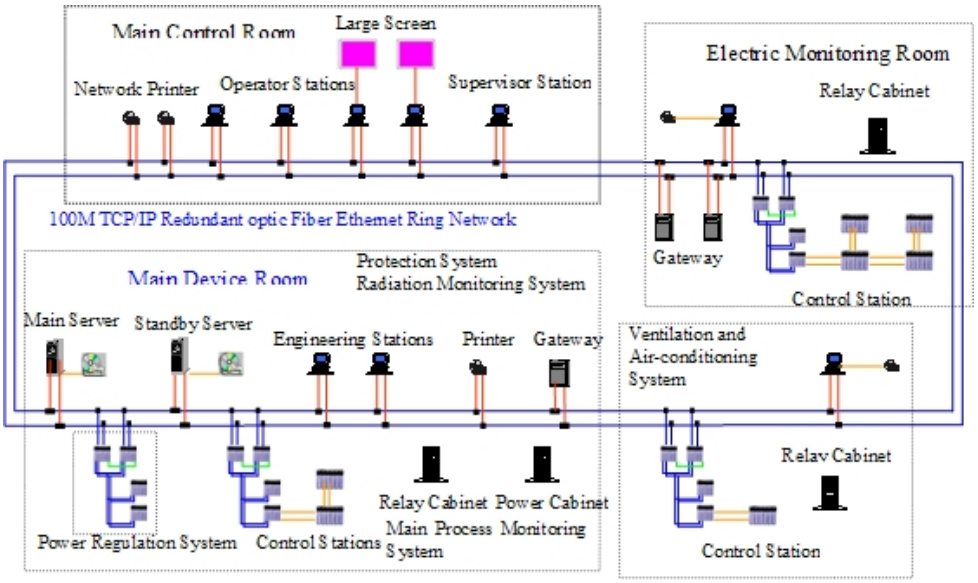

Fig.1 Monitoring and control System Network Diagram of CARR

The reactor protection system adopts high quality commercial grade computers, related modules and components, It functions as the safeguard of CARR, whenever the initial postulated events should happen and reached the setting value, the system would trigger the breakers and make the reactor shutdown safely and prevent it from deteriorating.

In case the reactor cannot shutdown by dropping the control rods due to some common cause failure or control rods blocking, the mitigating system for ATWS will send an additional signal to executive device of protection system for shutdown the reactor, it will further trigger the heavy water discharging valves and make the reactor trip in this case.

3. Advantages using digital technology

CARR's C&P design relies upon a technical line with complete computerization, standardization and commercial grade for devices chosen and general techniques applied. Practice has indicated that the digital technology applied in research reactor shows superiority whatever in human factor engineering, logical algorithm, facility amount used and man power required for commissioning, easy mastering for running, etc.

3.1 Convenient operating and data visual

The application of digital technology considerably decreases the amounts in system facilities so reducing the burden for operating and maintenance. Take the protection system as example, there are 7 display and monitoring stations set in protection system, three independent channel stations isolated physically and electrically in three rooms, two independent display and monitoring stations in main control room, two display stations in auxiliary control spot, all trip parameters and status information can be displayed on real-time and compared with each other. Any changes in protection variables or status information will instantly catch the sight of operators and maintenance workers, which is much favorable to making quick judgment and response for these changes. All these data and parameters in protection system are transmitted through redundant optic fibers, which considerably reduce the usage of normal cables resulting in lowering the work load for installation and commissioning.

Due to the usage of digital technology, the requirement for human factor engineering is easily

realized in design of main control room lay out, circumstance conditions and functions applied, which greatly improve the situation of shortages in analog technique. Real time and precise display, handy buttons and switches, control action and on-time feedback information combined with friendly communicated man-machine interface make the reactor operating and control convenient with least load so assuring the reactor operating safely and effectively under all conditions of normal operation and accident.

As comparison, Fig.2 and Fig. 3 shows the appearance of main control rooms, HWRR (heavy water research reactor also sited in CIAE) and CARR respectively.

Fig.2: The main control room of HWRR

Fig. 3: The main control room of CARR

3.2 The realization of complicated algorithm

The application of digital technique has changed the restriction that only simple algorithm can be conducted in analog mode. In CARR's digital C&P system, many complicated algorithms are realized through the application of computer.

Among protection variables, some are based on complicated algorithm and some are resulted from intricate protection logic. Through digital technology all these situations are possible to be realized. Some setting values for alarming and protection variables, such as inlet pressure and flow-rate of reactor coolant, inlet pressure of the main pipe in secondary loop, flow-rate of heavy water, temperature difference of reactor coolant between inlet and outlet of the reactor core and temperature difference of heavy water between inlet and outlet of heavy water tank, can be automatically changed according to reactor operating conditions without manual interference.

Here is an example to show how the complicated logic to dealt with when the heat sink loss accident would happen. When the secondary loop pressure drops down and flow-rate loss, the temperature of main coolant would rise up, two protection parameters "low pressure" and "temperature high", would result in trip of the reactor. The residual heat removing is still needed within a certain period by running the main coolant pumps. However, the running of main pumps will further heat up the coolant because of the loss of heat sink. So, an additional logic condition has to be applied to the C&P system, i.e., when the power of reactor lowers to less than 1 MW, switch off the main pumps automatically.

Because CARR possesses the small and compact core with quite large worth of 4 control rods, in order to avoid power distribution distortion resulted from too large of insertion level difference between control rods, the algorithm for power regulating adopts the logic of pulling the control rods in same bank level as much as possible. During manually withdrawing or inserting, the level difference among 4 compensating rods is not over 6mm, while in automatic regulating mode, the difference among 3 compensating rods is still kept not over 6mm and for the regulating rod the

level difference from other three is not over 24mm. Practice shows that the digital system of CARR has successfully accomplished the requirements mentioned.

3.3 Be adjusted easily

During the commissioning phase, the related devices, interfaces among systems, conditions and requirements raised by commissioning tests of the reactor are not consistent with those required in normal operation status, correspondent adjustments are always needed at different commissioning stages. Such demands are easily conducted in digital technique. On the contrary, if analog technology was used, the difficulties whatever in technique approach and work load are unimaginable.

The quick data sampling is quite important for testing the characteristics of various loops during their commissioning tests. Different tests want definite parameters, sampling frequencies and total sampling durations. Because for normal operation, the highest communicating speed rate between configure software and PLC is once per second which can not meet the requirements raised by the related commissioning tests. Therefore, special designed quick sampling codes are made with neither any impacts on normal data sampling and display nor adding any investment for hardware, and successfully accomplish the tests.

When conducting the first physical start up experiment, in order to avoid the blind monitoring of neutron population, some ionization chambers used in protection system for normal operation have been moved into near core channels. For getting approximate the same neutron signals among three ionization chambers, the method used in analog technology was frequently and manually adjusting the position of related ionization chamber, it was quite difficult to obtain the ideal conditions and some times it would bring about safety problems. However, because of the use of digital technology, this problem can be easily solved by changing the related coefficients in the formulae of nuclear power signal calculations to approach the reasonable adjusting.

4. Problems brought about by digital tech

4.1 Unaccustomed to the display by operators

Certain embarrassments and awkward feelings will be given rise to at the beginning stage on digital system for the operators who have been trained, worked along with and accustomed with the operation or observation with analog systems.

To take the display of measuring parameters as an example, in analog system mechanical indicator was adopted to show the measuring data, the indicator hand swings a little or even no moving when measuring value fluctuating suddenly due to the mechanical inertia. However, in digital mode all measuring data are displayed in numeric style, the precision of system facility is much higher than that in analog one, the numeric display is always changing in every second which makes operators not accustomed to the frequent changing and sometime nervous in visual sense especially in the situation of reactor period display.

The reactor period meter face in analog system is adopted the dichotomizing scale, if the value of reactor period reaches a certain value, say, above 100 seconds, the scale of indicator is not so sensitive even with quite large fluctuation in real period value. In this case, operator will consider the rector being under safe condition because its power shown in quite steady state. But in digital system, the display of real-time period value changes from time to time. Especially during low power stage, the period value changes a lot due to statistical fluctuation of neutron population which always brings about some impacts to operators mentally.

Moreover, in CARR’s situation, the symbols “+” and “-” are used to show the reactor power

measured being increasing or decreasing, as a result, ever changing display accompanied with symbols “+” and “-” even the reactor power being steady lets operators unaccustomed. Especially the period with a minus symbol always makes operators inadaptable because in analog mode the period never appears negative one.

4.2 Disadvantages resulted from too much functions easily set

The use of digital technology supported by smart computers makes many functions realized very easy. For creating alarming function, it is only required to set alarming threshold values of certain parameters in related files，then the alarming of each parameter works. Due to less communication in DCS designing stage, the software designer prefers to set parameters as many as possible. As a result, too much undue alarms disturb operators annoyingly during the commissioning stage.

Moreover, the same situation exists in parameters display on computer screen. Different colors are used to show parameters consistent with the results of logic judgment. However complicated logic results in quite many colors which make operators confusing in their response.

4.3 Be liable to make fault

In analog technology, once finishing the commissioning of various reactor systems, their configurations or features are not changed at will. But just inverse in digital technique, engineers may easily adjust the conditions of various systems on computers according to different requirements. Nevertheless, it would bring forth troubles beyond expectation if these adjusting did not pass through appropriate QA procedures or without communicating with each other.

Here is an example. During a physical experiment the power of reactor was under auto-regulated by the regulating rod and the operator was adjusting the level of other control rods, suddenly the reactor was shut down due to power over. After the efforts to find out where the positive reactivity came from that making the reactor power rising up were failed, the real reason was found at last that the auto-regulating function failed because one control rod has got to the top end position according to demand of experiment. In normal operation procedure later, there is a restriction condition for auto-regulating function, which is “all control rods are neither at the top end position nor at the bottom end position”. The careless on this limit condition and no strict QA measures brought about this unexpected reactor shutdown event.

5. Conclusion

The use of digital technology with its significant features on intelligence, flexibility, powerful functioning and easy modifying makes variety requirements realized easily, which in analog technique not realized or realized under great costs paid. Just as industrializations in other fields, the application of digital technique in research reactor field will be an irreversible trend. The practice in CARR’s C&P system with digital technology has shown its incomparable advantages no mater in technical points or in project costs. However，every thing has its two sides, some problems like unnecessary functions added at will due to its powerful performance, operator’s knowledge talent not matched with the application of digital technology, especially the feature of easy modification of digital technique would bring about troublesome casually. Anyway, these problems can be solved or avoided by compiling software codes, or through strict managing and QA measures.

REFERENCE

[1] Hai Zeng, etc., IMPLEMENTATION OF DIGITAL CONTROL & PROTECTION SYSTEMS OF CHINA ADVANCED RESEARCH REACTOR, ICON13-50610

IMPLEMENTATION OF INTEGRATED MANAGEMENT SYSTEMS FOR OPERATING ORGANIZATION OF RESERACH REACTORS

J.P. BOOGAARD
RRSS/NSNI/IAEA
E. Bradley
RRS/NEFW/IAEA

Wagramerstrasse 5, PO Box 100, 1400 Vienna - Austria

1. Introduction

Over the years the IAEA requirements to establish and implement a quality assurance programme for research reactors and its associated experiments to ensure safe operation have been developed from Quality Assurance in 1988 through Quality Management in 1996 to Integrated Management Systems in 2006.

Based on the IAEA safety standards on Quality Management of 1996 the majority of the operating organizations developed different quality assurance programmes for operation, utilization, maintenance, radiation protection and emergency preparedness, resulting in a patch work of programmes and procedures by which the responsibilities to ensure safe operation and safety of the workers and public were spread out over the different programmes.

With the introduction of GS-R3 “The Management System for Facilities and Activities” [1], it was required that “a management system shall be established, implemented, assessed and continually improved.” To ensure safe operation; all safety, environmental and occupational health aspects should be integrated in one management system which should be an integral part of all operational activities.

The IAEA requirements and guidance use the term ‘management system’, rather than ‘quality assurance’. The term ‘management system’ reflects and includes the initial concept of ‘quality control’ (controlling the quality of products) and its evolution through ‘quality assurance’ (the system to ensure the quality of products) and ‘quality management’ (the system to manage quality).

Although the IAEA publications “Application of management systems for facilities and activities” (Safety Guide GS-G-3.1) [2], provides generic guidance to aid establishing, implementing, assessing and continually improving a management system and Safety Guide GS-G-3.5 [3], “Application of management systems for nuclear installations”, provides specific guidance for research reactor operating organisations, the need for practical examples on the implementation of an integrated management system for operating organizations of research reactors was requested by member states.

Upon this request the IAEA developed a case study on the implementation of management systems. The draft case study [4] presents an example of processes of an integrated management system to ensure safe operation of nuclear facilities.

2. Implementation of an Integrated Management System

The senior management (Head of Operating Organization) is responsible for ensuring that the management system is implemented and consequently the senior management should

appoint a project leader and assign the resources for the project team to develop a project plan for the establishment and implementation of the Integrated Management System.
This project plan should present clear milestones, the required resources and the implementation and communication strategy. This project plan should be approved by the senior management to ensure the required commitment for the implementation of an Integrated Management System. To ensure the required commitment it is recommended that each division manager appoints a member of the project team, who has the authority to make decisions on his behalf and to assign staff members within the division for drafting and review of the documentation which has to be developed.

The senior management should also discuss and identify the relevant processes in the organization. The preparatory work for the identification of the work processes might be carried out by the project team, but the work processes for an organization should be established by the senior management team.

The project team should identify the applicable (inter)-national regulations and standards which have to be obeyed, including the applicable IAEA safety standards to ensure safe operation of the activities being carried out by the operating organization as well as the IAEA Safety Standards for management systems (GS-R-3; GS-G-3.1 and GS-G-3.5).

As a next step the tasks and responsibilities for the different activities of the work processes, the interfaces with other processes and the relevant documentation which are part of the processes should be identified, described. The procedures describing the processes should be approved by the senior management.

The processes and the corresponding documentation are the basis for a gap analyses to prepare an overview of the documents which need to be drafted or which need to be reviewed. The project team is responsible that these documents are drafted, reviewed and approved as a part of the implementation plan.

To ensure proper implementation all staff should be trained to achieve proficiency and to ensure they understand the management processes that apply to the performance of their work. A detailed audit programme should be developed and implemented to assess the effective implementation of all stages and to identify areas for additional implementation activities and areas for improvement of the processes and related documentation.

The project and implementation plan must be communicated to all involved staff and must be implemented at a time that is commensurate with the activities it covers.

With the applicable regulations as a reference basis a gap analyses should be performed in order to identify whether all prescribed safety, environmental and occupational health provisions are in place. Beside the nuclear safety and radiation protection provisions also sufficient attention should be given to the environmental and occupational health provisions which are prescribed. The gap analyses normally results in areas of improvement, which should be prioritised based on the gain in safety level, the required resources for the implementation and the investment costs. The implementation of these, normally hardware, investments might be carried out as a different project.

3. Process development

A management system conform to the requirements of GS-R-3 is process based, but a single ‘process catalogue’, listing the processes which will apply to every organization, cannot be given. Each organization should determine the applicable processes based on the nature of the organization’s activities, its overall strategy and the applicable regulatory and statutory safety requirements.

Normally the processes are being developed using a top-down approach and are hierarchically linked. The corporate processes should describe who is responsible for which activity, what are the requirements or boundary conditions for the specified action and what the outcome of the action is or what is being produced. Although the corporate processes can be described in a document, it is commonly used to present them as flow charts. The descriptions of the activities are more detailed the closer they are to the technical or task level. At the technical level a procedure or instruction might be more appropriate. A hierarchal structure is presented in figure 1.

Figure 1: Hierarchical structure of a management system

The operational framework within an organization is typically made up of a number of processes, most of which have interfaces across the organization. The processes might be divided in core processes, management processes and supporting processes.

The core processes describe activities of which the output is critical to the success of the organization, e.g. isotope production, neutron activation analyses, irradiation services.
The support processes describe the infrastructure necessary which is necessary for the core processes and the management processes should ensure smooth and efficient operation of the entire management system. At the development of the processes special attention should be paid to the safety related processes. An overview of common support and management processes is given in table 1.

Table 1: Overview of possible processes

Management Processes	
Planning and reporting	Organization Structure
Management system administration	Safety related organizational changes
Resource management	
Recruitment, Selection and Appointment	Employing Temporary Workers or Outsourcing
Performance, Assessment and Training	
Process implementation	
Generic Management System Processes	
Control of document	Control of records
Control of products	Measuring and test equipment
Purchasing	Managing organizational change
Communication	
Processes Common To All Research Reactors	

Project Management	Waste Management
Quotation management	Health, Safety and Environment of Operations
Incoming and Outgoing Correspondence	Near misses
Archiving	Accident and/or Emergency
Numerical Calculations	Operation of Installations and Laboratories
Software Administration	Administration and Maintenance of Equipment and Installations
License, Occupational Health and Safety Assessment	Requests to Reactor Safety Committee
Monitoring and Measurement	
Management system review	Self-assessment
Internal audits	Complaints and product non-conformances
Improvement proposals	Feedback of operational Experience

4. Graded approach

Although the establishment and implementation of a management system is a requirement for an operating organization of a research reactor, the application of the requirements of GS-R-3 and the controls of a management system can be performed using a graded approach in order to deploy the appropriate resources.

The graded approach should be based on the hazards and potential impact (risks) associated with safety, health, environmental, security, quality and economic related elements. Special attention should be given to the grading process with regards to the consequences of a design error, technical failure, wrongly implemented modification or utilization, human error or technical failure. But also the utilization of a research reactor, e.g. irradiation of experiments, isotope production and scientific research could be taken into account for the grading aspects of the management system.

For the grading process the following aspects should be considered:

- Safety analyses and engineering judgement
- License, Operational, Limits and Conditions
- Regulatory requirements
- Significance and complexity of each product or activity
- Safety classification of the structures, systems and components
- Safety classifications of the utilization
- Complexity of the organization
- Maturity level of the technology
- Operating experience associated with the activities
- Lifecycle stage of the facility

Typical examples of grading are more or less stringent inspection and audit requirements, more or less stringent review and approval routes; more or less detailed procedures and instructions, training and retraining programme, self-assessment programme, etc.

5. Examples

OPERATION OF INSTALLATIONS AND LABORATORIES

1. Division Manager
- appoints Line Manager responsible for daily operations of plants/laboratories/experimental set-ups and buildings
- establishes mandates

Line Manager
- appoints supervisor for plants/laboratories/ experimental set-ups and buildings

2. Line Manager
- determines necessity for and nature of Technical Information Package (TIP)/written instructions
- determines (Emergency) drills based on corporate Emergency Plan

3. Supervisor
- co-ordinates preparation of TIP/instructions/ preventive maintenance programme

4. Line Manager
- approves TIP/instructions/preventive maintenance programme

5. Line Manager
- is responsible for operation in accordance with instructions and within technical specifications/ legal framework and licensing requirements
- provides additional instructions
- implements regular HSE inspections/tests and Emergency drills
- is responsible for adequate handling of malfunctions
- initiates procedures regarding complaints and non-conformances if required

6. Division Manager
- evaluates operation with Operational Plan as reference annually
- initiates contract amendment if necessary in consultation with Finances and Commercial Services

Line Manager
- assesses necessity of amendments in operation
- assesses necessity for contract amendments

7. Line Manager
- is responsible for:
  - * approval procedure for amendments
  - * adaptation of documentation
  - * adaptation of HSE inspection programme

8. Line Manager
- co-ordinates data recording
- supervices reportings
- initiates (partial) invoicing if necessary

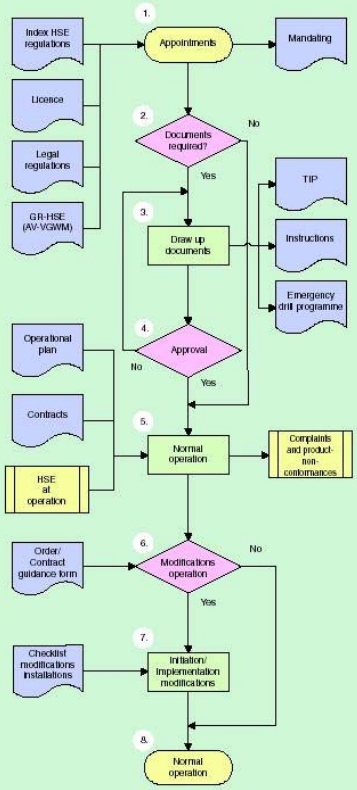

ADMINISTRATION AND MAINTENANCE OF EQUIPMENT AND INSTALLATIONS

1. Line Manager
- appoints administrator
- determines nature and necessity of description and (technical) information package

Administrator
- co-ordinates drawing up description and (technical) information package

2. Line Manager
- determines necessity and scope of preventive maintenance/inspection programme

3. Administrator
- drafts, as necessary, maintenance/inspection programme and adjusts as necessary

4. Line Manager
- evaluates maintenance/inspection programme and/or adjustments and approves

5. User
- notifies malfunctions to administrator

Administrator
- prevents, if necessary, further use after malfunctions
- co-ordinates corrective maintenance
- approves futher use
- informs Line Manager

6. Line Manager
- assesses whether maintenance/inspection programme needs to be adapted
- assesses whether installation needs to be modified

7. Line Manager
- is responsible for:
  - * approvals required for modifications
  - * adaptation of documentation
  - * adaptation of maintenance/HSE inspection programme

8. Administrator
- co-ordinates execution, recording of data and archiving

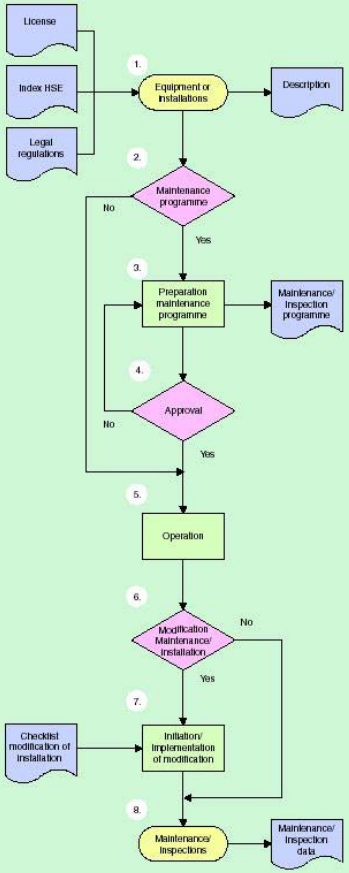

6. Conclusions

An integrated management system based on GS-R-3 integrates all relevant aspects to ensure safe operation with sound working conditions, within the environmental and security requirements by which the economic aspects to ensure sufficient resources for long term safe operation are taken into account.

The work processes should be based on the nature of the organization's activities, its overall strategy and the applicable regulatory and statutory safety requirements.

7. References

1. The Management System for Facilities and Activities; IAEA Safety Requirement GS-R3; Vienna 2006;
2. Application of management systems for facilities and activities; IAEA Safety Guide GS-G-3.1; Vienna 2006;
3. Application of management systems for nuclear installations; IAEA Safety Guide GS-G-3.5; Vienna 2009;
4. Implementation of a Management System for Operating Organizations of Research Reactors, A Case Study; NE Technical Report Series; Draft 08 November 2010.

European Nuclear Society
Rue Belliard 65
1040 Brussels, Belgium
Telephone: +32 2 505 30 50 - FAX: +32 2 502 39 02
rrfm2011@euronuclear.org
www.rrfm2011@euronuclear.org